ACTIVE FLOW CONTROL OF LAB-SCALE SOLID POLYMER ELECTROLYTE FUEL CELLS

A Thesis
Presented to
The Academic Faculty

by

Scott B. Leahy

In Partial Fulfillment
of the Requirements for the Degree
Master of Science in Mechanical Engineering

Georgia Institute of Technology

March 2004

Active Flow Control of Lab-Scale Solid Polymer Electrolyte Fuel Cells

Approved by:

Dr. David E. Parekh, Co-Advisor

Dr. Comas L. Haynes, Co-Advisor

Dr. William J. Wepfer

Date Approved: March 29, 2004

ACKNOWLEDGEMENT

I would like to thank my co-advisors, Dr. David Parekh and Dr. Comas Haynes for their assistance throughout the course of this project. I would also like to express my gratitude to Dr. Bill Wepfer for his participation as a member of my reading committee. I would also like to thank the staff in the ATAS division of GTRI, in particular Allan Williams, Dr. Gary Gray, and Grover Richardson. Each made significant contributions to this project over the past two years.

Furthermore, I would like to thank United Technologies Corporation, and specifically Michael May of UTC for their sponsorship of my research over the past year. Finally, I must acknowledge Motorola and Allison Fisher, in particular, for the direct methanol fuel cells donated to GTRI.

TABLE OF CONTENTS

LIST OF TABLES

LIST OF FIGURES

LIST OF SYMBOLS

c_2	Concentration of methanol at anode
D	Diffusion Coefficient
Δc	Concentration difference between cathode and anode
Δh_f	Enthalpy of formation
ΔP	Pressure difference between cathode and anode
E	Nernst Potential
F	Faraday's Constant
f_i	Fugacity
G	Gibbs' Free Energy
HHV	Higher Heating Value
I	Current
j	Molar diffusion rate
K	Effective hydraulic permeability
m	mass flow rate
M	Molarity
n	number of moles
n	molar flow rate
NOS	Number of Stoichs
P	Power
p_i	Partial Pressure
R	Resistance
R	Universal gas constant
t_m	Membrane thickness
u_f	Fuel utilization
V	Voltage/Potential
η	Efficiency
η	Polarization
λ	Electro-osmotic drag coefficient

SUMMARY

The effects of actively pulsing reactant flow rates into solid polymer electrolyte fuel cells were investigated in this thesis. First, work was conducted to determine the magnitude of voltage response to pulsed reactant flow on a direct hydrogen proton exchange membrane (PEM) cell. The effects of pulsed reactant flow into a direct methanol fuel cell (DMFC) were then considered.

The PEM work showed substantially greater response to pulsed air flow than to pulsed fuel flow. It was found that several parameters affect the magnitude of cell response to active flow control (AFC). Increasing current load, increasing the magnitude of flow oscillation, decreasing the frequency of oscillation, and decreasing the average level of excess reactant supplied were found to maximize both the amplitude of voltage oscillations and the decrease in cell power from steady state performance. The (voltage) response of the cell to pulsed air flow was substantially greater than the response to pulsed hydrogen flow; possible explanations are given.

In contrast, pulsed fuel flow showed the greatest response in the study of DMFC technology. In this case, time averaged cell voltage was found to increase as fuel flow was pulsed. The increase in average cell power is the result of a reduction in methanol crossover; sustainable increases of up to 6% in power output were measured. The parameters found to effect the increase in cell power observed include the frequency of oscillation and the time-averaged NOS_{fuel}. Pulsed air flow on the DMFC did not show any such rise in voltage, supporting the hypothesis that a reduction in methanol crossover is the phenomenon which brings about enhanced performance.

1. Introduction

With the supply of readily available fossil fuels dwindling, there has been an increased search for efficient and effective energy conversions devices in recent years. Of the various alternative energy conversion devices, fuel cells are regularly identified as one of the most promising due to their high efficiencies and their potential for being zero-emission sources. In particular, polymer electrolyte fuel cells (PEFCs) are readily identified as a power source for small scale and portable applications. PEFCs that incorporate a methanol-water solution as fuel, known as direct methanol fuel cells (DMFCs), are well suited to replace batteries in low power applications (e.g., mobile phones and laptop computers). The generic name 'Proton Exchange Membrane' (PEM) fuel cells often refer to polymer membrane fuel cells using hydrogen as a fuel. PEM cells are considered to be most applicable to transportation systems. These two types of PEFCs are considered in the present thesis.

In general, fuel cells operate by electrochemically combining hydrogen and oxygen to produce DC electric power, water and heat. This power is produced with higher efficiencies than prevalent heat engine systems in today's market, such as gas turbines and internal combustion engines. Figure 1 shows the operation of a typical PEFC. Hydrogen based fuel enters into the anode side of the cell, where the hydrogen molecules are electro-oxidized into electrons and positively charged hydrogen nuclei. The hydrogen nuclei pass through the polymer electrolyte membrane and combine with oxygen molecules and returning electrons to form water on the cathode side of the cell. The nitrogen then carries this water away and any excess oxygen left from the inlet air stream. The electrons produce electric power by flowing from the anode through the electronic load placed on the cell before returning to the fuel cell at the cathode side.

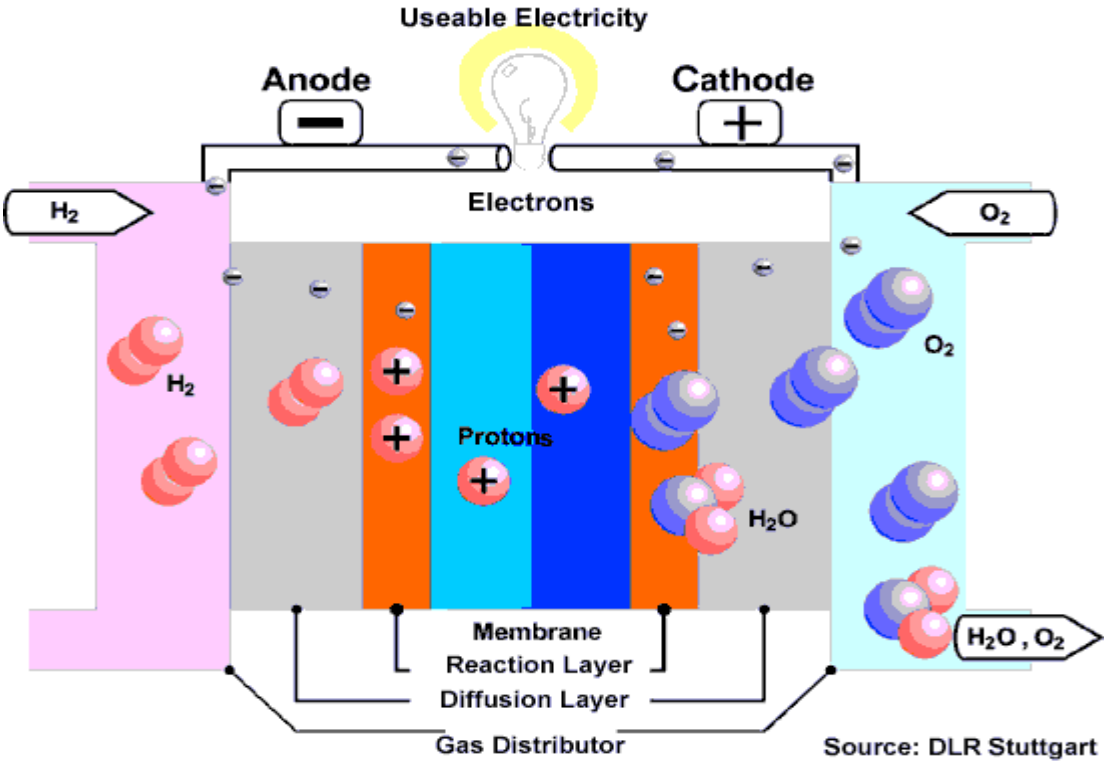

Figure 1.1. Generalized PEFC operation (courtesy www.solarserver.de)

Before fuel cells can become a viable replacement for current means of power generation, several issues must be overcome. Chief among these concerns are the reduction of associated capital costs and increasing the power output from the fuel cell stack. Figure 2 shows the composition of a typical fuel cell system, consisting of a reforming system, the fuel cell stack itself, and a power conditioning system. Collectively referred to as the "balance of plant," the reformer and power condition unit comprise up to 2/3 of the capital cost of a fuel cell system. The reformer takes a hydrocarbon-based fuel and through chemical processes, provides hydrogen rich fuel for the cell stack. Assuming a distributed generation scenario, the power conditioning unit takes the DC electricity output from the fuel cell stack and converts it into grid quality AC power and meets any periodic variations in electric load.

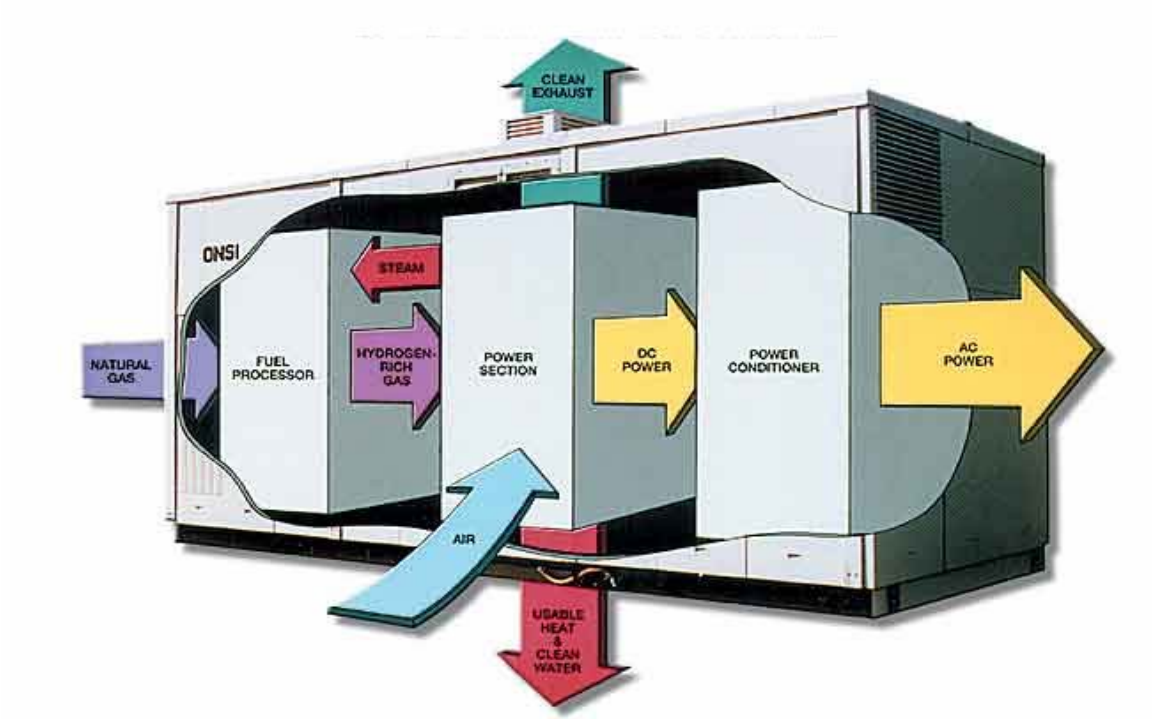

Figure 1.2. Fuel cell system schematic (courtesy of www.usps.com)

To improve the performance of fuel cells and thereby reduce the associated cost, further fundamental research is required. Previous studies of PEFCs, including both direct hydrogen and direct methanol cells, have quantified steady state performance quite well, but few studies have been conducted that focus upon transient cell performance. Further, the vast majority of transient studies that have been published consider the effects of transient electric loading on a cell or are models of transient fuel cell performance. This thesis experimentally considers the effects of transient reactant flow rates on both direct hydrogen and direct methanol fuel cells. This is a manifestation of Active Flow Control (AFC), which is a generic practice by which fluid flow is actively controlled or modulated.

Fuel cells are normally operated under steady state conditions, including a steady electrical load demand, nominally constant temperature and flow rates. All of

these factors will affect the performance of a fuel cell stack. In particular, the reactant flow rates have a large affect on cell performance. Supplying more reactant than is required to sustain a load current (as specified by Faraday's Law) is common practice. By changing the rate of reactant supply, the power produced by the cell can be drastically increased or decreased. Based on this fact and attendant realizations, it was hypothesized that AFC could be used to enhance fuel cell performance.

AFC has been shown to be a viable means of manipulating cell potential. This has been achieved through pulsed air flows to a lab-scale direct hydrogen cell model. As an example, sinusoidally varied flow rates resulted in a low-distortion sinusoidal cell potential at sufficiently low frequencies. A variety of frequencies and amplitudes were studied over a range of current loads to quantify the cell's ability to respond to periodic input flows. It was found that a periodically repeating voltage signal could be obtained with input frequencies in the range of a few Hertz (Hz). Identical tests were performed on the fuel (hydrogen) side of the direct hydrogen cell. Here the frequency threshold at which voltage oscillations become negligible was found to be substantially less than on the oxidant side of the cell. The frequency limit on each side is related to rate limiting transport and electrochemical phenomena. A theoretical explanation of these phenomena will be offered.

A similar study was performed on the DMFC where again both fuel (a methanol/water solution) and air flows were pulsed. In this case, in addition to studying a variety of input frequencies and amplitudes over a range of loads, a variety of wave form shapes were studied. Because of the differences in cell size and in inherent reaction kinetics, AFC showed substantially different effects. However, several trends were observed which promote a periodic voltage response from both the PEM cell and the DMFC.

2. Overview of Pertinent Fuel Cell Operation & Systems

2.1 Structure/Assembly & Fuel Options associated with PEFCs

2.1.1 Structure and Assembly of PEFCs

Fuel cells are most often identified by the electrolyte used, such as phosphoric acid fuel cells (PAFC), solid oxide fuel cells (SOFC), and polymer electrolyte fuel cells (PEFC). PEFCs contain a polymer membrane that selectively allows hydrogen cations (H^+) to flow through the membrane while preventing the flow of electrons across the electrolyte.[1] This electrolyte forms the center of the typically five-layer membrane-electrode assembly (MEA), including gas diffusion layers (GDLs). The MEA is the core of the fuel cell; the other major components of a PEFC are the bipolar and endplate hardware.

The electrolyte at the center of the MEA is generally composed of "sulphonated" polytetrafluoroethylene, or PTFE (known by the trade name Teflon). The sulphonization process results in a polymer with a sulphonic acid (SO_3^-) side chain replacing a fluoride ion. This polymer is produced by several manufacturers, most notably by Dupont under the brand name Nafion®. Nafion has the following properties that are useful to fuel cell operation (Larminie, 2000):

- Highly chemically resistant
- Acidic
- Able to be made in thin films
- Water absorbent
- Good proton conductor if hydrated

[1] A small amount of electrons do pass through the membrane; this phenomenon is known as internal current (Larminie, 2000).

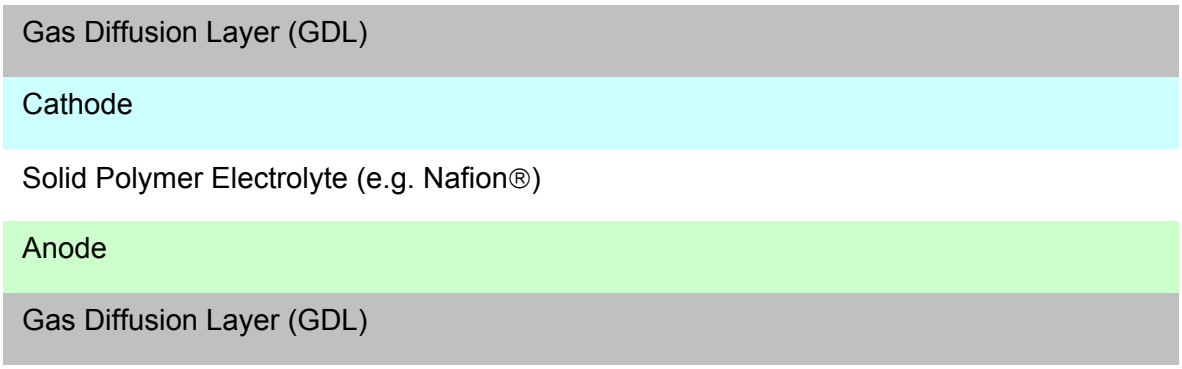

Figure 2.1: Schematic representation of 5 layer membrane-electrode assembly (MEA)

The last bullet item is the most essential to cell performance—by ensuring that the Nafion membrane is properly hydrated, the conductivity of the membrane will be maximized, yielding higher power density. Also important to the operation of PEFCs is the fact that Nafion and other such materials prevent the large scale crossover of entire fuel molecules; rather, the electrolyte layer permits only protons to migrate through to the cathode.[2]

The layers that are immediately bonded to the electrolyte are the electrodes. The electrodes are generally composed of carbon-backed layers doped with a catalyst. For direct hydrogen cells this catalyst is platinum (Pt) on both anode (hydrogen) and cathode (air) sides; for direct methanol cells this catalyst is a combination of platinum and ruthenium (Pt-Ru) on the fuel (methanol) side and pure platinum on the cathode side. At the anode (negative electrode), the catalyst facilitates the electro-oxidation of the hydrogen based fuel. On the cathode (positive electrode), the platinum doped carbon increases the rate of oxygen reduction and provides a site for the hydrogen nuclei to combine with oxygen ions to form water.

[2] In DMFCs, the phenomenon of methanol crossover has been observed where methanol fuel passes through the membrane and combusts with air on the cathode side of the cell. This is a significant limitation on the performance of such cells.

The outermost layers of the MEA are the gas diffusion layers (GDLs). The GDL actually serves three purposes: first, to promote the diffusion of reactant to the electrode and to promote diffusion of water away from the electrode; second, to provide mechanical strength to the MEA; third, to provide an electrical pathway for electrons. The GDL is constructed of a carbon-based material, usually in the form of a cloth or a thinner "paper." To prevent the collection of water in the GDL, it is impregnated with PTFE.

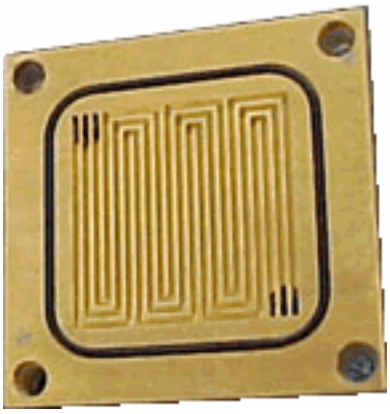

Figure 2.2: Photograph of serpentine flow channels on Lynntech endplate

(Courtesy of Lynntech Industries, www.lynntechindustries.com)

Reactant gas is delivered to the MEA via flow paths in the endplate structure. These paths are classically serpentine, though other flow field designs have been shown to yield superior performance.[3] The endplates are typically made of a material such as carbon or titanium. Current collectors may be incorporated into the flow channel plates or they may be separate parts of the endplate structure.

[3] Nguyen, et al. (1997) have shown the benefit of interdigitated flow fields

2.1.2 Fuel Options Associated with PEFCs

PEFCs can use a variety of hydrogen-based fuels. The most common of these fuels are hydrogen gas and liquid methanol. Though similar in structure, hydrogen fueled PEM cells and DMFCs offer substantially different power densities. This is due to a number of reasons, most notably the differing rates of reaction and the energy content of the two fuels. The higher rate of reaction of hydrogen allows for larger current densities; performance levels achieved with a DMFC using air are in the range of 180-250 mA/cm^2, while hydrogen fueled PEM cells are able to attain approximately five times this current density when operated at ambient pressure (Dept. of Energy, 2002).

Though hydrogen fueled cells provide much better performance, DMFCs have a distinct advantage in the energy content of the fuel when compared to the energy content of pure hydrogen gas. Methanol has an energy density of 4.42 kWh/L whereas hydrogen gas stored at 20 MPa has an energy density of only 0.53 kWh/L (www.hydrogen.org). This order of magnitude difference gives DMFCs a distinct advantage over hydrogen powered PEM cells as the designer of a hydrogen fuel cell system must allow for a large volume devoted to either the storage of pure hydrogen or to the reformation of a denser fuel source. Furthermore, methanol has the advantage of being readily available and compatible with the current infrastructure, whereas hydrogen is not easily produced or transported within today's means of delivery.

2.2 Electrochemical & Chemical Fundamentals

2.2.1 Basic Chemical Reactions in PEFCs

The basic reaction in any hydrogen fuel cell can be described as

$$2H_2 + O_2 \rightarrow 2H_2O \tag{2.1}$$

This net reaction is no different than the combustion of hydrogen to produce water and thermal energy. However, as discussed above, the electrolyte membrane prevents large-scale crossover of fuel, thus forcing the flow of electrical current through an external load (and thus the production of electrical energy) rather than allowing combustion to occur (and thus producing thermal energy). As the reaction described in equation 2.1 does not occur in one vigorous step as assumed of combustion, it is appropriate to decompose it into the actual anodic and cathodic reactions. For a PEM cell using pure hydrogen as its fuel, the resulting chemical reactions are

Table 2.1: Anode and cathode half-reactions for a hydrogen-fueled PEM fuel cell

Anode	$2H_2 \rightarrow 4H^+ + 4e^-$ (2.2)
Cathode	$O_2 + 4e^- + 4H^+ \rightarrow 2H_2O$ (2.3)

As mentioned above, the electrons produced in the reaction at the anode (equation 2.2) are first passed through the electronic load before reaching the cathode (refer to Figure 1.1).

When the fuel used is more chemically complex than pure hydrogen, the reactions at the anode and cathode will of course be more complex than described in equations 2.2 and 2.3. DMFCs, which use a methanol/water solution as fuel, are described by the following reactions:

Table 2.2: Anode and cathode half-reactions for a DMFC

Anode	$CH_3OH + H_2O \rightarrow 6H^+ + 6e^- + CO_2$ (2.4)
Cathode	$1.5O_2 + 6e^- + 6H^+ \rightarrow 3H_2O$ (2.5)

Here, the anode reaction again produces an electrical current and protons migrate through the MEA. However, unlike the case of directly using hydrogen as a fuel, carbon dioxide is produced on the anode and is expelled along with excess water.

2.2.2 Nernst Potential

The Nernst Potential of any electrochemical reaction gives the maximum difference in electric potential (voltage) between the two electrodes. This value is relevant to this discussion in that it is used in the computation of cell efficiency. From thermodynamics, the total change in chemical energy (enthalpy change) for a given

(isothermal) process is comprised of the change in Gibbs Free Energy, ΔG, and the change in the product of temperature and entropy, $T\Delta S$. That is,

$$\Delta H = \Delta G + T\Delta S \tag{2.6}$$

As the $T\Delta S$ term is thermodynamically unavailable for work, the total electrical work that may be done through any electrochemical source is given by

$$W_{electrical} = -\Delta G = nFE \tag{2.7}$$

where n is the moles of electrons transferred per mole of fuel reacted, F is Faraday's constant (96,487 coulombs/g-mole electron) and E is the ideal potential of the cell—the Nernst potential. At standard conditions (P = 1 atm), the following equation is true:

$$\Delta G^o = -nFE^o \tag{2.8}$$

Given a generic chemical reaction of the form

$$\alpha A + \beta B \rightarrow cC + \delta D \tag{2.9}$$

the Gibbs Free Energy of a reaction at any temperature and pressure can be related to the standard state by the equation

$$\Delta G = \Delta G^o + RT \ln \frac{f_c{}^c f_D{}^\delta}{f_A{}^\alpha f_B{}^\beta} \tag{2.10}$$

In equation 2.10, f_i is the fugacity of the substance. Fugacity is used in here in place of pressure to allow for deviation from the ideal gas law associated with liquid and solid reactants. Now substituting equation 2.8 into equation 2.10 and allowing for more products and reactants yields an expression for the Nernst Potential for any chemical reaction of ideal gases:

$$E = E^o + \frac{RT}{nF} \ln\left(\prod_i p_i^{\nu} \right) \tag{2.11}$$

In this equation, R is the ideal gas constant, T is the absolute temperature of the reaction, p_i is the partial pressure of the constituent, and ν is the stoichiometric coefficient of the constituent. For the fuel cells considered in this thesis, the Nernst Potentials are given as the following values (Larminie, 2000):

Table 2.3: Nernst Potential of selected fuels

Fuel	Nernst Potential (V)
H_2	1.23
CH_3OH	1.21

Using the Nernst Potential, the efficiency of a fuel cell operating at a particular voltage can be readily calculated. The cell efficiency, η, depends only on the enthalpy of formation (or latent heat) of the reaction and the cell potential. The enthalpy of formation

is taken as the Higher Heating Value (HHV) here because the water produced by the cells considered was in liquid form.

$$E_{HHV} = \frac{-\Delta h_f}{nF} \tag{2.12}$$

Using the Nernst Potential obtained from equation 2.12, the efficiency of the fuel cell can be computed using equation 2.13:

$$\eta = \frac{V_{act}}{E_{HHV}} \tag{2.13}$$

However, it should be noted that this assumes that all fuel and oxygen passed into the cell is reacted to produce electric power and liquid water. This is not the case; excess reactant is always required to maintain cell performance. The fuel utilization factor, u_f, is defined as

$$u_f = \frac{\dot{m}_{fuel,reacted}}{\dot{m}_{fuel,in}} \tag{2.14}$$

Combining equations 2.13 and 2.14 to obtain the overall fuel cell efficiency gives

$$\eta_{total} = u_f \frac{V_{act}}{E_{HHV}} \tag{2.15}$$

Without compensating for incomplete use of fuel, the maximum efficiency of a hydrogen fueled PEFC at standard conditions is 83%, while the maximum energy conversion efficiency of a DMFC at the same conditions is estimated to be in the range of 80-90%. However, actual operating efficiencies for both cells are much lower at this time, in the range of 40%.

2.2.3 Typical Voltage-Current Behavior and Polarization Losses

The Nernst Potential gives the ideal voltage at which a fuel cell will operate. However, in reality, there are certain irreversible losses associated with the operation of the fuel cell. These are divided into three types of electrochemical losses: activation polarization, ohmic polarization, and concentration polarization. Each will be described briefly.

Activation Polarization: Activation polarization is the result of activation energy required for the aforementioned chemical equations to occur. This is the dominant cause of loss at low current load. It is given by the semi-empirical Tafel Equation, which is

$$\eta_{act} = \frac{RT}{\alpha nF} \ln\left(\frac{i}{i_o}\right) \tag{2.16}$$

In the Tafel Equation, the coefficient α is the electron coefficient of the reaction at the electrode being addressed and i_o is the exchange current density (Dept. of Energy, 2002).

Ohmic Polarization: Ohmic polarization occurs as the result of internal resistance to the flow of current. Ohmic polarization can be reduced by increasing the conductivity of the electrolyte (e.g., by increasing the humidity of the membrane). Ohmic losses are most

prevalent at middle range current densities—beyond activation polarization dominance and before losses due to low reactant concentration largely influence response. The ohmic losses are given by

$$\Delta V_{ohm} = iR \tag{2.17}$$

where *R* is the internal resistance measured and *i* is the current load demanded from the cell.

Concentration Polarization: As the name implies, concentration polarization is the result of an insufficient supply (or concentration) of reactant. Faraday's Law shows that a given flow rate of reactant can produce a specific maximum current, i_L. In *The Fuel Cell Handbook, 7th Ed.*, it is shown that concentration losses can be expressed as

$$\eta_{conc} = \frac{RT}{nF} \ln\left(1 - \frac{i}{i_L}\right) \tag{2.18}$$

By combining these losses, the cell potential at a given current can be determined. The cell voltage is given as

$$V_{cell} = E_{cell} - \sum_{anode} \eta - \sum_{cathode} \eta - iR \tag{2.19}$$

where E_{cell} is the Nernst potential along the cell and the summations include the activation and concentration polarizations on each electrode. The shape of a typical V-J curve is shown in Figure 2.3, with each electrochemical loss highlighted.

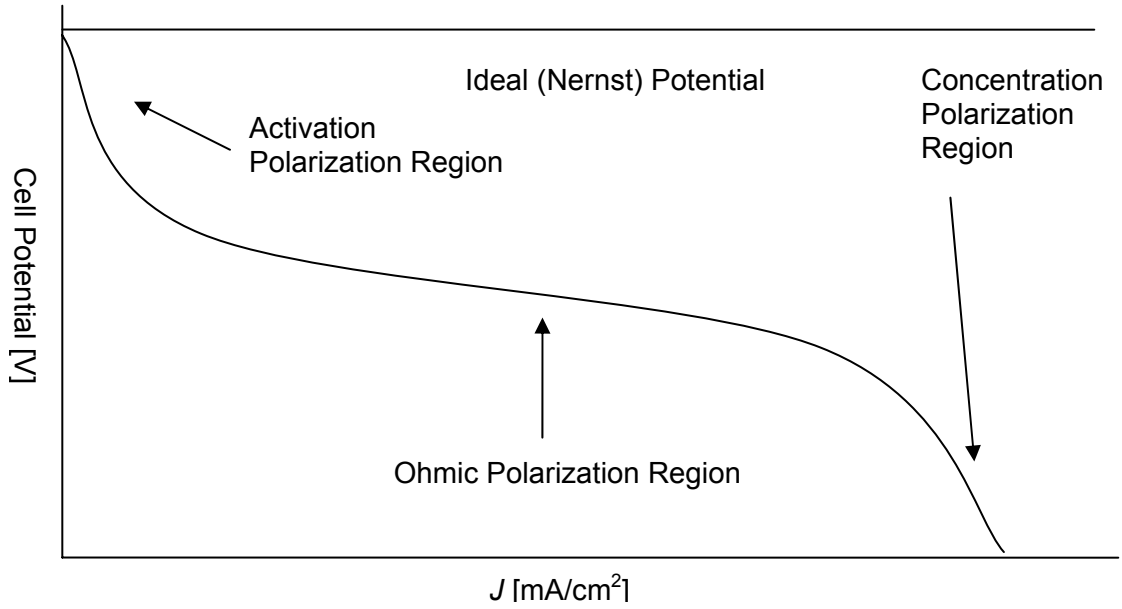

Figure 2.3: Typical V-J curve highlighting polarization losses

One may readily see that as the current load on the cell is increased the measured cell potential quickly falls away from the Nernst Potential due to the various losses discussed above. To maximize cell efficiency, a fuel cell must be operated at the highest possible voltage. However, maximizing cell potential also requires that the current load on the cell be minimal. As the electric power produced by the cell is the product of the cell potential and the current load on the cell, or

$$P = IV \tag{2.20}$$

the maximum power output of the cell is normally found to be in the region of maximum current load before concentration polarization occurs. Thus competing design criteria exist—a fuel cell system can be designed to operate in a region of high efficiency or it can be designed to operate in a region of high power density.

2.3 Basic Power Conditioning Subsystems

Fuel cells are not normally capable of operating as “stand alone” power sources; often they require a fuel reformation system and a power conditioning system, collectively known as the balance of plant, as discussed in the introduction chapter. This section will discuss the basic functions of power conditioning systems as it is relevant to the scope of this project.

2.3.1 Functions of a Power Conditioning Subsystem

A power conditioning subsystem has two essential functions: inverting stack voltage to produce AC voltage and regulating stack voltage. Other functions can be incorporated into the power electronics to improve system performance, but voltage inversion and regulation are essential at any level of sophistication. This thesis is concerned with the regulatory functions of power conditioning systems; therefore voltage inversion will be introduced on a basic level.

Devices powered by electricity often use AC electrical power; fuel cells produce DC power. To make this DC power usable in most applications, it is necessary to use inverters to convert to AC electricity. A simple single-phase inverter utilizes four switches, a configuration called an “H-bridge.” By varying the on-off cycles of each of the four switches, the steady current produced by the fuel cell is converted into an approximately sinusoidal current signal. Fuel cell systems that produce AC power of sufficient quality are capable of supplying power to electric grids for public consumption.

DC Voltage regulation is necessary for a variety of reasons. Switching devices can be used to step up or step down the voltage from a fuel cell stack to meet the power requirements of the electric load. More relevant to the work of this thesis, switches can

also be used to meet low frequency transient load demands on the cell stack. Using power electronics, so-called “buck” voltage regulation is achieved using a switch, drive circuit, a diode, and an inductor, as indicated in Figure 2.4(a). “Buck” voltage regulation is defined as reducing voltage in order to satisfy transient load demands; “boost” voltage regulation is the opposite process, whereby voltage is increased to meet transient demand. When the switch is on, current flows through the inductor and the load. The inductor produces a back EMF, making current gradually rise. The switch is then turned off. The stored energy in the inductor keeps the current flowing through the load, using the diode. The result of this on-off switching is a time varying current through the load and time varying voltage across the load. The variation of current with time is shown in Figure 2.4(b). The voltage signal can be smoothed using capacitors as necessary. Because each switch between on and off requires power to the circuit, this technique consumes more power to meet higher frequency transients. In all systems, the overall efficiency is better than 90%; in high voltage (>100 V), efficiencies of up to 98% are possible (Larminie, 2000, p. 254-5).

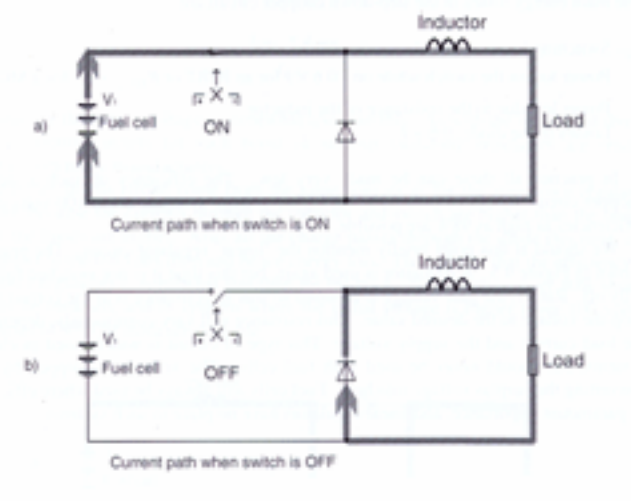

Figure 2.4(a): Circuit diagram showing the operation of a switch mode step down regulator (courtesy of Larminie, 2000, p. 255)

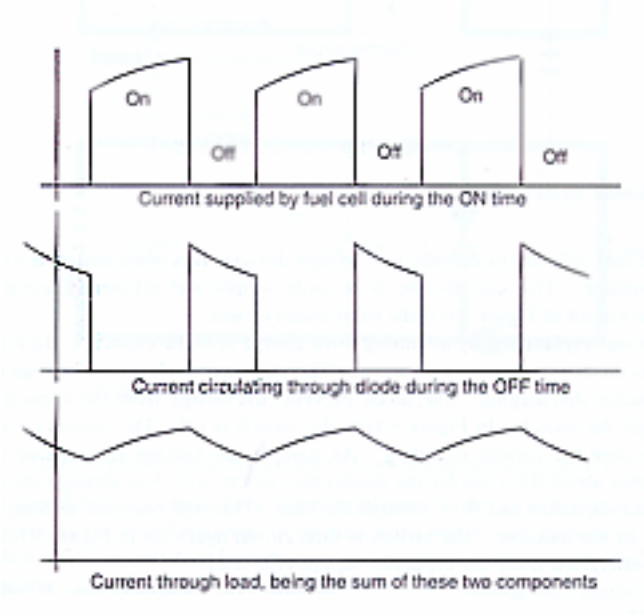

Figure 2.4(b): Currents in the step down switch mode regulator circuit (courtesy of Larminie, 2000, p. 255)

3. Review of Related Literature and Patents

To date, little variable flow experimental data is available through the literature. However, a review of pertinent publications presenting experimental results of the transient operation of PEFCs is given below.

Argyropoulos, *et al.* (1999) published the first relevant transient experimental work based on direct methanol fuel cell technology. Here, experimental results showing the effects of transient current loads on DMFCs were reported. Various loading scenarios are presented, including on-off load pulsing, ramped loads, and simulated drive cycles like those that would be encountered if a DMFC were to be used as the power source for a car. This article is relevant in that it establishes a significant basis for transient experimental work. In particular, the results presented in the work of Argyropoulos, *et al.* show that pulsed cell loading can temporarily enhance cell performance. The authors cite several factors contributing to the dynamic response of the DMFC; among them is the methanol crossover phenomenon. Argyropoulos, *et al.* observes that a pulsed current load results in a reduction of diffusion across the MEA, thus reducing, and potentially reversing methanol crossover and thereby improving cell performance.

A second relevant article focusing on direct methanol cells was written by Sundmacher, *et al.* (2001). This article presented ground-breaking experimental work showing the effects of pulsed flow on DMFC performance. The effect of transient methanol flow concentration is considered by the authors, including the effect of periodically discontinuing the methanol flow into the cell and pulsing the methanol concentration. These tests are similar to trials conducted as part of this thesis. Sundmacher, *et al.* show that when the supplied methanol flow is brought to zero, a temporary rise in cell potential is realized while the cell is subjected to a constant current

load. Furthermore, a pulsed methanol flow concentration is shown by the authors to produce a periodically repeating voltage signal under constant load. This test also shows a 10% increase in average cell power. As stated above, Sundmacher, *et al.* varied the methanol concentration to obtain these results. A constant liquid (water) flow rate was maintained while the concentration of methanol injected into the water inlet flow was pulsed. This is in contrast to the work performed for this thesis, where the flow rate of the methanol-water solution was varied with time while methanol concentration in the flow was held constant. The two flow control techniques are represented schematically in Figures 3.1(a) and (b).

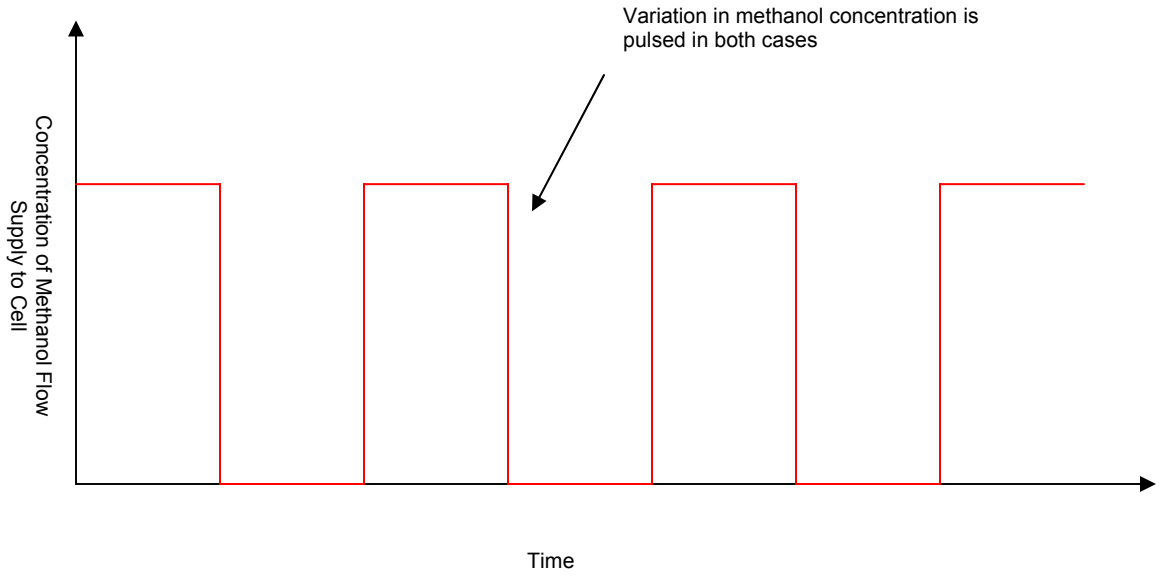

Figure 3.1(a): Variation in concentration of methanol supply to cell with time

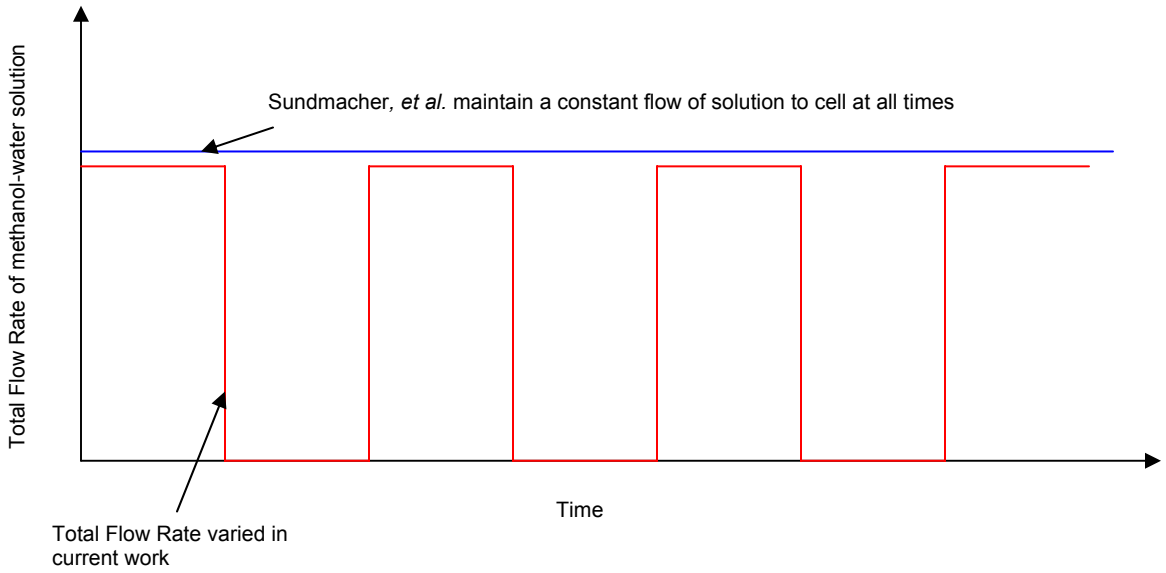

Figure 3.1(b): Variation in total flow rate of fuel solution to cell with time

In both the work presented here and the work conducted by Sundmacher, *et al.*, the concentration of methanol flowing to the cell is pulsed, as shown in Figure 3.1(a). However, as Figure 3.1(b) shows, the flow to the anode is held constant by Sundmacher, *et al.*, whereas the present results were obtained by varying the total flow past that anode. The different pulsing schemes give rise to possible differences in quantitative and qualitative results. A brief comparison of qualitative differences follows; quantitative results are presented in Chapter 6.

By temporarily turning off the flow of the 1 M methanol-water solution as was done in the present work, a small reservoir of fuel was effectively created in the flow channels of the DMFC. The cell exhausted the methanol in this pool before any change in methanol crossover was realized. In contrast, by maintaining a constant flow of water through the cell and varying the concentration of methanol between 1.5 M and

0 M, two important differences would likely arise. First, as water was continuously flowing through the cell, there was no reservoir affect as there was in this study; rather, excess methanol was purged by the feed water, making the minimization of methanol crossover occur more quickly. Similarly, this resulted in quicker decay in cell potential after peak voltage was realized. Furthermore, because the maximum concentration of methanol was 1.5 M, more methanol crossover occurred during periods when the methanol flow was on resulting in a larger improvement in cell performance was realized when methanol flow was turned off.

A significant benefit of pulsing the flow rate instead of varying fuel concentration in the flow is the potential for improved fuel efficiency. The scheme employed by Sundmacher, *et al.,* removes excess methanol from the anode flow channels whereas the current method allows for excess methanol to be electro-oxidized by the cell. Thus an improvement in single-pass fuel utilization is realized by pulsing the fuel flow rate while maintaining constant methanol concentration. Increasing single-pass fuel utilization introduces the possibility of further improving cell performance by eliminating the need for fuel recirculation pumps, which introduce parasitic losses to the system.

Scott, *et al.* (1997) published significant work modeling the steady state performance of DMFCs. Of particular importance is the group's quantification of methanol diffusion through a membrane-electrode assembly during steady state operation. This equation introduced by Scott, *et al.* identifies three major factors that contribute to the phenomenon of methanol crossover: the methanol concentration gradient across the MEA, pressure difference between the anode and cathode, and electro-osmotic drag of methanol through the MEA. Electro-osmotic drag occurs naturally and is proportional to the current load on the cell; as positively charged ions migrate from the anode to the cathode, a small number of methanol molecules are "dragged" across as well. As will be shown in Chapter 6, the steady state equation

introduced by Scott, et al. that quantifies methanol crossover is readily adapted to provide both qualitative insight into the potential for dynamic DMFC operation and quantitative values for the maximum change in methanol crossover that could be realized via dynamic operation.

Patent number 6,096,048, held by Ballard Power Systems and dated August 1, 2000, concerns a method and apparatus for operating a fuel cell with temporary, periodic fuel starvation at the anode. The claims of the patent extend this technique to general solid polymer-electrolyte fuel cells achieving the desired fuel starvation through a number of procedures, including diluting the fuel stream (similar to the method used by Sundmacher, *et al*.) and simply turning off all fuel flow (similar to the present work). Further claims of the patent extend to implementation of pulsed fuel flow incorporating a feedback control system that controls fuel flow in response to a cell operating parameter and also to using pulsed cell loading to realize an increase in cell potential. Like the work of Sundmacher, *et al*., and the work presented here, the Ballard patent shows that by temporarily reducing fuel flow to the cell, an increase in cell potential is observed. The crucial difference between this patent and the present work is the primary phenomenon cited that results in the observed rise in voltage. Ballard claims that the rise in cell potential is achieved as a result of removal of electrocatalyst poisons from the anode electrocatalyst. While this may be an ancillary benefit realized over long periods of cell operation, the present work will show that the immediate rise in cell potential is primarily the result of reduced methanol crossover. As methanol crossover results in detrimental effects at the cell *cathode*, the relevance of this difference is immediately obvious.

Pukrushpan, *et al*. (2002) developed an experimentally based model to describe the performance of their air flow based “super-charger” for a hydrogen fueled PEM stack. The super-charger was designed to quickly increase air flow into the fuel cell

stack in order to meet increases in load demand. This concept is similar to the work conducted in this thesis in that transient oxidant flow was used to modulate cell power output. While Pukrushpan, *et al.* focused on the effects of a sudden increase in air supplied to the cell, the effects of both increasing and decreasing oxidant flow rates are reported here. Pukrushpan, *et al.* show that the control loop proposed to modulate air flow actually results in a net power output loss; the extra power required to sufficiently increase the air flow into the stack is greater than the increase in cell power produced.

Nguyen, *et al*. (2002) discusses the use of active control of oxidant flow in a PEM fuel cell. This article shows that by selectively "dead-ending" cathode exhaust ports in a PEM stack for short periods of time, substantial performance improvement is realized due to increased water removal from the cathode and higher oxygen utilization. Dead-end operation involves blocking the exhaust port of a cell or a stack of cells. It is a technique often employed on the anode side of the cell when pure hydrogen is used as fuel. The result of dead-end operation is an improvement in fuel efficiency. Similarly, in the paper now discussed, it is shown that by using the dead-ending technique the oxidant utilization is substantially increased. Experimental data showed that stable cell performance is achieved with only 10% excess oxidant supplied (~91% oxygen utilization). This selective dead-ending process is patented as US patent number 6,503,651. The work of Nguyen, *et al.* is similar to the research discussed in this thesis in that oxidant flow is actively controlled through the use of solenoid valves.

4. Experimental System

The work performed for this thesis involved the development of a novel experimental system capable of transient fuel cell operation. In particular, transient reactant supply rates were considered. The experimental setup used to perform this study of transient PEFC operation, the error associated with this system, and the manner in which the system was developed will be discussed in this chapter.

4.1 Experimental Setup

Due to the nature of the project, a specialized control system was developed capable of accurately controlling and measuring the transient performance of the fuel cell. The major components of the system were a DC Electronic Load, mass flow meters coupled with proportional solenoid valves, temperature controllers, an oscilloscope to capture data at a high sampling frequency, and the fuel cell. Figure 4.1 shows a schematic of the experimental setup for which a LabView program was written to control the system.

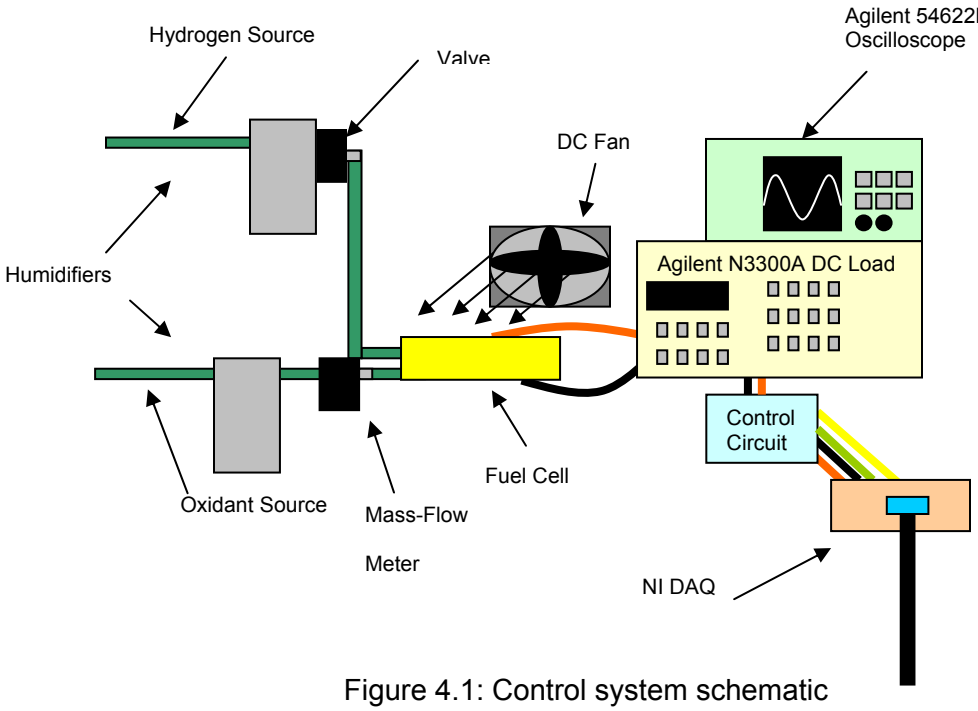

Figure 4.1: Control system schematic

The DC Load was purchased from Agilent Technologies, model number N3300A. The load module used in this experiment was model number N3302A. The system was operated under galvanostatic conditions. When operating in this mode, the DC Load held current constant to within ±0.1% of the desired value. The measured voltage is accurate to within ±0.05% of the actual cell voltage. The load was controlled through an Ethernet-based GPIB connection with the control software.

The mass flow meters used in this project were from the Omega Engineering FMA-1600 series. These meters simultaneously reported the flow rate on both digital and analog signal lines. The computer recorded the digital signals using a data acquisition card; the 0-5 V linear analog signal was used in conjunction with the oscilloscope. Flow rates were measured accurately within ±1% full scale for both steady and pulsed flow scenarios. This is equivalent to an accuracy of ±10 sccm of hydrogen

flow and ±50 sccm air flow for the PEM fuel cell and an accuracy of ±0.01 sccm of water-methanol solution and ±2 sccm air flow for the DMFC. The error associated with air flow on the PEM differs from the air flow error on the DMFC because substantially greater (10x) air flow rates were required for the PEM cell. Thus, a larger capacity flow meter was required, resulting in a larger absolute measurement error. The meters have a response time of 10 ms, which allowed for an assumed accuracy in measure of flow oscillation up to 25 Hz. The frequency limit associated with the 10 ms response time is a result of the Nyquist Criterion, which states that it is necessary to sample a waveform at a minimum of twice the highest signal frequency observed in order to avoid aliasing of the signal (http://mathworld.wolfram.com). With a response time of 10 ms, the flow meters are capable of sampling at 50 Hz; thus the maximum (accurately) measurable flow rate frequency is 25 Hz.

To verify the accuracy of these mass flow meters, a differential pressure sensor produced by SenSym ICT was used. The sensor measured differential pressures from zero to four inches of water (0-0.01 atm) on a linear voltage scale at frequencies up to 60 Hz. This sensor was especially useful in collecting data for the transfer functions that were developed as part of the project. The pressure differential was measured between the cell inlet or outlet and ambient.

Proportional solenoid valves were used in conjunction with the mass flow meters to regulate the flow rate of reactant into the cells. The Pneutronics Division of Parker Hannifin Corporation produced these valves, model numbers E-20568 (for methanol-water solution) and E-20336 (for gaseous reactants). The valves operated on a 0-5 VDC input signal, which was controlled by the data acquisition card. Measurements were repeatable to within ±0.5% and pulsed flow accurately up to 20 Hz. As the frequency of oscillation was increased, the maximum amplitude response of the valve decreased

substantially. At frequencies below 20 Hz, the response of the valve was sufficient to reliably modulate reactant flow over the required amplitude range. However, beyond 20 Hz, the proportional valves did not allow for the 50% amplitude modulation needed to acquire data consistent with that acquired at lower frequencies.

Temperature control of the direct hydrogen PEM fuel cell was achieved using a MicrOmega CN7700 Series temperature controller and a DC fan. The controller powered four 120 VAC cartridge heaters that were inserted into the fuel cell. The PEM fuel cell manufacturer, Lynntech Industries, recommended this thermal control scheme. The temperature controller measured cell temperature to within 0.5°C with a response time of 0.7 s. The temperature controller supplied up to 192 W to the cell through the heating rods distributed symmetrically about the cell, as dictated by the computer control system, again through the data acquisition card. The temperature of the DMFC was not controlled; however, after several hours of normal cell operation, the DMFC temperature was regularly found to be approximately 30°C. Room temperature operation of the DMFC was allowed for several reasons, most importantly that as potential small scale power sources for laptops and mobile phones, DMFCs would ideally be used as close to room temperature as possible. Furthermore, due to the small size (4 cm^2 electro-active area) of the DMFCs used, no simple, economical means of heating the cells was available.

An Agilent oscilloscope, model number 54622D, was used to capture pulsed flow data at a sufficient sampling rate. The oscilloscope was configured to capture data up to 1 kHz. The DC measurements made by the scope were accurate to within ±10 mV and the AC noise in the signal was ±1 mV, making all measurements accurate to within ±11 mV of the actual value. In order to report and record the most accurate voltage measurements possible, the voltage signals captured by the oscilloscope were

compared to the values recorded by the data acquisition system. Because the data acquisition card sampled within a smaller error range, data was recorded through it whenever possible (e.g. for sub-hertz flow oscillations); at higher frequencies, the maximum, minimum, and average voltage readings from the DAQ and the oscilloscope were compared. Normally, the two measurements agreed well; if the readings differed by more than 5 mV, the test was repeated until reliable measurements were obtained. Communication with the oscilloscope was established through a GPIB connection. The oscilloscope was generally used to simultaneously capture the cell voltage signal and the analog signal from the mass flow meter measuring pulsed flow. The oscilloscope was also used to measure the voltage signal from the differential pressure sensor.

Reactant gases were supplied at 20 psia from the lab supply gases that are part of the fuel cells lab infrastructure. The reactant gases were humidified using deionized water prior to flowing into the PEM cell. When either gas flow was pulsed, the gas passed through a pressurized bubbler prior to flowing through the mass flow meter and then the proportional valve before ultimately passing into the fuel cell. This arrangement allowed for the optimal control of the flow rate waveform that passed to the cell. For the DMFC, air was again supplied at 20 psia from the lab supply. However, in this case the air was not humidified. A 1 M methanol-water solution was supplied to the DMFC using a pressurized tank, which held up to 40 L of solution. The tank was pressurized to 18 psia using ultra-high purity Nitrogen, again from the lab's gas supply system. As with the gas supply lines, the solution was passed through the mass flow meter then through the proportional valve before entering into the fuel cell.

Lynntech Industries supplied the PEM fuel cell used in this project. A detailed schematic of the cell is shown in Figure 4.2. The cell consisted of two titanium end plates coated with gold, which served as current collectors. The rationale for using titanium in the endplates is to greatly reduce the bulk resistivity of the endplate (as compared to

using graphite or stainless steel). The gold coating helps to avoid oxidation of the titanium and, therefore, corrosion of the MEA. Additionally, each endplate has serpentine flow channels that make turns and multiple passes along the electro-active area; the flow paths covered an area of 25 cm^2. A Teflon gasket on the anode side of the cell and a rubber O-ring on the cathode side of the cell serve to prevent reactant leaks out of the flow paths. The cell is bolted together with ⅜" x 2" hex screws and nuts. The membrane-electrode assembly (MEA) was also supplied by Lynntech Industries. Each MEA used in this project had an electro-active area of 25 cm^2. The membranes were made using Nafion® 112 with 0.5 mg/cm^2 platinum loading on each side. The gas diffusion layers consist of a carbon cloth based material, ELAT.

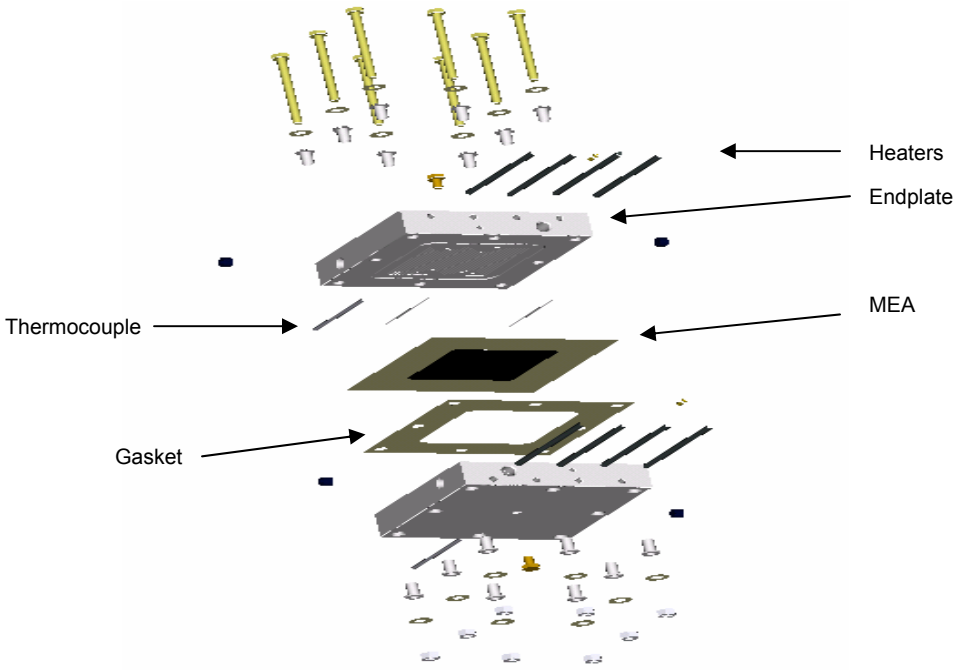

Figure 4.2: 25 cm^2 Lynntech PEM fuel cell schematic, exploded view

Motorola donated the DMFCs used in this project to Georgia Tech Research Institute. The MEAs installed in these cells used Nafion 117 with 4 mg/cm^2 Pt loading on the cathode and 4 mg/cm^2 Pt-Ru loading on the anode. Endplates were made from Dupont 951 ceramic green tape with serpentine flow fields and gold current collectors. Reactant was supplied to the cell via 5/64" diameter inlet ports and exhausted through ports of the same size. The cell was operated in accordance with the recommendations of Motorola. These recommendations include operating the cell in a vertical orientation with the fuel inlet tube attached to the upper anode port and the fuel outlet attached to the lower anode port. This allowed for gravity to assist in the flow of the methanol-water solution through the flow channels on the anode. Motorola further recommended that dry air be fed into the cell's cathode at the lower port and humid air exhausted from the upper cathode port. This allowed for better removal of water vapor from the cell. The flow rates recommended by Motorola were 0.25 sccm 1 M methanol-water solution flow rate and 60 sccm air flow rate, for maximum power conditions (Correspondence with A. Fischer, Motorola). Figures 4.3(a) – (c) schematically represent the construction of the DMFCs.

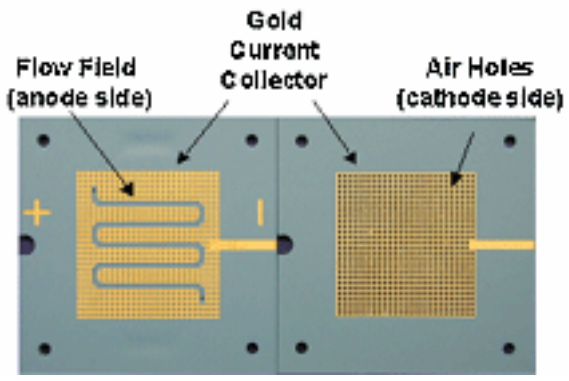

Figure 4.3(a): Motorola DMFC flow fields, current collectors, and endplates

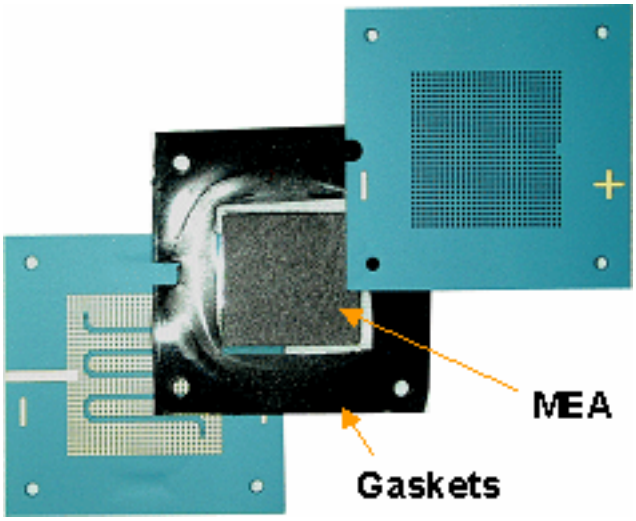

Figure 4.3(b): Exploded view of DMFC highlighting gasket and MEA

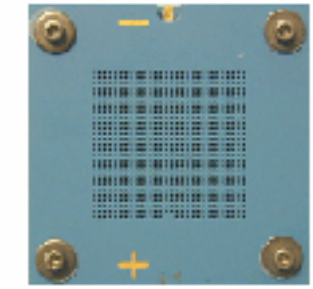

Figure 4.3(c): Assembled DMFC (all DMFC schematics courtesy of Motorola)

4.2 Control Program

The system was controlled through a LabView program developed specifically for this project. It managed all inputs to the cell, including flow rates, cell current (or voltage), cell temperature, and input flow waveform, if desired. The program also recorded the corresponding measured values, in addition to recording data captured by the oscilloscope during periods when the flow rate was pulsed. The methods employed to control cell temperature, electronic load, and reactant flow rates will be presented here; data collection techniques also will be discussed. Furthermore, the novel capabilities of this program will be covered.

Communication with the assorted control and measurement devices was established through a National Instruments data acquisition card (Model # NI AT-MIO-16XE-50), an Ethernet-based GPIB device, and serial ports, as discussed above.

The MicrOmega temperature controllers, as previously stated, controlled the cell temperature. As the temperature controllers themselves were capable of PID (proportional-integral-derivative) control, the LabView code needed only to input the temperature set point to the controllers. The PID constants were determined iteratively and input directly into the temperature controllers. The temperature controller was set to (continuously) stream data to the computer. The LabView code recorded this data into the output file once per iteration through the code.

The control program was capable of controlling the cell both potentio- (prescribed cell potential) and galvano- (prescribed cell current) statically. As necessary, the program updated the load set point (either current or voltage) and recorded values of both the control and dependent variables once during every iteration through the main while loop. For the vast majority of cases, galvanostatic control was used; therefore, current was normally set to the desired value and both the actual current demanded of

the cell and the resulting cell potential (voltage) were recorded. The control program communicated with the load using simple SCPI command lines to both write and read data. The write string was automatically formatted by the program based on the user input set point. The reply string from the DC Load was interpreted within the program before being recorded to the output data file.

Reactant supply in constant flow rate mode was achieved using a closed loop PID scheme. Flow rates were first calibrated against the DC voltage applied to proportional valves. Based on this calibration and the flow rate input by the user, an initial “guess” voltage was sent to valves. This initial voltage was simply the result of linear interpolation of the calibration data. The control program then compared the measured flow rate against the desired flow rate and adjusted the voltage sent to the valve by the DAQ card accordingly. Adjustments to the output voltage were made based upon the proportional and integral constants in the PID loop; derivative control was not necessary to obtain satisfactory control. The control constants were adjusted to attain quick convergence on the set point while avoiding substantial “wind up” error. Wind up error is associated with an integral control constant that is too large. Wind up error is characterized by large oscillations about the desired value.

The most distinct feature of the control program is the ability to generate transient flow rates based upon arbitrary input waveform. In theory, the system is able to realize any desired flow pattern. This was achieved by recording the desired waveform into a text file. This file was then read by the control program and loaded into the DAQ card’s onboard memory, where the pattern was repeated until it was removed from memory by the control program. The user set the frequency of repetition.

Another distinct feature of the code is the ability to automate experiments. Rather than manually changing control values, a script could be written that would automatically set the control variables to the desired values for the user determined time

period. The automation of the control program was exceptionally useful for the following reasons: it allowed for consistent and repeatable experimental conditions, it organized output data files in a user-friendly manner, and it allowed for continuous data collection over long periods of time.

Data was automatically recorded by the program into a comma separated value (*.csv) file at the rate specified by the user. Due to the amount of serial communication required for each iteration through the control code, each loop took roughly 0.3 seconds. Thus, the maximum sampling frequency of the control program was 3 Hz. Data recorded into the output file by the program included cell voltage, current, reactant flow rates, cell temperature, and water generation rate. As previously mentioned, the high sampling frequency of the oscilloscope allowed for the collection of high frequency oscillations in flow rate and in cell potential as necessary. Data obtained from the oscilloscope was recorded as a waveform file (*.wfm), which was accessible through MS Excel.

4.3 Experimental Procedure

4.3.1 Steady State Operation

For both steady and pulsed flow studies in the given thesis scope, the important parameters for maintaining reliable operating conditions were reactant supply rates and electronic load upon the cell, as well as cell humidification level and cell temperature in the case of the direct hydrogen PEM cell. As described above, the user controls each of these parameters either directly or indirectly. Values for each parameter were sought that provided consistent, reliable cell performance.

As discussed in Chapter 2, fuel utilization, u_f, is a non-dimensional parameter that indicates the level of excess reactant supplied. Fuel utilization is equal to the ratio of the actual current generation/demand to the theoretical current producible by the fuel supply (per Faraday's Law). Standard values of u_f range from 70-90%. For this study, u_f was set at 83.3%.

The inverse of fuel utilization is known as NOS, or number of stoichs. For the purposes of this study, it was often more intuitive to express flows in terms of NOS. To adhere to prevalent terminology, results are reported here in terms of fuel utilization, except in cases where insight is gained by expressing flow rates in terms of NOS. The standard fuel utilization incorporated corresponded to $NOS(H_2) = 1.2$ for the Lynntech PEM cell.

When operating the Lynntech PEM cell, NOS values were held constant as current load changed. That is, reactant flow rate was increased proportionally as current demand was increased. In the case of the Motorola DMFCs, flow rate was held constant regardless of current load on the cell. This is procedure recommended by Motorola.

It is generally unsafe to operate a fuel cell with a reactant NOS less than one. This is based on the definition of NOS, the ratio of current ideally produced by a flow rate of reactant to the current load demanded of the cell. If NOS is less than one, this means that more current is demanded than the reactant supply will allow for. The result is threatened cell performance and reliability. An example is potentially dangerous, visible holes (from localized burnout at low operating voltages) within the MEA that could allow for hydrogen and oxygen to come into direct contact and result in combustion.

It was determined that the PEM fuel cell technology used in this study is particularly sensitive to NOS_{air}. This is because of the substantially larger volumetric airflows that are required to produce a given current in comparison to the fuel flow rate to produce the same current. Practically, the airflow must be five times larger than the fuel flow to achieve the same maximum current. This substantially greater flow rate allows for a large amount of water to be removed from the cell with the exhaust air, thus affecting the MEA's humidification level, and hence its performance. Cell performance has been measured at NOS_{air} levels ranging from 2 to 4, and it was determined that $NOS_{air} = 2$ provided the most latitude in the AFC portion of the project while still maintaining consistent cell performance.

Other parameters have been sought that provided repeatable PEM cell performance. The temperature value that provides the most reliable cell performance is 50°C. Below this temperature, the power density of the cell is exceptionally low due to greater electrochemical losses, whereas at higher temperatures the cell suffers substantial dry out, which also leads to exceptionally low power density.

In order to ensure that the PEM MEA remained sufficiently hydrated to yield reliable results, the MEA was often soaked in deionized water. This was done until the MEA was visibly saturated with water. The MEA was then reinstalled into the cell and the experiment begun immediately thereafter. This procedure increased the

repeatability of the cell's performance substantially. Over-saturation was not found to be an issue.

Comparatively speaking, the operating procedure for the DMFCs used in this study is significantly simpler. As previously mentioned, Motorola specified that constant flow rates be used and the cell be operated at room temperature. The only procedural requirement given by Motorola was to vent all methanol from the cell when the cell was not in use. Ensuring no methanol was stored in the cell's flow paths prevented methanol from diffusing through the MEA and crossing over to the cathode.

Methanol crossover is one of the primary performance limitations of direct methanol cells. Methanol crossover occurs when methanol from the anode of the cell migrates through the methanol-permeable membrane and to the cathode. At the cathode, the methanol is able to react chemically with air. That is, the methanol can burn. This not only reduces the amount of oxygen to the cathode to drive electro-oxidation of methanol, but the combustion of methanol can have a harmful effect on the membrane and the rest of the cell's structure.

4.3.2 Active Flow Control Operation

As was described above, the control system was developed with the unique ability to introduce periodically repeating reactant flow rates to the respective fuel cells. To ensure high reliability of the input flow signal, a standardized procedure was necessary.

Waveforms of desired shape and amplitude were produced within MS Excel and the frequency of oscillation was controlled by the LabView code. This was achieved by loading the waveform into the DAQ board and repeating the waveform at the frequency entered into the LabView code. For the sake of repeatability, it was vital to ensure that

each waveform input, and thus the resulting reactant flow rate, had the correct amplitude and frequency. Accurate waveform data was acquired through the use of the oscilloscope. The measured minimum and maximum flow rates were observed on the oscilloscope and recorded. An appropriate waveform was developed and tested to ensure that it met the desired minimum and maximum flow rates. An iterative procedure was followed until the necessary flow range was achieved. The need to use such an approach was due to hysteresis effects encountered with the control of the proportional valve.

5. Results of Direct Hydrogen PEM Study

5.1 Steady State Characterization

The performance of the PEM fuel cell was characterized over a range of NOS_{air} values under steady flow conditions. Control variables such as temperature and fuel utilization were held constant; for these tests, temperature was set to 50°C and fuel utilization set to 0.833. Characteristic V-J and power density curves can be seen in Figure 5.1. Cell performance was studied over the range of NOS_{air} values from 1.5 to 4; the results shown in Figure 5.1 depict data at NOS_{air} = 1.5, 3, and 4. These values were used as they spanned the range of test conditions used in the AFC portion of the study.

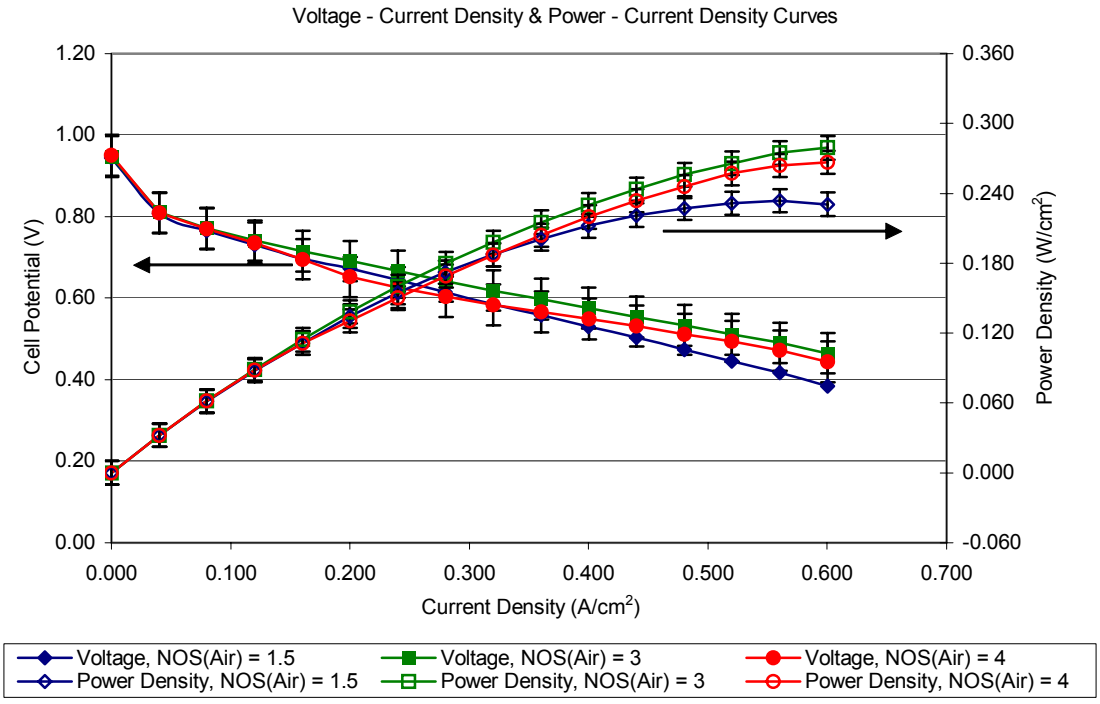

Figure 5.1: Steady state characterization of PEM cell performance

Figure 5.1 reveals that optimum performance was achieved when air was supplied at three times the theoretically necessary rate. At the low air flow rate of NOS_{air} = 1.5, insufficient oxygen was supplied to support electro-reduction, and thus the power output of the cell was adversely affected. Furthermore, at this low flow rate, insufficient product water may have been removed from the cathode. In contrast, at the higher air flow rate associated with NOS_{air} = 4, the assumption is that too much water was removed from the cathode, thus dehydrating the membrane. As discussed in Chapter 2, the hydration level of polymer electrolyte membranes plays a major role in the performance of PEFCs. If the membrane is either over- or under- hydrated, cell performance (in terms of power output) will suffer; Figure 5.1 exemplifies this fact. The results of these tests provided a basis to determine if the cell was performing at a reasonable level during AFC trials.

5.2 Results of Active Flow Control Study

In the consideration of Active Flow Control (AFC) on the PEM fuel cell, the effects of varying the following parameters were studied: frequency of oscillation, current load on the cell, amplitude of flow oscillation, and level of excess reactant supply (i.e. NOS). The effects of pulsing both air and hydrogen flow rates were studied.

5.2.1 Consideration of Pulsed Air Flow

The parametric study of the effects of pulsed air flow revealed several trends; the primary trend being the ability to regulate cell voltage, and thus power via modulation of air flow rate. Other trends identified indicate the effects of the frequency and amplitude of oscillation as well as the effect of pulsing air flow about different time-averaged NOS levels.

The primary variable considered was the frequency of oscillation. The response of cell voltage to transient air flow at 1 Hz and 6 Hz is shown in Figures 5.2 and 5.3, respectively. The test conditions for the data in Figures 5.2 and 5.3 are I = 10 A, u_f = 0.833, 25% input oscillation in air flow amplitude, and T = 50°C. It is notable that over this range of input frequencies, the input sine wave air flow pattern produces a low-distortion voltage response thus confirming the basic hypothesis of this study, that modulation of reactant flow rate can have a substantial effect on cell potential. Also of note is the diminished amplitude of oscillation in cell potential at the higher frequency. This trend is made clearer in Figure 5.4, which shows the amplitude of voltage oscillation over the range of frequencies studied for several current loads.

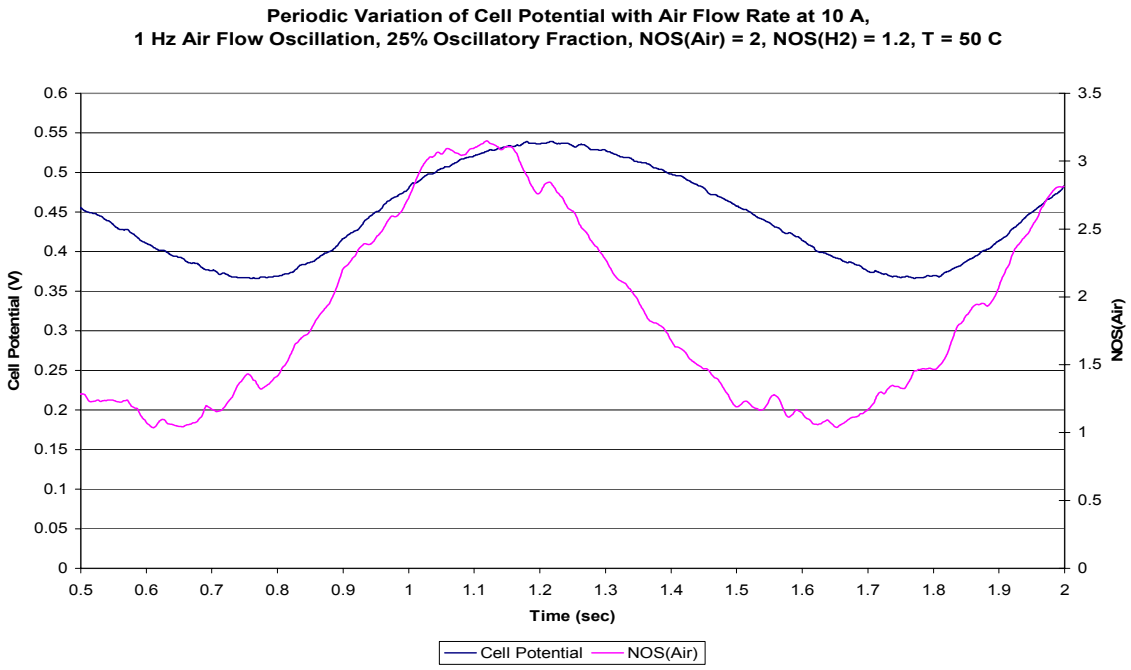

Figure 5.2: Variation in cell potential with 1 Hz pulsed air flow

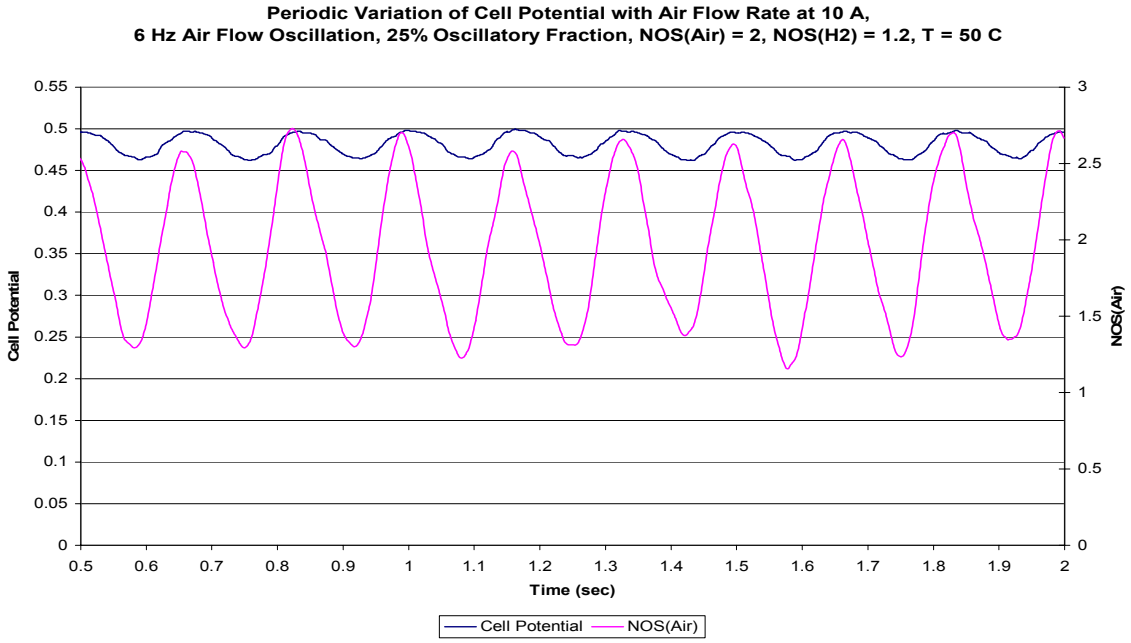

Figure 5.3: Variation in cell potential with 6 Hz pulsed air flow

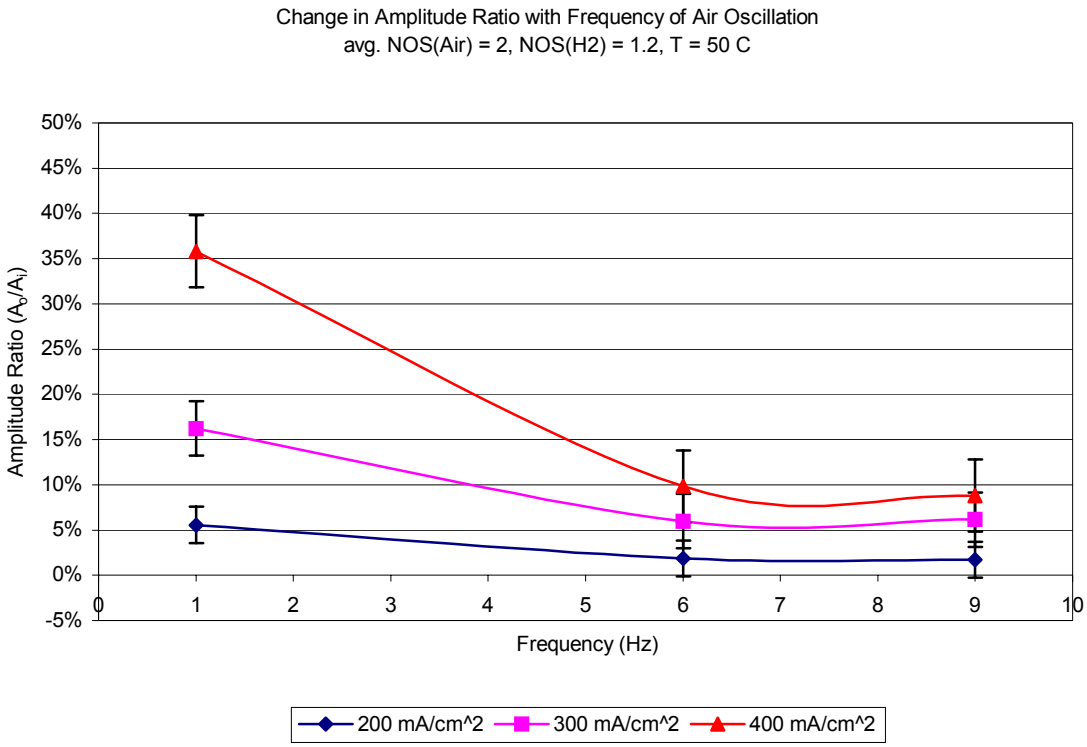

Figure 5.4: Change in voltage oscillation with frequency of air oscillation at 200 mA/cm^2, 300 mA/cm^2, and 400 mA/cm^2 (5, 7.5, and 10 A); nominal air oscillatory fraction = 25%

Figure 5.4 clearly displays two trends that have been identified through the course of this investigation. First, the oscillation in cell potential that occurs as a result of reactant pulsation decreases as the frequency of reactant oscillation is increased. This is understood to be true because at higher frequencies of oscillation, the periodicity of modulated reactant supply is too small for substantial cell response (i.e., the variable stimuli of lower supply rate is offset by higher supply rates in too rapid a manner). At low frequency, when the periods of low and high flow are considerably longer, the relative abundance or scarcity of reactant has a substantial affect on cell potential. The second

trend revealed in Figure 5.4 is that an increase in current load promotes an increase in voltage oscillation. Referencing the discussion of Faraday's Law in Chapter 2, higher current load requires an increased reactant supply. Considered another way, a fixed supply of reactant will be used more quickly at higher current load. In the galvanostatic approach used, the result of increased current load is greater oscillation in cell potential at fixed NOS because the reactant supply is exhausted more quickly. This is true in spite of the fact that the relative level of reactant supply is held constant (i.e. NOS is constant) over the range of current densities studied. It is hypothesized that the greater amplitude ratio at higher current densities is realized because of reduced reactant presence in the respective electrodes, also referred to as a reactant capacitive effect, due to the need for higher mass transport from the free stream to the electroactive sites. This results in a smaller concentration gradient within the electrode, which in turn results in greater sensitivity to fluctuations in reactant supply rate. A second possible explanation for the greater amplitude ratios measured at higher current densities is related to membrane humidity. The higher air flow rates associated with elevated current densities have a substantial effect on membrane humidity, which is believed to be a key factor in modulation of cell voltage via active flow control.

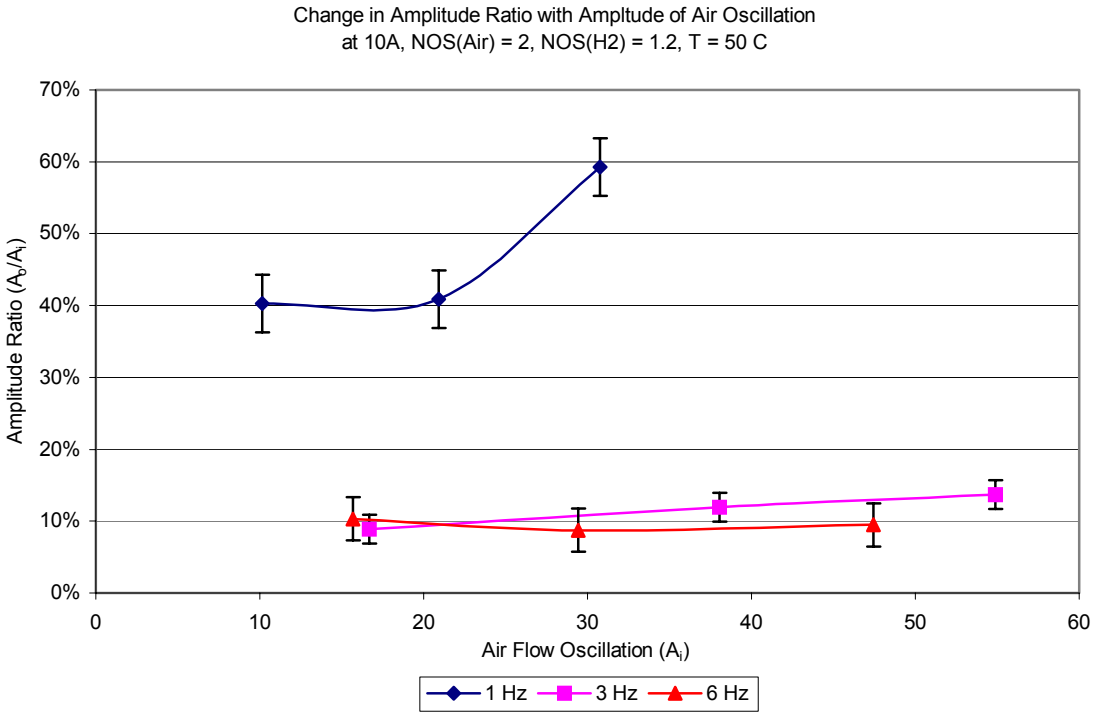

Figure 5.5: Change in voltage oscillation with amplitude of air oscillation at 1 Hz, 3 Hz, and 9 Hz

The next parameter varied in the study was the amplitude of flow oscillation. These results are presented in Figure 5.5, which shows the voltage oscillation at a 10 A current load (400 mA/cm^2 current density) at 1 Hz, 3 Hz, and 6 Hz, with NOS_{air} = 2, u_f = 0.833, and cell temperature set to 50°C. The data here demonstrate that by amplifying the oscillation of air flow, thus amplifying the relative abundance or scarcity of reactant, the corresponding voltage oscillation is increased. Though not practically possible, if the flow oscillations had been taken to extremes of 0% and 100% oscillation[4], no oscillation in flow would be observed when the reactant flow was held constant (0%

[4] The oscillatory fraction or percent oscillation is defined as the difference between the maximum (or minimum) change from the average NOS divided by the average NOS. By way of example, with an average NOS of 2, 100% oscillation means that a maximum flow rate equivalent to NOS = 4 and a minimum flow rate of NOS = 0 are achieved.

oscillation) and a large oscillation in cell potential would be produced by a full (100%) oscillation in flow. Figure 5.5 also further supports the trend that increased frequency of reactant oscillation yields a decreased oscillation in cell potential. The oscillation in cell potential at 1 Hz is roughly four times greater than the oscillation observed at 3 Hz. This indicates that voltage regulation via reactant flow modulation is maximized at sub-hertz frequencies.

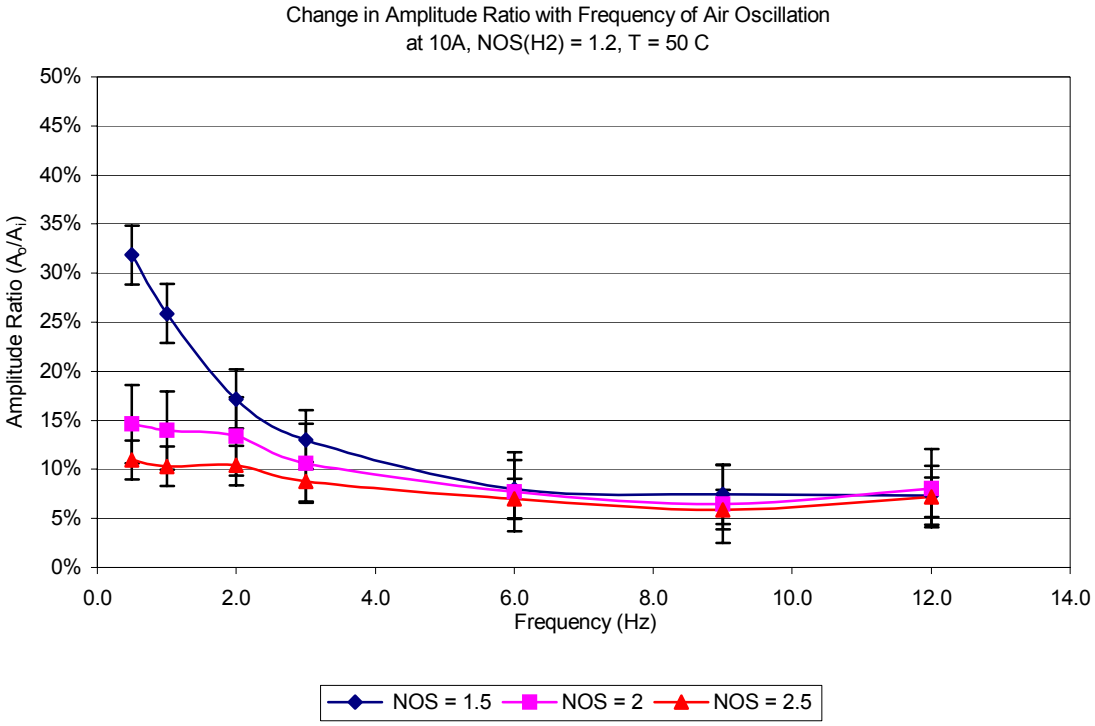

Figure 5.6: Effect of average level of reactant supply on change in voltage oscillation with frequency of air oscillation at NOS_{air} = 1.5, 2, 2.5

The final parameter studied to determine its effect on voltage oscillation was the level of excess air flow, NOS_{air}. Figure 5.6 depicts the results of this portion of the study, where NOS_{air} was varied from 1.5 to 2.5 with a 10 A current load (400 mA/cm^2 current density) with u_f = 0.833 and T = 50°C. Data was collected at 0.5, 1, 2, 3, 6, 9, and 12 Hz. Figure 5.6 shows that by minimizing the level of excess reactant an increased oscillation in cell potential is realized. This is driven by the fact that at reduced average NOS, any change from that average value will have an amplified effect on the overall cell performance. Conversely, at a high average NOS value with the same percentage change in flow rate, the cell's performance will be less affected by the changes in flow rate. This is another manifestation of the reactant capacitance effect discussed above. A fixed percent oscillation in flow rate will have less effect on cell potential as time-averaged NOS is increased because of reactant capacitance because a lesser concentration gradient would be observed with pulsed reactant flow at a higher NOS.

A side effect of pulsing air flow is a decrease in cell power. This trend is shown in Figure 5.7, which shows the change in cell power from steady flow operation as a function of frequency over a range of NOS_{air} values. Cell temperature was set to 50°C and fuel utilization was 0.833; the current load on the cell was 10 A. The data presented here are from the same trials shown in Figure 5.6. In all cases shown in Figure 5.7, the power output of the cell was less than the power produced under comparable steady flow conditions. The power drop was most pronounced at low frequency, regardless of level of excess air supply. A comparison of Figures 5.6 and 5.7 reveals that the greatest power loss measured coincides with the greatest oscillation in cell potential. Therefore, there is a trade-off to be made in terms of time-averaged power output in realizing maximized oscillation in/control of cell potential. It has been suggested above that changes in membrane humidity are possibly responsible for the modulation of cell voltage observed due to reactant flow modulation. This variation in membrane humidity

may result in periods of either (or both) the membrane becoming too wet (during periods of low flow) or too dry (during periods of high flow). Recall from Chapter 2 that if the membrane is too dry, its internal resistance will increase, resulting in increased ohmic polarization losses and reduced power output. Conversely, if the membrane is too wet, product water on the cathode will inhibit the reduction of oxygen in the air stream, resulting in a concentration polarization loss and reduced cell performance. It is thus believed that pulsed air flow leads to reduced power output from the cell as both excessively high and excessively low flow rates lead to undesirable polarization losses.

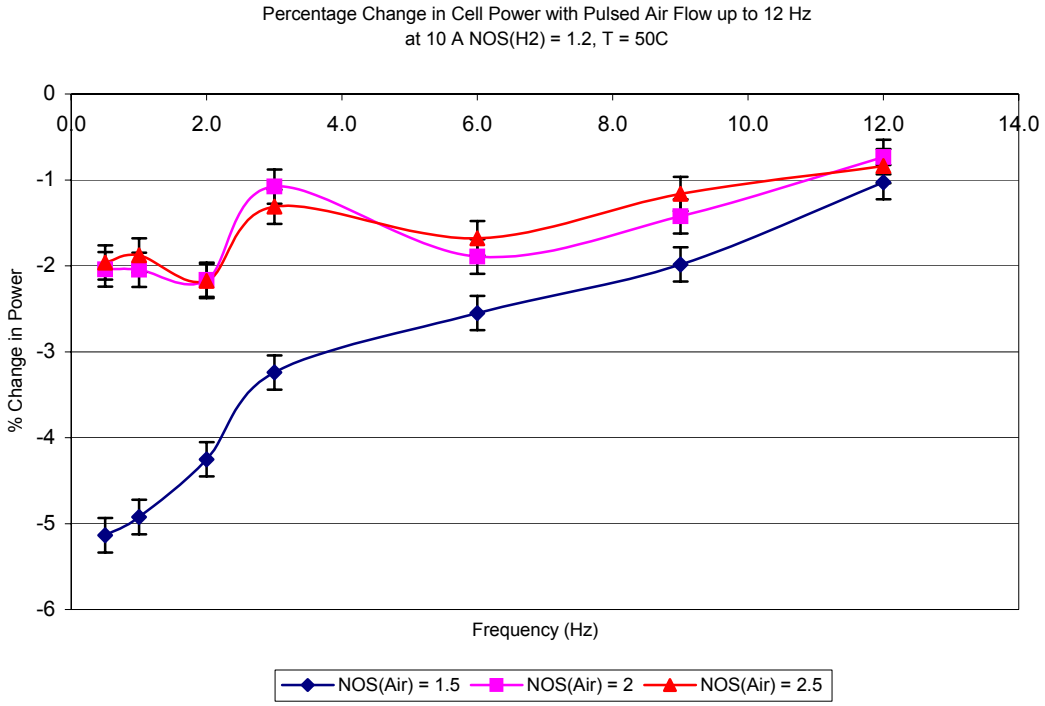

Figure 5.7: Change in cell power with respect to steady state as a function of frequency of air oscillation at NOS_{air} = 1.5, 2, 2.5

To verify that cell response was indeed diminishing as frequency increased, an empirical transfer function was developed based upon step changes (or impulses) in flow. These tests were again run with a constant current load of 10 A, u_f = 0.833, T = 50°C. The initial NOS_{air} value was 1.2, and then the impulse increased NOS_{air} to values of 1.5, 2, and 2.5, respectively. The averaged data of the NOS_{air} = 1.2→2 case is presented in Figure 5.8.

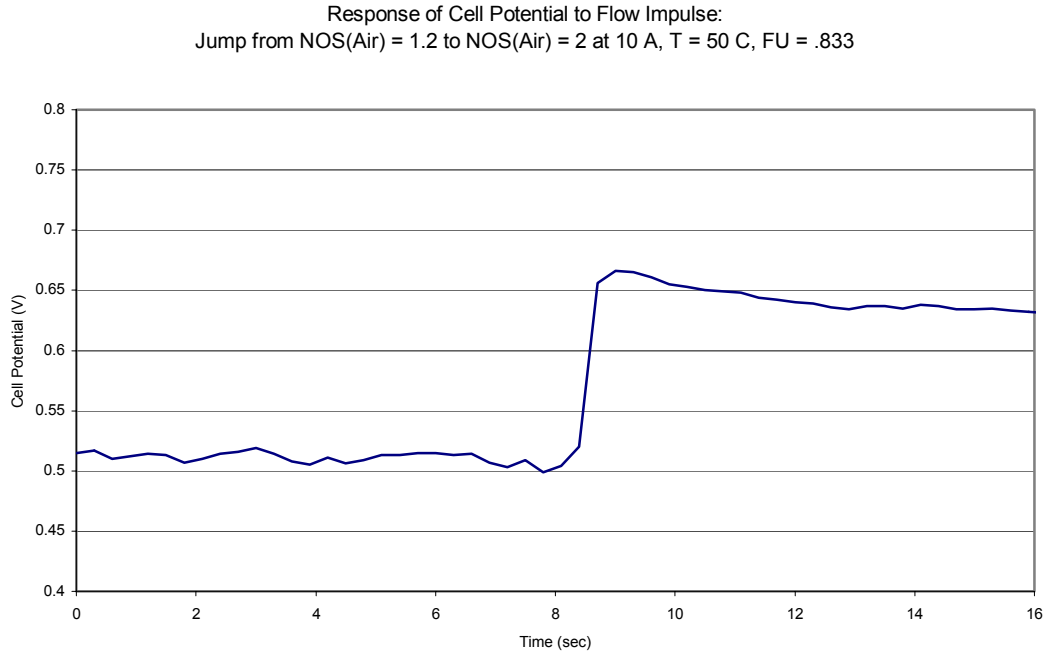

Figure 5.8: Cell voltage response to air flow impulse

The data obtained indicated a first order (Laplace) transfer function would be sufficient to accurately predict cell response to transient flow rates. Such transfer functions are of the form

$$H(s) = \frac{K}{s + a} \tag{5.1}$$

In this equation, *K* and *a* are empirically determined coefficients where *K* is a scaling factor based upon the instantaneous voltage jump realized in Figure 5.8. Converting (5.1) to the time domain yields equations of the form

$$H(t) = Ke^{-at} \tag{5.2}$$

The resulting transfer functions are plotted in Figure 5.9. These mathematical results accurately predict the level of voltage oscillation at each level of reactant supply when compare to Figure 5.6. Figure 5.6 indicates the voltage oscillation observed at 12 Hz was minimal; Figure 5.9 supports this and furthermore indicates that voltage oscillation goes to a noise level response by 15 Hz. Noise level response is anything less than a 1% voltage oscillation and is indicated by the dashed black line in Figure 5.9.

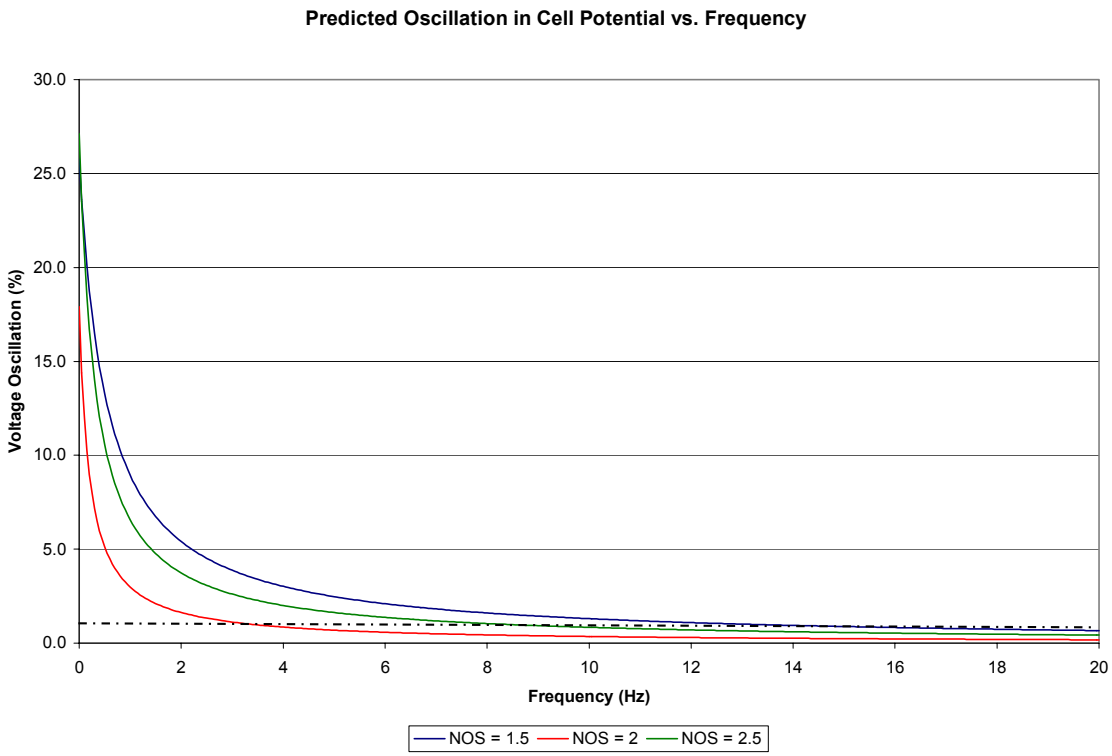

Figure 5.9: Voltage oscillation predicted by empirical transfer function

The work presented here raises the possibility of using AFC to regulate air flow rate into a PEM fuel cell or cell stack in order to meet low frequency variations in cell load. The most potential for such an application is in "buck" voltage regulation (introduced in Chapter 2), whereby a temporarily reduced voltage output is required of the fuel cell system. Rather than using power electronics to meet the slow transient loading demands, a system utilizing active flow control could be implemented that allows reactant flow rates to modulate cell voltage rather than treating the fuel cell as a "black box" which puts out a constant current at a constant voltage and relying solely upon the power conditioning system to regulate cell power. An AFC system such as this could supplement circuits within the power conditioning system designed to manage load

variations at low frequency. The envisioned power electronics system would thus include an AFC circuit to regulate air flow into the cell to respond to low frequency changes in current load used in conjunction with the existing technology that has been developed to address high frequency fluctuations in current load. It is not uncommon in the field of power electronics to incorporate two different topologies in order to produce the most efficient power conditioning system. One example of such a system used in high voltage applications consists of vacuum tubes that are used to address low frequency fluctuations at high voltages combined with a transistor (usually a MOSFET, or Metal Oxide Semiconductor Field Effect Transistor) which regulates high frequency changes over a small voltage range.

5.2.2 Consideration of Pulsed Hydrogen Flow

The data obtained in the study of pulsed hydrogen flow showed little similarity to the study of pulsed air flow. While pulsing air flow had a predictable affect on the cell voltage, pulsing the hydrogen flow into the cell did not result in an oscillating voltage signal as was expected. The parameters varied in the consideration of pulsed hydrogen flow were identical to those considered in the study of pulsed air flow (current load, frequency, flow amplitude, and NOS).

The first step taken in the consideration of pulsed fuel flow was to study the effects over a range of current loads. The results of this portion of the study can be seen in Figure 5.10. The conditions for this test were NOS_{air} = 2, average NOS_{fuel} = 1.2, and T = 50°C. A 50% flow oscillation was used and the current loads studied were 5 A, 7.5 A, and 10 A (current densities of 200 mA/cm^2, 300 mA/cm^2, and 400 mA/cm^2, respectively). In contrast to similar tests performed using pulsed air flow (see Figure 5.4), limited response was observed as a result of pulsed hydrogen flow over the same

range of current loads. Only at a 10 A current load with flow oscillations at 1 Hz was a significant oscillation in cell potential observed. This general trend of limited or trivial oscillation in cell voltage was consistently observed throughout the course of this portion of the study.

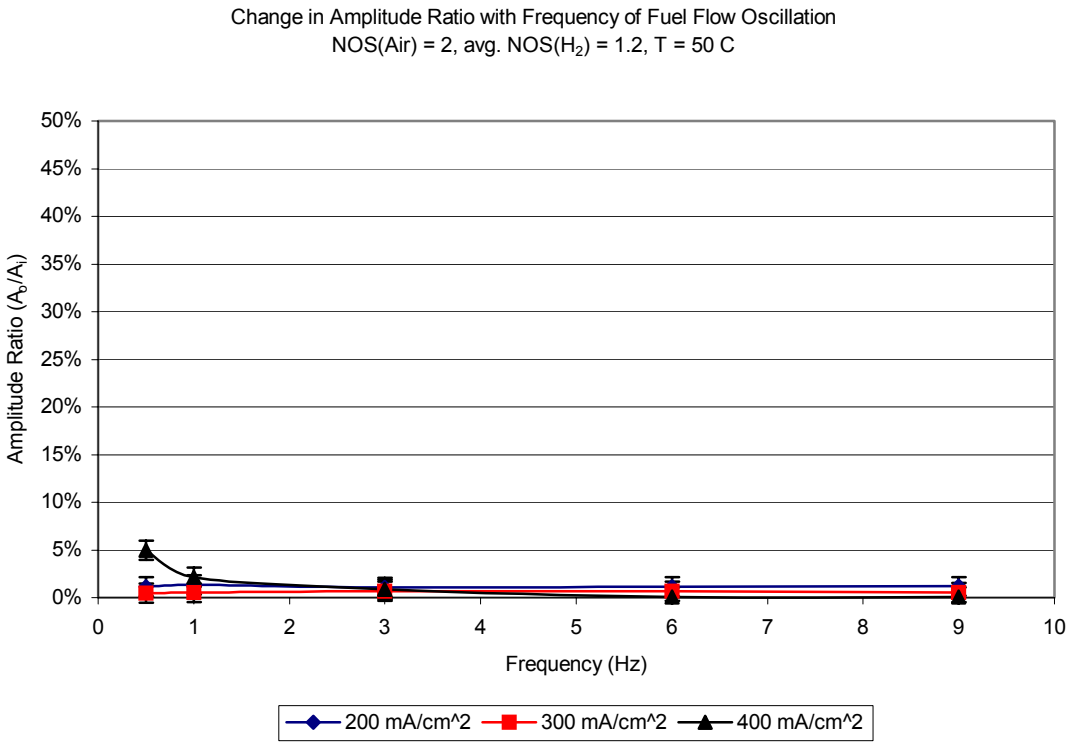

Figure 5.10: Change in voltage oscillation with frequency of fuel oscillation at 200 mA/cm^2, 300 mA/cm^2, and 400 mA/cm^2 (5, 7.5, and 10 A); nominal fuel oscillatory fraction = 25%

Figure 5.11 shows the effect of varying input amplitude on voltage oscillation. These tests were performed at the following conditions: I = 10 A (400 mA/cm^2 current density), NOS_{air} = 2, average NOS_{fuel} = 1.2, T = 50°C. At all frequencies studied, no

significant, repeatable oscillation in cell potential was observed. The data presented in Figure 5.11 are comparable to the pulsed air flow data shown in Figure 5.4 in that the test conditions (i.e. cell temperature, reactant supply rates, and current demand) are identical. Comparison of these two figures thus shows that pulsed air flow resulted in significant oscillations in cell potential whereas pulsing fuel flow in an identical manner under identical conditions resulted in negligible voltage oscillation.

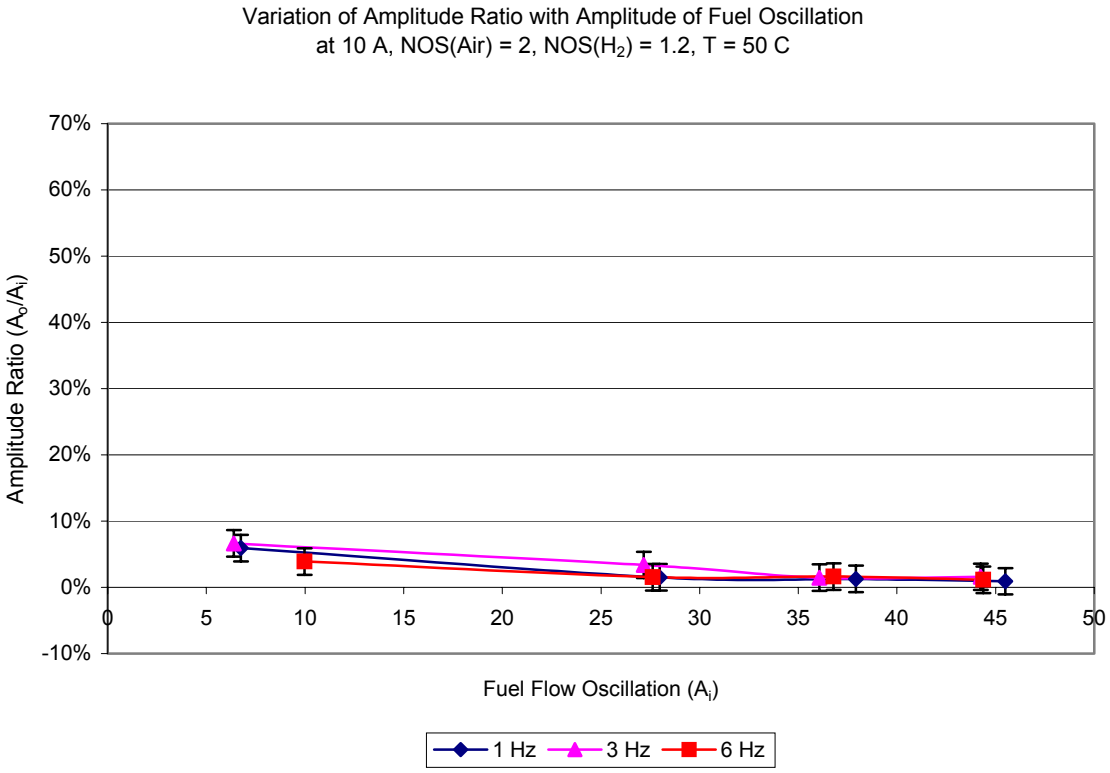

Figure 5.11: Change in voltage oscillation with amplitude of fuel oscillation at 1 Hz, 3 Hz, and 6 Hz

It should be noted that because the average hydrogen flow rate was only 20% above the theoretically required flow rate, the large flow oscillations (i.e. ≥~25%) shown

actually supplied less hydrogen than theoretically necessary to drive the reaction at the given current load; reactants capacitance within the electrodes and/or gas flow channels is understood to have maintained the required electrochemical stoichiometry. If either cathode or anode reactant supply is exhausted, even briefly, cell performance will suffer; an example of such behavior is shown below in Figure 5.12.

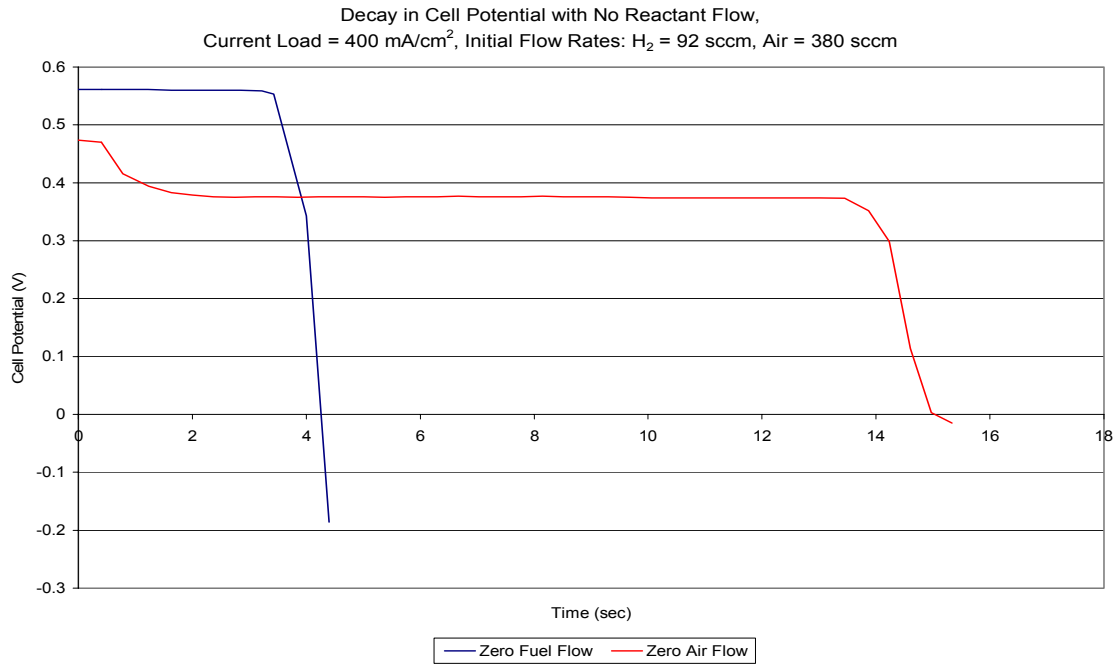

Figure 5.12: Decay of cell potential with discontinued reactant supply

Figure 5.12 shows the effect on cell potential when either reactant stream is turned off under constant current load. After a brief delay during which all available reactant is used, the cell potential rapidly goes to zero. This indicates that varying the reactant flow rate, especially in such a way that less than the theoretically required flow rate is temporarily supplied, should have an effect on cell performance. Also of note is that Figure 5.12 indicates that the cell potential holds steady longer after air flow is cut

off than in the case when fuel flow is cut off. This implies that pulsed hydrogen flow should have an effect on cell potential up to a higher frequency limit than was found when air flow was pulsed; at lower frequencies, such as 1 Hz, the voltage oscillation observed due to pulsed hydrogen flow should be larger than the voltage oscillation measured as a result of pulsed air flow. A comparison of the data in Figures 5.4 and 5.11 indicates that this is not the case. This implies that electrochemical reaction rates are not the dominant factor in realizing voltage regulation via active flow control. Rather, the data in Figure 5.12 considered with Figures 5.4 and 5.11 strengthens the proposed hypothesis that membrane humidity is the dominant effect in realizing time-varying cell potential via reactant flow modulation.

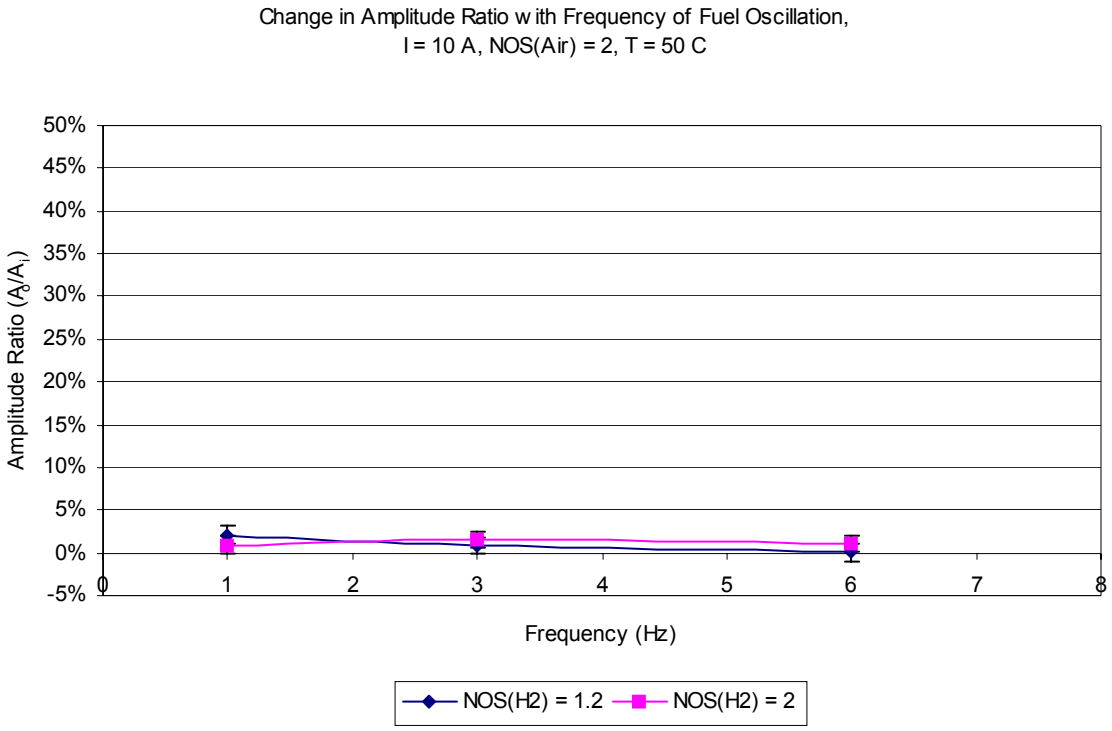

Figure 5.13: Change in voltage oscillation with frequency at NOS_{fuel} = 1.2 and NOS_{fuel} = 2

Figure 5.13 shows the effect of varying fuel utilization levels on voltage oscillation. The test conditions were I = 10 A, NOS_{air} = 2, T = 50°C, and a 50% input fuel flow amplitude. This test was performed so as to allow a full comparison between the data collected in pulsing air flow into the cell to data collected in pulsing fuel flow into the cell. As was previously discussed, by pulsing reactant flow and maintaining a mean flow rate close to the theoretical limit (i.e. NOS close to 1) greater cell response should be observed. This was in fact the case when pulsed air flows were studied. However, here again, pulsing hydrogen flow showed no greater than noise-level oscillations in cell potential.

5.3 Repeatability Issues Encountered with PEM Cell

At times during the course of this study, erratic PEM cell performance was observed in spite of steps taken to ensure consistent performance (see Chapter 4). As can be seen in Figure 5.14, large variations in cell potential occurred while under identical operating conditions. Figure 5.14 depicts the results of an active flow control study where the effects of air flow were studied. The test conditions were 1 Hz pulsed air flow at a mean NOS_{air} = 2, the fuel utilization, u_f, was 0.833, cell temperature was set to 50°C, and the current load on the cell was 10 A. The data shown in Figure 5.14 were taken on different days but within a week of each other. The same MEA was used for both trials.

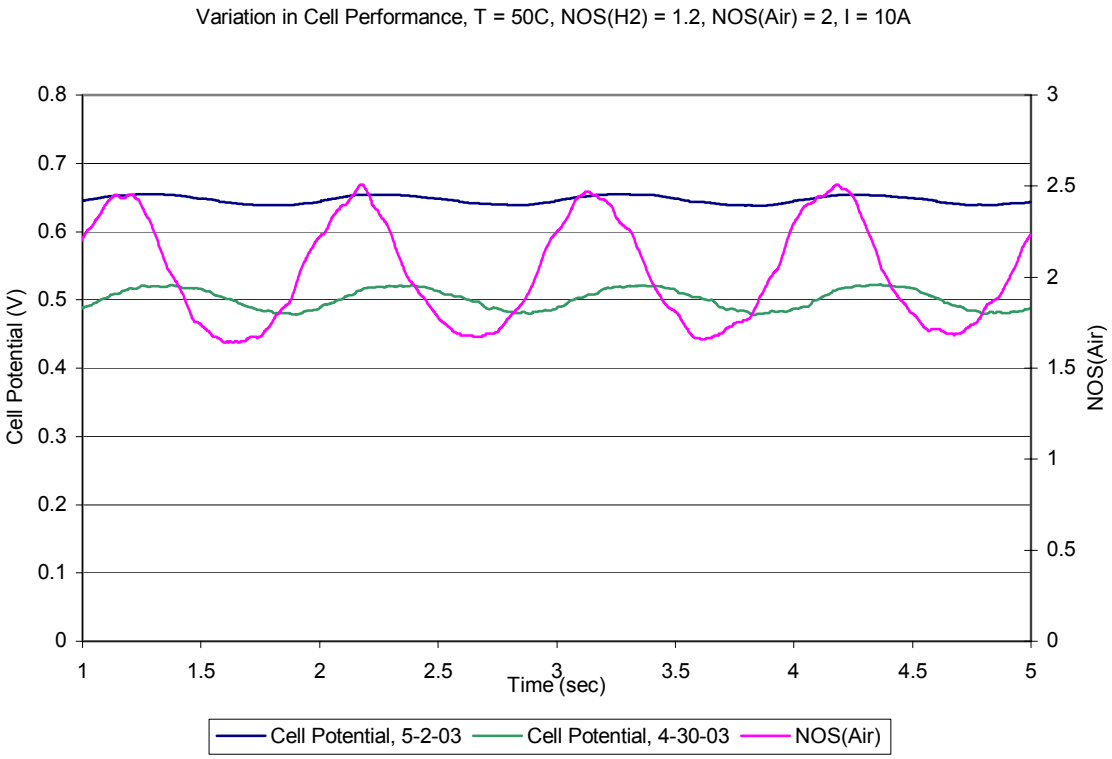

Figure 5.14: Variability of PEM fuel cell performance

Variability such as that shown above was observed, whereby the cell would perform poorly, such as shown in Figure 5.14 on April 30th, before performing as expected, as on May 2nd. After maintaining the expected performance level for a period of several days, performance would sharply decline to the point where the cell could not meet any substantial current demand. There are several corroborating factors that could lead to such unreliable performance. As discussed above, membrane humidity plays a vital role in cell performance. Therefore, a new, unhydrated MEA would need to go through a "break-in period" during which the MEA becomes sufficiently hydrated. Once the MEA is sufficiently humidified, consistent performance can be expected for a period of several days before performance begins to degrade. Such degradation could be explained by the MEA becoming over hydrated and thus reducing conductivity. However, numerous MEAs were dried out at high temperature (80°C) to remove water in such a way as to not damage the MEA.[5] In spite of these attempts to "recondition" the MEA, no return to acceptable performance was observed. The break-in period and useful lifetime of each MEA varied widely; break-in times ranged from 30 minutes to several hours and lifetimes ranged from 60 hours to 300 hours. Possible reasons for this variation in lifetime are most likely due to contamination of the MEA as a result of direct contact particulate matter during installation or reconditioning (Correspondence with J. Layton, Lynntech Industries).

Each MEA followed the same pattern of break-in, *reliable performance,* and degraded performance. To ensure repeatability of the results presented here, several replicates of each data set were taken while the cell was performing as expected, and only those results obtained during this period of "normal" operation are reported. Every

[5] Polymer-electrolyte membranes are temperature sensitive; permanent damage to the MEA is likely to occur if temperature exceeds 100°C.

time data was collected, a test case was run to determine that results obtained would be comparable to other data. The test case run was as follows: $NOS_{air} = 3$, $u_f = 0.75$, T = 50 C, I= 12.5 A (500 mA/cm^2 current density). Given these conditions, the cell was determined to be operating acceptably if the measured voltage across the cell was a minimum value of 0.62 V. The test case conditions were obtained through conversations with Lynntech.

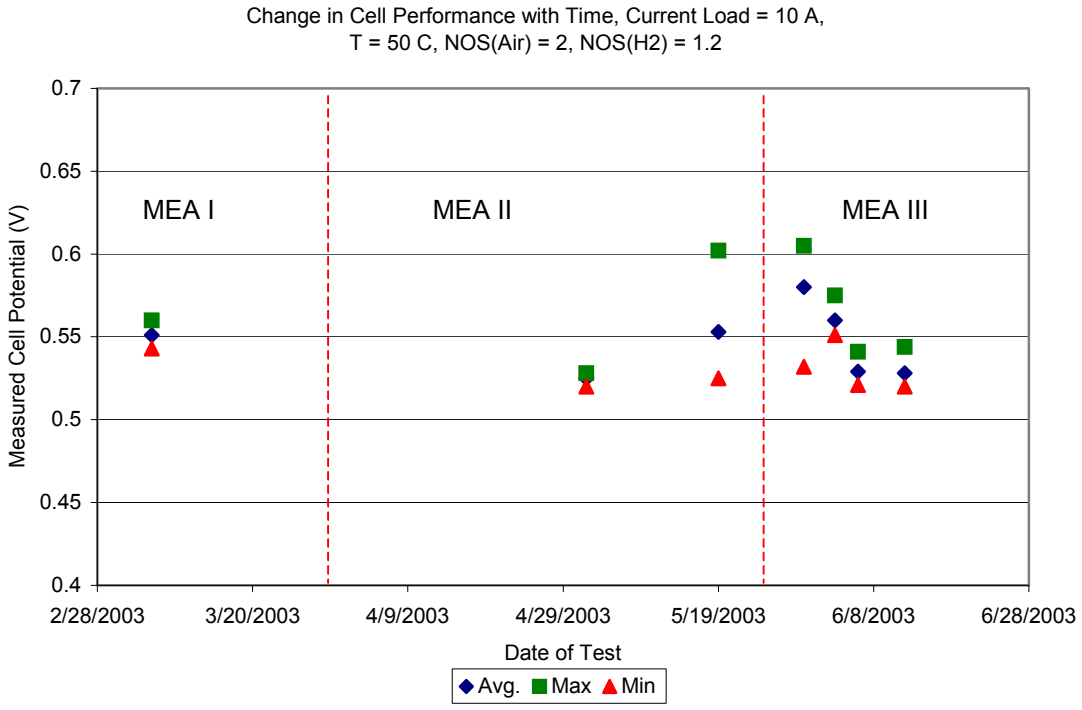

Figure 5.15: Day-to-Day variation in cell performance on relevant dates

Using this procedure to ensure comparable results worked well; Figure 5.15 shows the variation of cell potential on days when data presented here were recorded. The conditions for each test were a 10 A current load with $NOS_{air} = 2$, $u_f = 0.833$ and T =

50°C. The dotted red lines denote a change in MEA. The cell was deemed to be operating acceptably if the measured voltage was greater than or equal to 0.52 V. This new test condition was used as it utilized common parameter values such as NOS_{air} = 2, u_f = 0.833, and I = 10 A, whereas the test case suggested by Lynntech prescribed reactant supply rates not commonly used in this study.

5.4 Summary of Observations in Considering AFC on PEM Fuel Cell

Several trends were identified in the above sections. They are reviewed here and in Table 5.1 below for the reader's convenience. The primary trend identified is that low frequency, pulsed air flow produced a repeatable, low-distortion voltage signal whereas pulsed fuel flow over the same range of input variables did not produce a significant voltage response. The ability to modulate cell potential through controlling the air flow rate to the cell is significant as it introduces reactant flow regulation as a possible means to modulate cell power output to meet changes in voltage/power demand.

The difference between the response measured for air flow oscillation and response measured for hydrogen flow oscillation *may* be explained by the substantial difference in the absolute humidity of each flow. As has been discussed previously, membrane humidity has a substantial effect on cell performance. As a matter of simple stoichiometry, the air flow rate into the cell is multiples of the fuel flow rate at a fixed current load. Because of this substantial difference in flow rate, significantly more water is transferred both to and from the cell via the air stream. Thus, oscillations in air flow rate have a greater effect on membrane water content as significantly more water is transferred via the oxidant flow than by the fuel flow. The large change in membrane humidity attributable to pulsed air flow likely causes a larger change in membrane conductivity, and in turn, substantially alters cell performance (Correspondence with J. Layton, Lynntech Industries). This provides further support for the hypothesis that membrane humidity, and not electrochemical reaction rates, is the driving factor that produces substantial oscillation in cell potential as a result of pulsed reactant flow rates.

The role of humidity in this process is not fully understood and requires further study to confirm or refute the present hypothesis. Such a study must control MEA

humidity and further measure inlet and outlet humidity. This would allow for one to compare the variation in membrane humidity with time to variations in flow rate and cell voltage. If the resulting data indicates good agreement between variation in MEA humidity and oscillations in cell potential, the present hypothesis would be supported.

Table 5.1: Summary of identified trends

Parameter Varied	**Current Load Increased**	**Frequency Decreased**	**NOS Decreased**	**Flow Amplitude Increased**
Effect on Voltage Oscillation	+	+	+	+
Effect on Average Cell Power vs. SS Performance	-	-	-	-

Parameters that have been identified as having a substantial effect on the degree of the cell's voltage response include frequency of oscillation, average amount of excess reactant supplied, and current load on the cell. Additionally, it has been shown that cell power is reduced as result of pulsed reactant flow and that the drop in power is largest under the same conditions that maximize oscillation in cell potential.

6. Results of Direct Methanol Fuel Cell Study

6.1 Steady State Characterization

As with the direct hydrogen PEM fuel cells in this study, the performance of the Motorola DMFC was first characterized under steady state conditions. The conditions used for this initial characterization were those recommended by Motorola, including 1 M methanol flow rate of 0.25 ccm and an air flow rate of 60 sccm. Cell temperature was allowed to vary freely (i.e. the cell was without thermal control). As the effects of methanol supply rate to the cell are the primary focus of this chapter, Figure 6.1 shows cell performance using both the recommended flow rate of 0.25 ccm as well as a reduced fuel flow rate of 0.125 ccm. The current densities considered here range up to 100 mA/cm^2. This current density was chosen since it is the greatest load place on the cell during the course of the pulsed flow studies discussed later in this chapter. However, the Motorola DMFC was able to operate at current densities beyond 140 mA/cm^2 if desired.

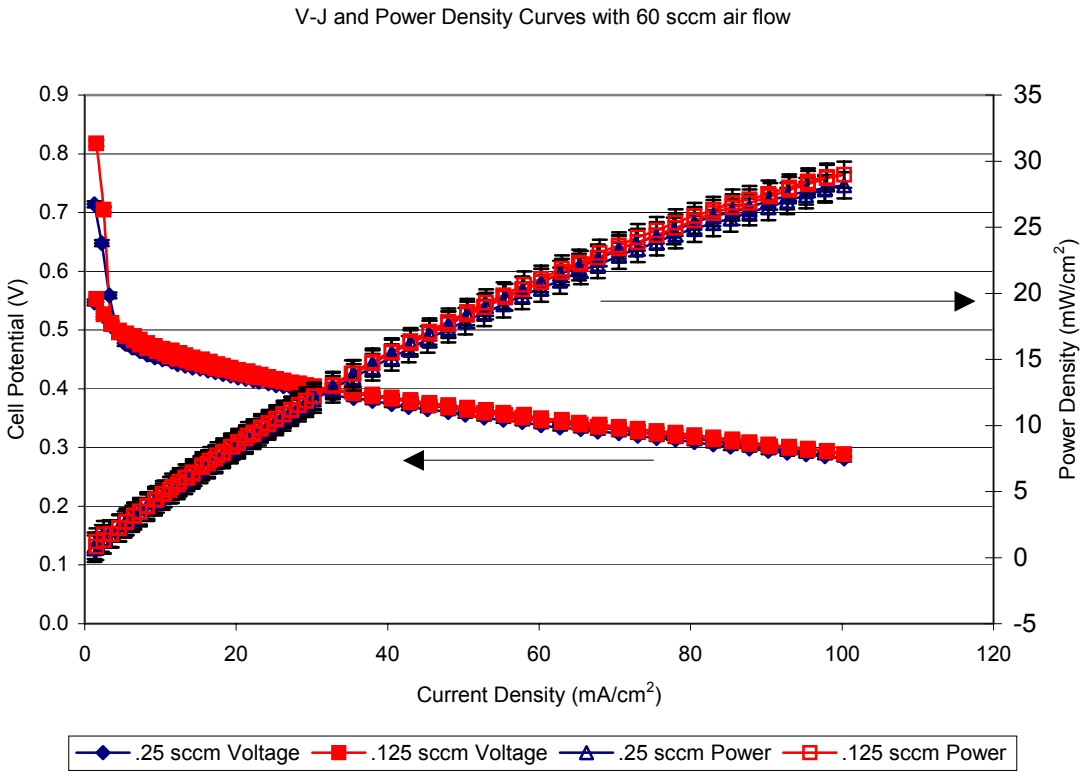

Figure 6.1: DMFC characteristic V-J and power density curves

Inspection of the data shown in Figure 6.1 shows virtually no difference between the 0.25 ccm flow rate and .125 ccm flow rate data sets; the sets show nearly identical power production up to the current load of 100 mA/cm^2; statistically, the difference in cell performance is indiscernible. That is, the difference in performance at these two flow rates is within the measurement error associated with the DC electronic load. The one statistically significant difference of note is the open circuit voltage (OCV) measured at a fuel flow rate of 0.125 ccm. The OCV measured in this case is significantly greater than that measured at the suggested flow rate of 0.25 ccm. This is likely due to the methanol crossover phenomenon mentioned in Chapter 2 and discussed in detail below. This undesirable phenomenon is a more significant problem at greater levels of excess fuel

supply (i.e. greater NOS_{fuel}). The maximum expected power output of the fuel cell was expected to be in the range of 20 mW/cm^2 to 25 mW/cm^2 (Communications with A. Fisher, Motorola); however, one can see from Figure 6.1 that power outputs of up to 30 mW/cm^2 were measured. The cell was thereby determined to be performing reliably.

6.2 Results of Active Flow Control Study

This study of active flow control on a DMFC considered the following parameters: current load on the cell, frequency of flow oscillation, and amplitude of oscillation. Both fuel and air flows were pulsed.

6.2.1 Consideration of "Turn-Off" Transients

As a first step in studying the effects of active flow control on methanol-fueled polymer-electrolyte cells, "turn-off" transients were studied. "Turn-off" transients are trials in which either air or fuel flow is turned off while current load is held constant and the change in cell potential with time is recorded. The trial to trial variance associated with the turn-off transients and the normalized plots presented later was found to be $\pm$4% for voltage measurements and within $\pm$7% for time measurements. Each test was repeated a minimum of three times to establish repeatability. Figures 6.2(a) and (b) show the respective results when air and fuel flow were turned off. In Figure 6.2(a), when air supply to the cell was discontinued, a monotonic decline in cell potential can be seen, after a short delay during which the latent air supply is exhausted. The time required for cell potential to reach 0 V after air flow was turned off varied inversely with the current load on the cell. Primarily, this is for the simple reason that at lower current density, the latent air supply is exhausted more slowly than at higher current density.

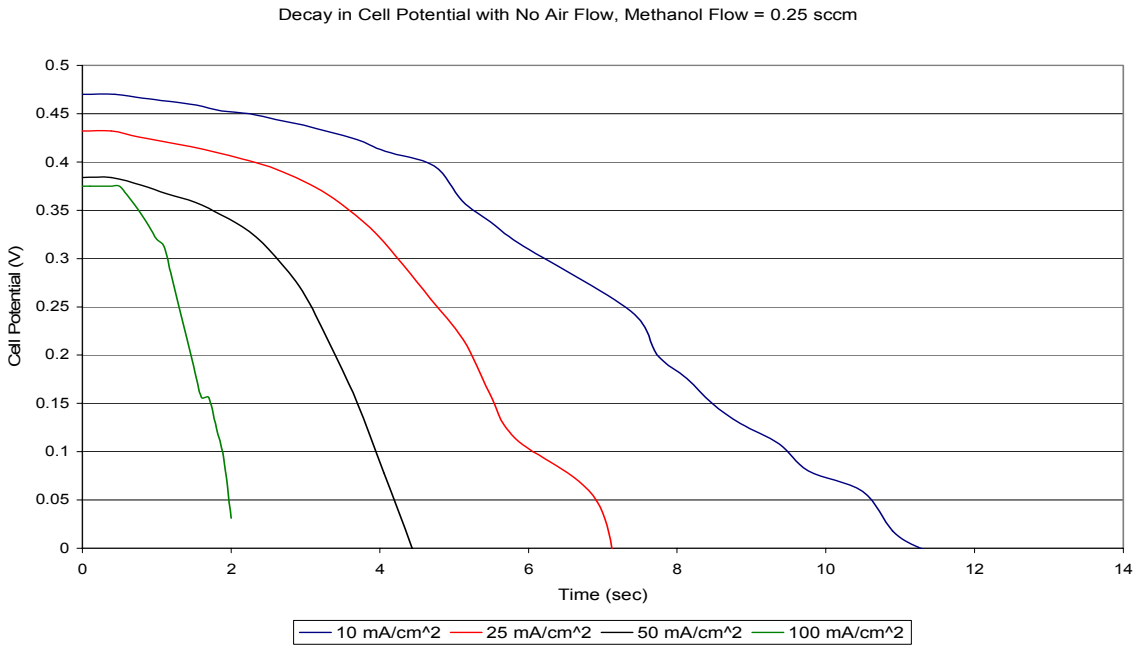

Figure 6.2(a): Decay in cell potential after air flow discontinuation at 10 mA/cm^2, 25 mA/cm^2, 50 mA/cm^2, and 100 mA/cm^2

Figure 6.2(b) shows the corresponding case where the supply of 1M methanol-water solution was discontinued. Again the time required to exhaust the latent reactant supply decreased as current load was increased. However, unlike the air flow case, in most cases cell potential briefly *increased* after initially remaining at the steady flow voltage and before ultimately decaying. This phenomenon was not observed at all current loads studied; in particular, at 100 mA/cm^2, the cell voltage was found to monotonically decrease as in the case of air discontinuation. *As will be discussed in detail later, the primary mechanism causing the observed rise in voltage is understood to reduction in methanol crossover*. The rise in voltage realized was greatest at lower current loads; the total decay time was also longest at lower current loads. Note that the difference in potential decay time for methanol discontinuation is approximately two

orders of magnitude greater than that of air. Aside from the unique phenomenon of initial potential rise, the larger time frame may also be attributable to a greater capacitance of methanol along the DMFC, in comparison to oxidant capacitance. This is subject to further investigation. To confirm that the data presented in Figure 6.2(b) represents feasible results, an energy balance was conducted to compare the energy content of methanol in the anode flow channels with the work done by the cell after fuel flow discontinuation. It was determined that approximately 1% of methanol in the flow channels was consumed during these trials; Appendix A details this analysis. Thus the energy balance indicates that the results presented here are not in violation of the first law of thermodynamics and are therefore possible. Methanol crossover phenomenon is next revisited.

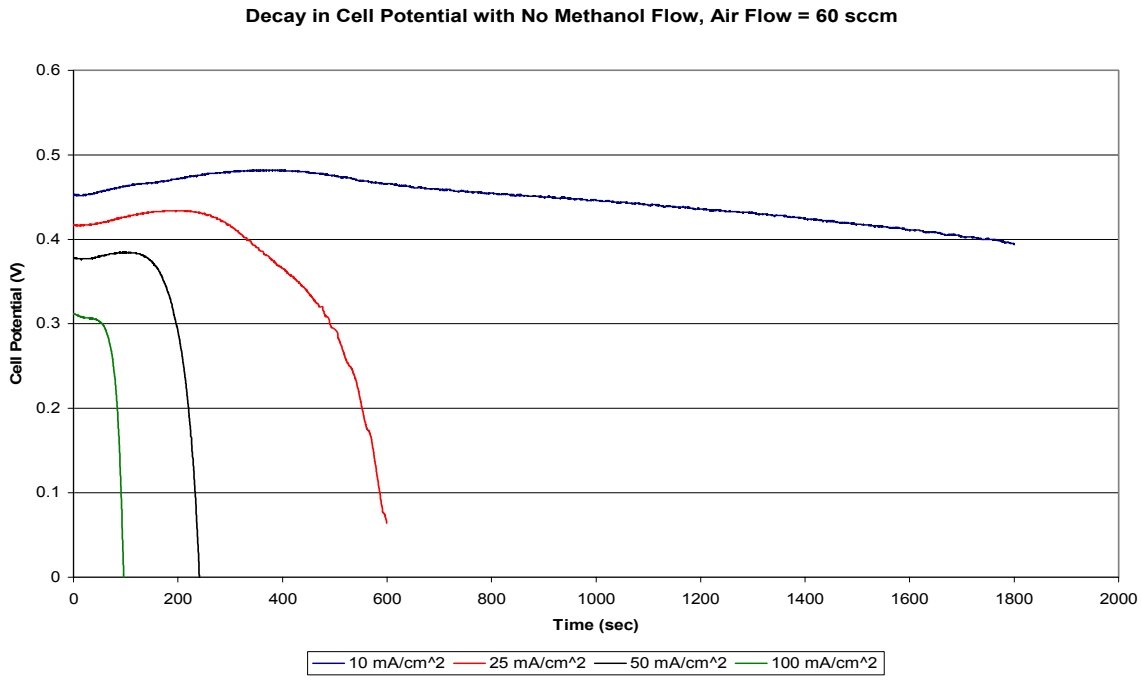

Figure 6.2(b): Decay in cell potential with after fuel (Methanol) flow discontinuation at 10 mA/cm^2, 25 mA/cm^2, 50 mA/cm^2, and 100 mA/cm^2

The phenomenon of methanol crossover is a substantial limiting factor in the performance of direct methanol fuel cells. As was discussed briefly in Chapter 2, methanol crossover is the diffusion of methanol from the anode side of the membrane-electrode assembly (MEA) to the cathode side of the cell. At the cathode, methanol can chemically react (i.e. combust) with oxygen. The migration of methanol to the cathode also results in a significant drop in voltage across the cell. This voltage drop is essentially another form of polarization that reduces both efficiency and cell power. Finally, DMFC lifetime may be adversely affected by methanol crossover. Normal start-up procedure for a fuel cell is to introduce reactant flow to both anode and cathode shortly before putting an electronic load on the cell. During this period where no load is on the cell, methanol crossover is particularly large due to the high concentration of unused fuel on the anode. This naturally results in higher diffusion through the membrane. Recall that this particular manifestation of methanol crossover was shown in the substantially different OCVs shown in the V-I curves in Figure 6.1. Furthermore, during loaded steady state operation, excess fuel is conventionally fed to the cell. That is, fuel utilization is less than unity (or NOS_{fuel} is greater than unity). Ideally, the excess methanol would flow through the cell, recirculate, and ultimately be electro-oxidized on a subsequent pass through the cell. However, in practice, some portion of the excess methanol will cross through the membrane (hence the term “crossover”), hindering cell performance.

As the same initial methanol supply was used for all current loads (as opposed to the same initial NOS), there was substantially more methanol present along the anode at low current loads; that is, for the same supply rate, the concentrations of methanol along the anode-electrolyte interfaces were negatively correlated to the electrochemical consumption of methanol via current generation. The result was that undesirable methanol diffusion through the electrolyte was exacerbated at lower current loads.

Thus, turning off fuel flow at lower current loads resulted in a greater impact via reduction of methanol crossover, leading to a greater improvement in cell voltage. This is illustrated in Figure 6.3 below, where the arrows pointing from the anode to the cathode represent the volume of methanol crossover under given relative loading conditions.

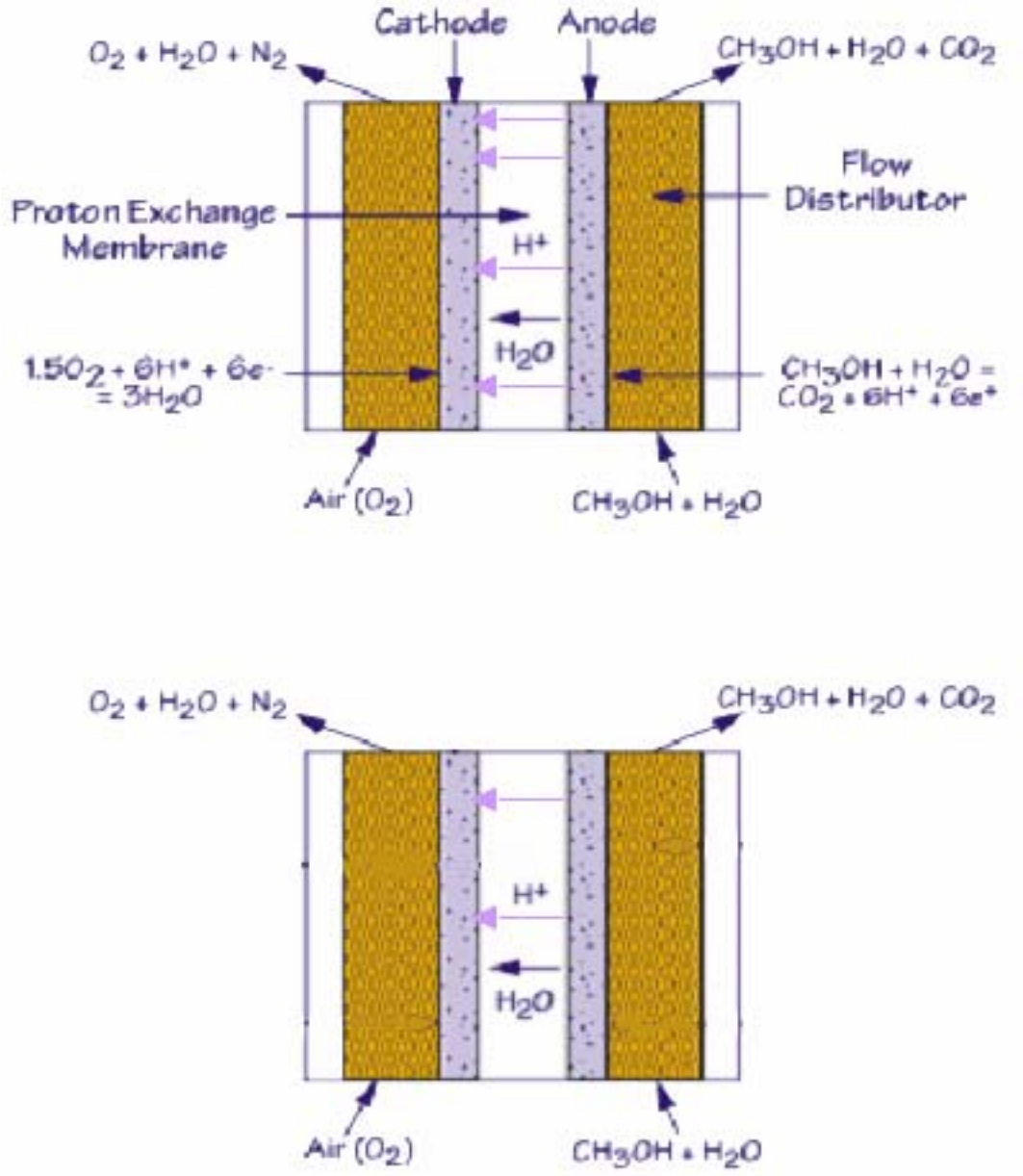

Figure 6.3: Schematic respresentation of methanol crossover

at low current load (top) and high current load (bottom)

The data in Figure 6.2(b) suggested that pulsed methanol flow could produce an increase in time-averaged cell voltage/power. Furthermore, the data suggested that there is an optimal frequency (or period) of oscillation that is dependent upon related excess fuel flow (i.e. NOS), the current load on the cell, and the concentration of methanol at the anode.

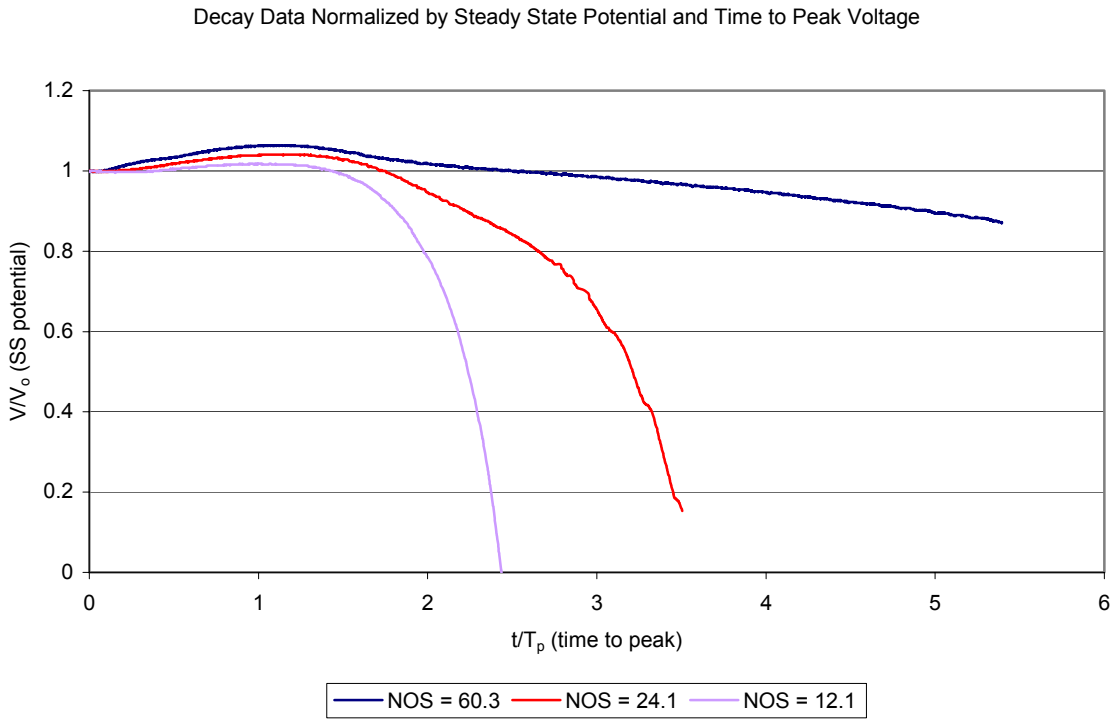

Figure 6.4(a): Decay data normalized by steady state voltage and time to peak voltage at initial NOS_{fuel} = 60.3, 24.1, and 12.1

(10 mA/cm^2, 25 mA/cm^2, and 50 mA/cm^2 current loads, respectively)

Figure 6.4(a) shows the same data presented in Figure 6.2(b), though here the data has been normalized. The instantaneous cell voltage measured is shown

normalized by the initial steady state cell voltage measured at the moment fuel flow was discontinued; the elapsed time since shut-off of fuel flow is normalized by the total time elapsed to attain peak voltage. The 100 mA/cm^2 data is excluded from this plot as a rise in voltage was not observed in this case. As previously stated, there was no rise in cell potential observed in this case because at high current load (low initial NOS) and a fixed fuel flow rate, there was substantially less methanol crossover than at lower current loads (higher initial NOS). This data also indicates a threshold NOS exists below which no rise in cell potential is observed due to insufficient reduction in methanol crossover in comparison to fuel depletion effects.

The data in Figure 6.4(a) reveals two trends. First, the rise in cell potential (on a percentage basis) varies inversely with the current load on the cell. Alternatively, it is equivalent to say that the percentage rise in cell potential varies directly with the initial NOS. As it is known that methanol crossover is greatest at low current loads (given the same supply rate) and that the greatest performance enhancement was realized at low current density, this trend supports the hypothesis that this phenomenon is the result of reduced methanol crossover as compared to normal, steady flow operation. The second trend brought forth by Figure 6.4(a) is that the time required for complete decay in cell potential varies inversely with current load. Again, it can be said that the time for total decay varies directly with initial NOS. This is indicative of the fact that at low current load (or high initial NOS_{fuel}), fuel consumption occurs more slowly, thus requiring longer times to exhaust latent fuel supply.

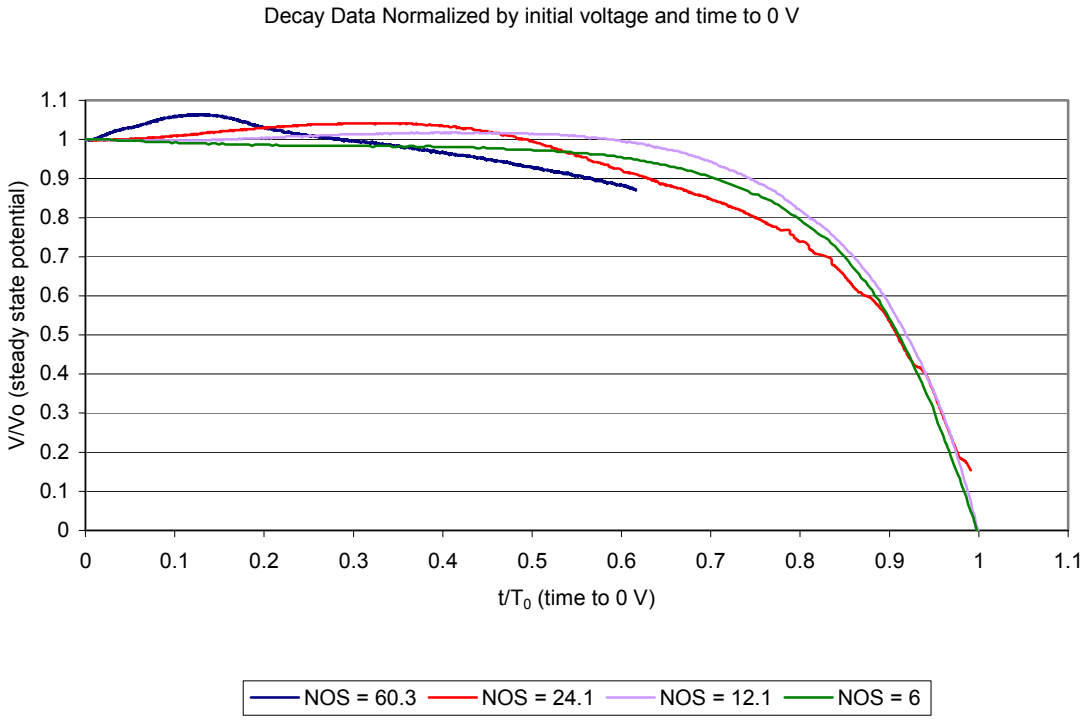

Figure 6.4(b): Decay data normalized by steady state voltage and time to 0 V

at initial NOS_{fuel} = 60.3, 24.1, and 12.1

(10 mA/cm^2, 25 mA/cm^2, and 50 mA/cm^2 current loads, respectively)

Figure 6.4(b) again shows normalized voltage decay data, though in this case the time scale has been normalized by the time required to reach the 0 V level; cell potential has again been normalized by the steady state cell potential. Note that for the initial NOS_{fuel} = 60.3 and initial NOS_{fuel} = 24.1 cases, the cell voltage did not decline to 0 V during the course of the trial. Thus, the existing data was extrapolated to determine the time required to reach 0 V. Normalizing the data by these benchmarks yields a family of curves that are generally similar. Even at low initial NOS when no rise in cell potential was observed, the curve maintains a similar latter-stage profile to the cases in which a

voltage rise was encountered. Before approximately 60% of time to reach 0 V has passed, normalized cell potential uniformly declined at a moderate rate after achieving peak voltage. However, beyond this point, the decline in normalized voltage becomes quite rapid. This indicates that in spite of the different NOS levels used, there is little variation in the normalized time required to realize the detrimental effects of reactant starvation. The energy balance carried out in Appendix A further supports the fact that the data collapse to form a family of self-similar curves as approximately the same amount of power is produced by the cell after flow discontinuation over the range of NOS levels studied.

As can be seen in Figures 6.5(a-c) below, at low initial NOS_{fuel}, the realization of peak voltage requires more time (on a relative scale) but substantially less time on an absolute time scale. Figure 6.5(a) shows the increasing time required to attain each benchmark level (peak voltage, return to stead state voltage, and 0 V) in absolute terms; Figure 6.5(b) repeats this same data with the exception of time to 0 V to bring out the similar trends in time to peak voltage and time to return to steady state voltage. Figure 6.5(c) shows these times on a normalized basis.

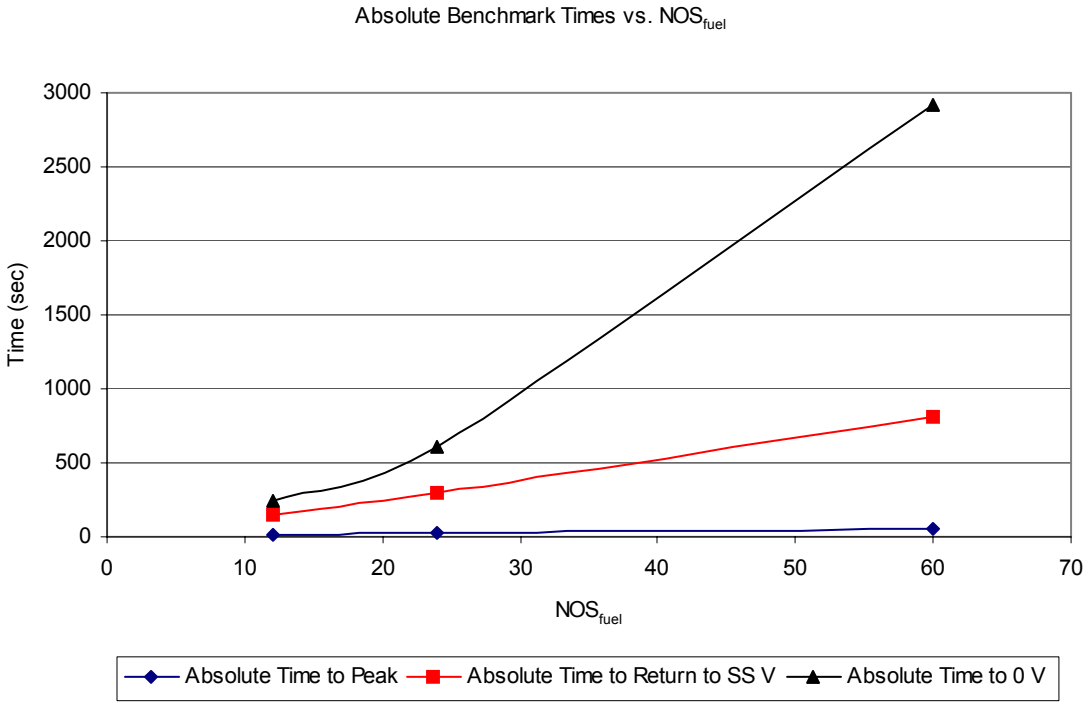

Figure 6.5(a): Variation in time required to attain benchmark voltages with NOS_{fuel}

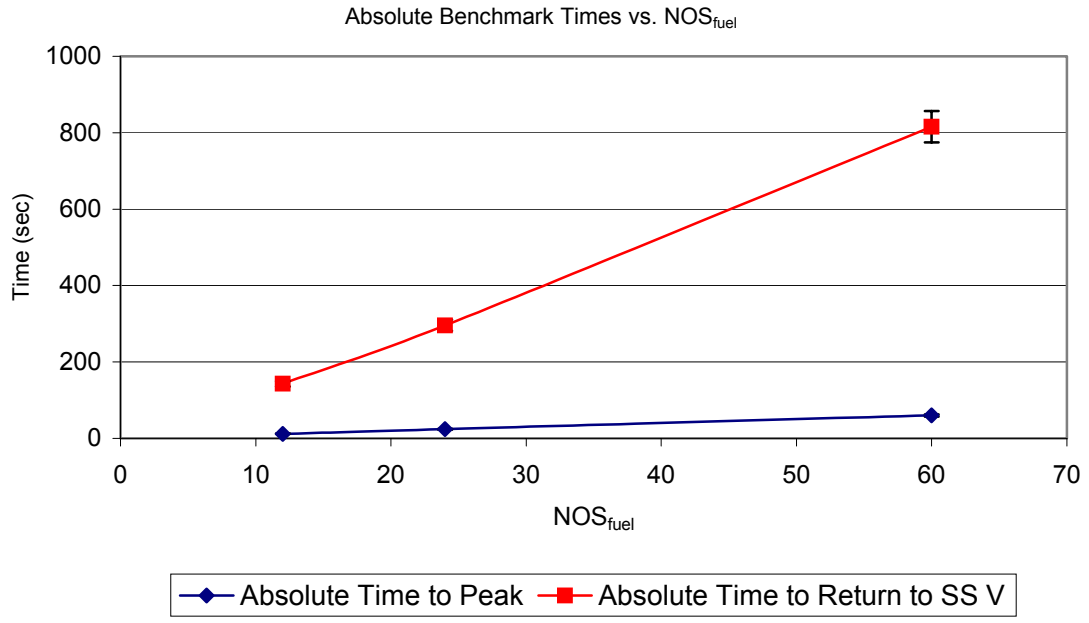

Figure 6.5(b): Variation in time required to attain benchmark voltages

(time to 0 V excluded)

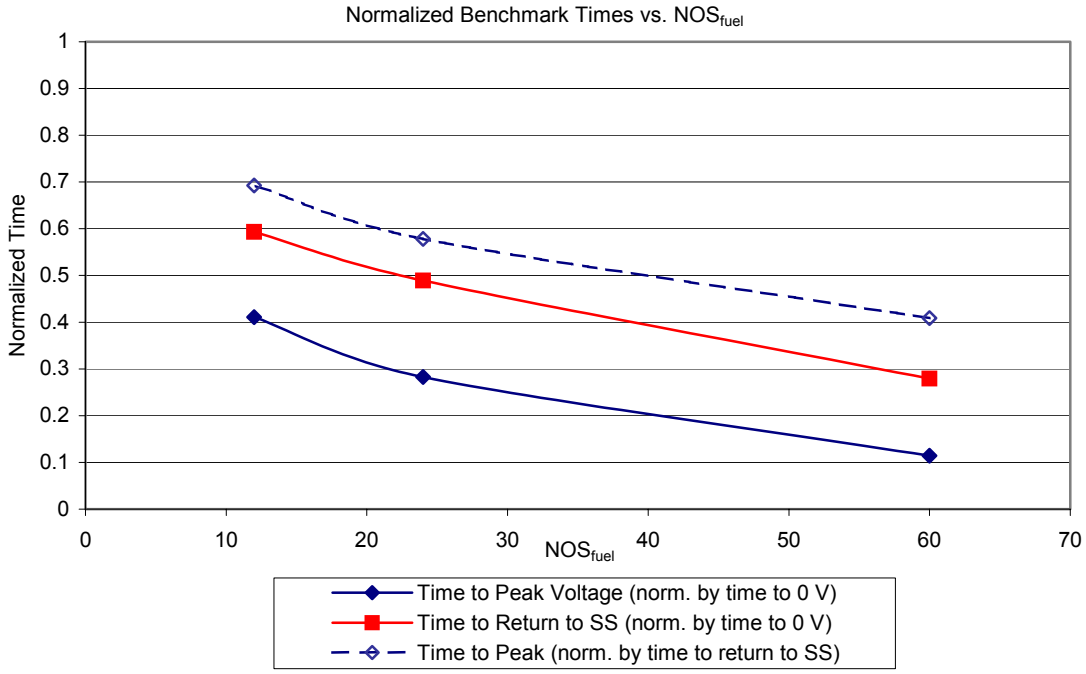

Figure 6.5(c): Variation in normalized time required to attain benchmark voltages

Figure 6.5(a) further shows the general trend that has already been stated—as NOS increases (equivalent to a decrease in current load), the time required to attain a specific benchmark cell potential increases. This is particularly true of the time required to reach 0 V. Figure 6.5(b) further speaks to this trend, though here the time required to achieve complete voltage decay is excluded to reveal the trend that both the time to attain peak cell potential and the time required to return to steady state voltage increase in what appears to be a logarithmic manner.

The fact that time to attain benchmark levels increases with NOS_{fuel} may be intuitive. The time to reach maximum voltage should increase proportionally with NOS_{fuel} because as the relative rate of consumption decreases, longer times are required to reduce methanol crossover via the virtual electrochemical sink. Furthermore, as has already been stated, methanol crossover is greater at high NOS_{fuel}, thus there is more

crossover to be mitigated in addition to the fact that the relative rate of methanol consumption is slower as compared to lower NOS levels. The increase in time to return to steady state voltage is also intuitive because of the rate of methanol consumption. Cell potential declines back to steady state levels (and below) as fuel starvation (or concentration polarization) becomes the dominant effect. The lower rate of methanol consumption associated with high NOS_{fuel} necessarily means that a greater period of time is required for fuel starvation to become dominant.

Figure 6.5(c) shows the change in normalized benchmark times with NOS_{fuel}. In contrast to the absolute times discussed previously, the normalized times decline as NOS_{fuel} increases. It should also be noted that at for the NOS_{fuel} levels considered, roughly 20% of the total trial length elapses between reaching peak voltage and returning to steady state voltage. Thus it is understood that higher initial levels of NOS_{fuel} extend the "post-peak" region of the decay curve.

The third (dashed) curve in Figure 6.5(c) gives the time to peak voltage normalized by the time to return to steady state voltage. This curve supports the trend that normalized time to benchmark levels decreases as NOS_{fuel} increases. Furthermore, it gives a measure of the overall symmetry of the voltage crest measured after fuel flow was terminated. At moderate levels of excess fuel supply, cell potential increases before rapidly declining because, as previously stated, reactant starvation becomes a dominant effect at lower NOS_{fuel} levels. Correspondingly, at high NOS_{fuel}, cell potential takes a significantly greater time to decline from peak levels due to the low rate of methanol consumption.

As a further step in analyzing the methanol decay data presented, the average increase in cell potential (on a percentage basis) for the duration of the voltage crest was computed for each NOS_{fuel} level. This is plotted along with a measure of crest symmetry in Figure 6.6 below. This is the same data presented in the third curve in Figure 6.5(c)

above. Crest symmetry is measured on a scale of zero to one. Crest symmetry is calculated as the difference between time to attain peak voltage after fuel discontinuation and the total elapsed time to return to steady state voltage after fuel flow discontinuation normalized by the total elapsed time to return to steady state voltage. Therefore, a crest symmetry value of 0.5 indicates that the time required to reach peak voltage is equal to the time required for voltage to decline back to steady state levels. A symmetry value of less than 0.5 indicates that voltage peaked relatively quickly and then returned to steady state levels over an extended period of time. A high symmetry value (greater than 0.5) indicates the converse case—that cell potential rose relatively slowly and then rapidly decayed back to the steady state voltage level.

Figure 6.6 shows reveals that the average power gain measured during the voltage crest is inversely related to the symmetry of the crest. As discussed above, at high NOS_{fuel} levels, a gradual decline from peak voltage is observed; this situation results in the largest gain in cell power (in both percentage and absolute terms). This is understood to be true as the low consumption rate associated with NOS_{fuel} allows for a maximum reduction in crossover while simultaneously maintaining an elevated cell potential.

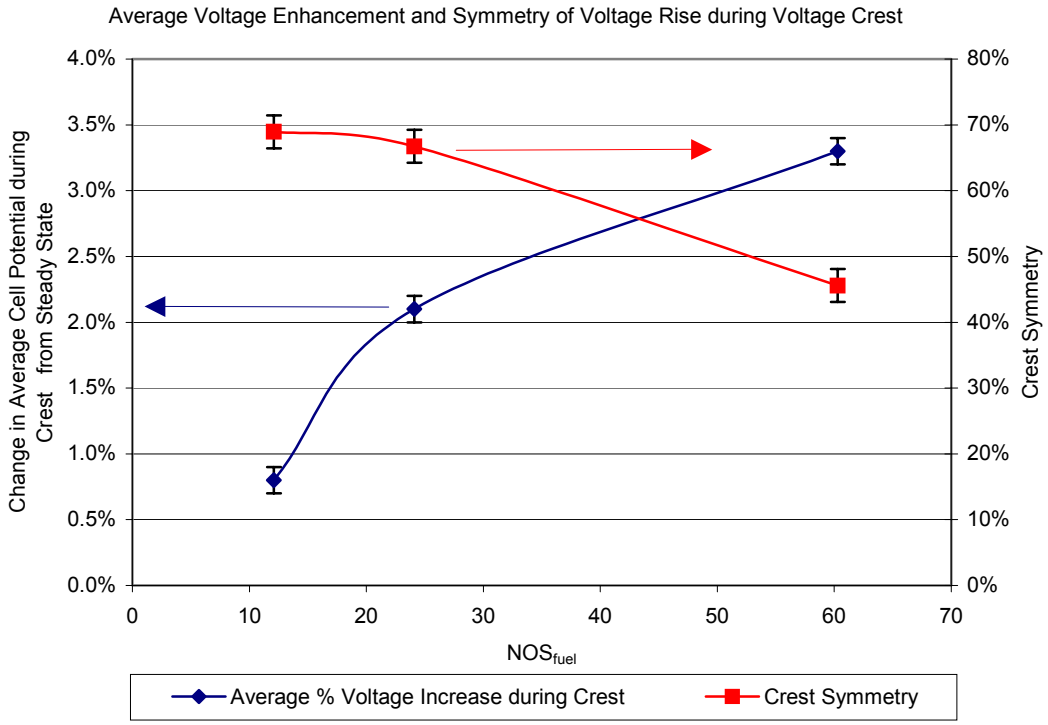

Figure 6.6: Percent increase in average cell potential during crest and crest symmetry

The crest symmetry value plotted in Figure 6.6 provides the fuel cell system designer with a design space that allows for optimization of power performance or of fuel utilization. To effectively implement the data here into an operational scheme that improves overall performance (in terms of power or in terms of fuel efficiency), the most important parameters for the designer are the time required to attain peak voltage and the time required to return to steady state voltage. The symmetry value in Figure 6.6 indicates the relative time between these two events; as previously stated, a high symmetry value (>0.5) indicates a relatively short window between realization of peak voltage and return to steady state voltage whereas a low symmetry value (<0.5) indicates a relatively long time between attainment of peak voltage and subsequent return to steady state levels.

Figure 6.7 below schematically represents the design space, which spans the range of time from the maximum increase in cell voltage to the minimum dome-averaged NOS_{fuel}. Both these goals—power maximization and NOS_{fuel} minimization—increase fuel efficiency. A designer who desires to maximize time averaged cell voltage would work to minimize the symmetry value. One who seeks to improve fuel efficiency must seek the optimal point in minimizing time averaged NOS_{fuel}.

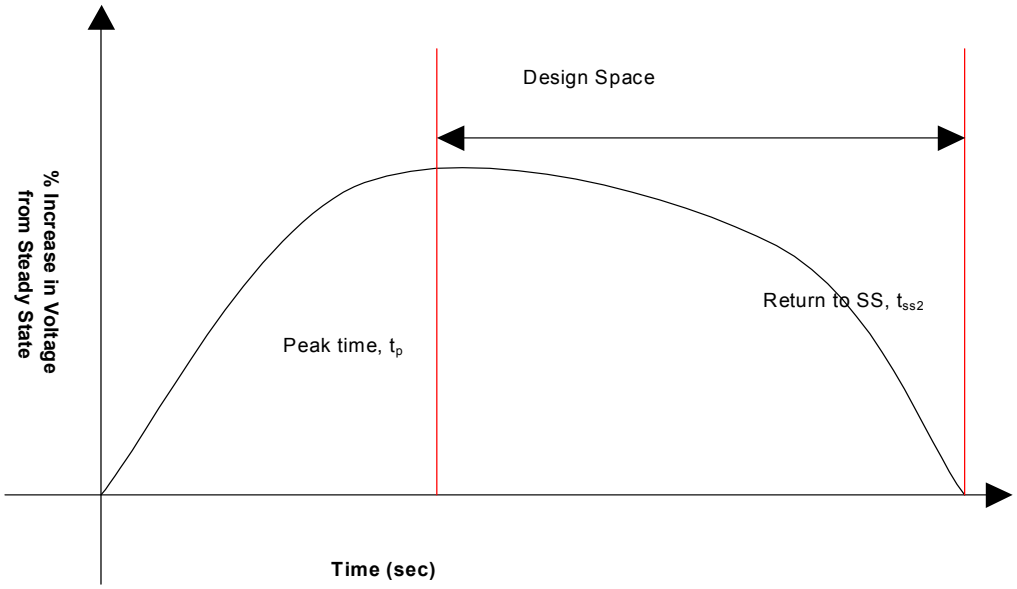

Figure 6.7: Schematic representation of optimal design space

The final step taken in the study of voltage decay due to fuel starvation was to compare the effects of initial flow rate to the effects of initial NOS_{fuel}. In Figure 6.8 below, five sets of decay data are plotted. Three curves are at a 50 mA/cm^2 current load with NOS_{fuel} ranging from 6 to 24.1. Also, of the five curves plotted, three are at a fixed

NOS_{fuel} of 12.1 with current loads ranging from 25 mA/cm^2 to 75 mA/cm^2. This combination of five data sets allows for three points to show the effect of varying NOS_{fuel} compared to three points that show the effect of varying the current density. By visual inspection of Figure 6.8, it appears that NOS_{fuel} is the parameter that most affects the shape of the curve and the voltage rise observed while constant current density on the cell during the trial appears to have the greatest effect on (absolute) benchmark times.

The initial NOS_{fuel} has a comparatively large influence over the general shape of the curve because, by definition, this parameter defines the latent fuel supply relative to the rate the fuel will be electro-oxidized. Thus at fixed NOS, there should be nearly identical levels of methanol crossover. This leads to a similar shape in the decay curve as the cell then goes through the an identical process for each case, regardless of current load, first utilizing latent methanol in the anode flow channels, then reversing crossover by extracting methanol from the MEA (and possibly the cathode) thus realizing a voltage increase before concentration polarization leads to a decline in cell potential. This process is discussed in more detail below.

While the shape of the curve is most influenced by the initial relative level of fuel supply, Figure 6.8 indicates that the absolute benchmark times vary due to the fixed volume of the anode flow channels and the rate of fuel consumption. At higher current densities, this latent supply is utilized more quickly; therefore, benchmark voltages are attained more quickly.

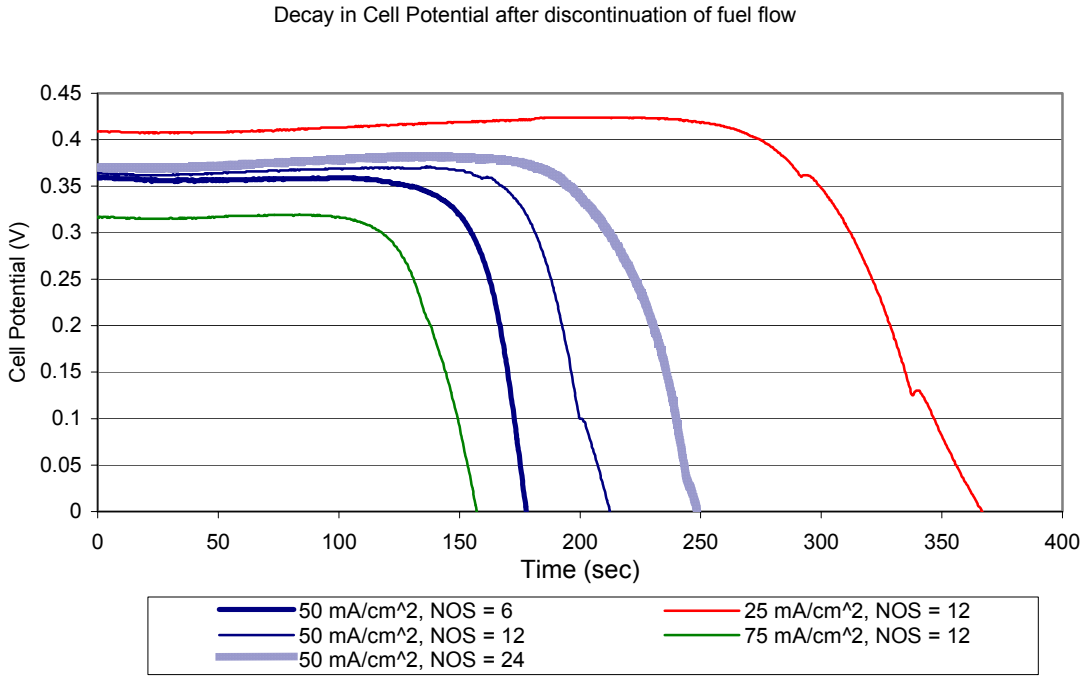

Figure 6.8: Effect of NOS_{fuel} and current density on decay in cell potential

For ease of reference, Table 6.1 below displays the above results quantitatively. Table 6.1 shows that it is the NOS parameter, rather than the current density parameter, which has a greater impact on cell performance. The low NOS case shown here (NOS_{fuel} = 6, j = 50 mA/cm^2) is substantially different from the other cases in terms of the rise in voltage observed as well as in terms of normalized benchmark times recorded. In contrast, the normalized benchmark times, and to a lesser extent the rise in cell potential, for the NOS_{fuel} = 12 cases show little variation. Therefore it is understood that NOS_{fuel} parameter is paramount in a variable flow scheme that seeks to realize enhanced DMFC performance.

Table 6.1: Numerical comparison of decay results

Current Density (mA/cm^2)	NOS_{fuel}	% Rise in Voltage	$\frac{T_{peak}}{T_{0V}}$	$\frac{T_{peak}}{T_{ss2}}$	$\frac{T_{ss2}}{T_{0V}}$
25	12.1	3.7	.562	.775	.726
50	6	0.3	.012	.546	.022
50	12.1	1.9	.645	.884	.730
50	24.1	3.2	.531	.727	.730
75	12.1	0.9	.532	.862	.617

6.2.2 Results of Pulsed Methanol Study

Based upon observations made in analyzing the above data, methanol flow was pulsed at what were hypothesized to be optimal periods of oscillation. The hypothesized optimal half-period for each respective current load was taken to be the time required for the cell to attain peak voltage after fuel flow was turned off. The minimum time of zero fuel flow was taken to be the time required for a measurable rise in cell potential to occur; similarly, the maximum period of discontinued fuel flow was taken to be the time required for the cell to return to steady state voltage. Note that this range is different than the optimal design space depicted in Figure 6.7; here, the time period of zero flow was selected with the goal of realizing a measurable voltage increase from the measured steady state potential.

Larger periods (i.e., lower frequencies) of oscillation were expected to result in fuel starvation becoming a dominant contributor to declining cell voltage; at lower periods (i.e., higher frequencies) of oscillation, minimal change was expected from steady state operation because little if any change in methanol crossover/fuel depletion

would have occurred. In a small range near the optimal period, an increase in cell power was expected, thus creating a dome shaped region in which cell performance could be improved via AFC. This hypothesis is described qualitatively in Figure 6.9 below.

Based upon this hypothesis, three distinct regions were proposed. In the first region, referred to as the capacitive zone, no significant change in cell potential was expected. While in the capacitive zone, the cell continues to operate normally by electro-oxidizing methanol in the latent pool along the anode. At this stage, neither the reduction in methanol crossover nor the detrimental effects of concentration polarization dominate; rather, the built-up fuel capacitances of both the flow fields and of the MEA itself dominate in this first zone. The second zone is marked by an increase in cell potential from steady flow levels. In this envisioned zone of maximized crossover mitigation, the latent supply of methanol has been exhausted to the point that a significant reduction in crossover occurs due to smaller concentration based driving forces, resulting in a rise in cell potential and a reduction in methanol crossover. The final stage is the fuel depletion zone during which cell potential declines below steady state levels as fuel starvation, or concentration polarization, becomes the dominant effect. It should be noted that each effect—consumption of latent fuel at the anode, reduced crossover, and finally fuel starvation are present at all times, though each effect is temporarily dominant as discussed above.

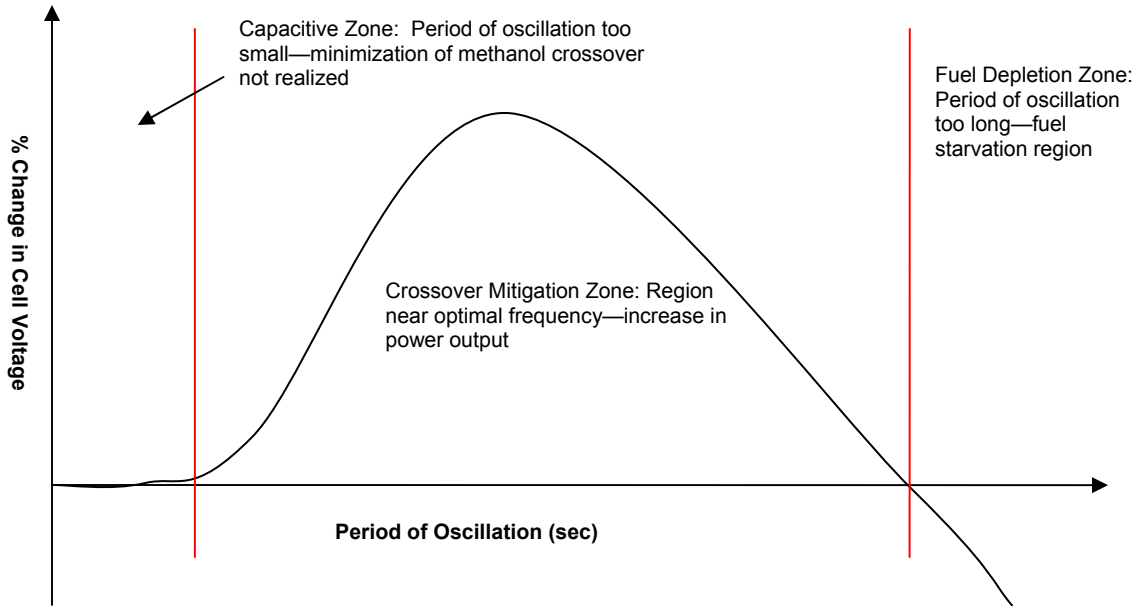

Figure 6.9: Qualitative description of effect of pulsed fuel flow

Figure 6.10 shows the time-averaged change in cell voltage from steady flow conditions with periodically pulsed methanol flow. For these trials, 1 M methanol flow was pulsed between 0 ccm and 0.25 ccm at the period indicated while current density and air flow were held constant. The waveform pattern used was a 50% duty cycle square wave. This figure shows that the anticipated dome shape was in fact observed. The data also indicate that the performance enhancement is greatest at low current densities. The range of acceptable zero-flow duration is also broadest at low current density. These trends are most prominent at low current density because this condition results in the greatest amount of methanol crossover. Thus, again reducing methanol crossover will have the largest impact at low current loads. It should be noted that the negative "Zone 1" values are observed in Figure 6.10 as a result of limitations in

measurement accuracy; the error associated with the measured cell potential is equivalent to ±1% of the reported value.

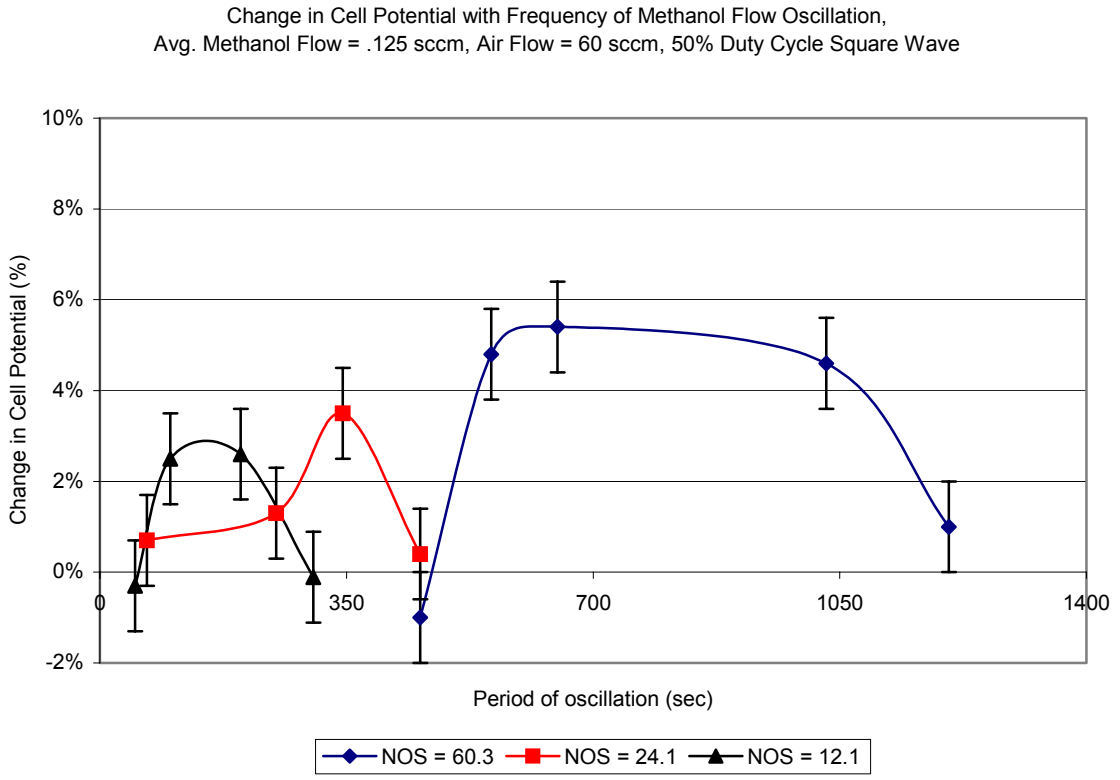

Figure 6.10: Change in average cell potential from steady state due to pulsed methanol flow at NOS_{fuel} = 60.3, 24.1, and 12.1 (10 mA/cm^2, 25 mA/cm^2, and 50 mA/cm^2)

Figures 6.11(a) shows the voltage-time effect of pulsed fuel flow. This plot gives the transient voltage response to fuel flow pulsed between 0 ccm and .25 ccm for 5500 seconds. The period of oscillation was 550 s (f = .0018 Hz). The current load in this case is set at 10 mA/cm^2, which corresponds to NOS_{fuel} = 60.3. The air flow rate is a constant 60 ccm. Like the decay data discussed in the previous section, the cell voltage

is observed to undergo a temporary rise after fuel flow is stopped before beginning to decline. When fuel flow is reintroduced to the cell, cell potential is again shown to rise before rapidly declining. The added surge is understood to be a result of reduced methanol crossover being complemented by added fuel reactant presence at the anode; however, the counter-effect of crossover build-up recurs. It should be noted that the mean cycle-to-cycle cell voltage declines throughout the duration of the trial (hence the negative slope of the mean voltage). This diminishing return brought about by the steady decline in mean voltage is a common characteristic of DMFC performance during steady flow operation as well (Correspondence with A. Fisher, Motorola). This trend is shown by the red curve, which is the change in cell potential over time with steady flow. It is observed that the rise in cell potential which is coincident with discontinuation of fuel flow is substantial as compared to the steady flow voltage. Similar data is presented in Figure 6.11(b) below.

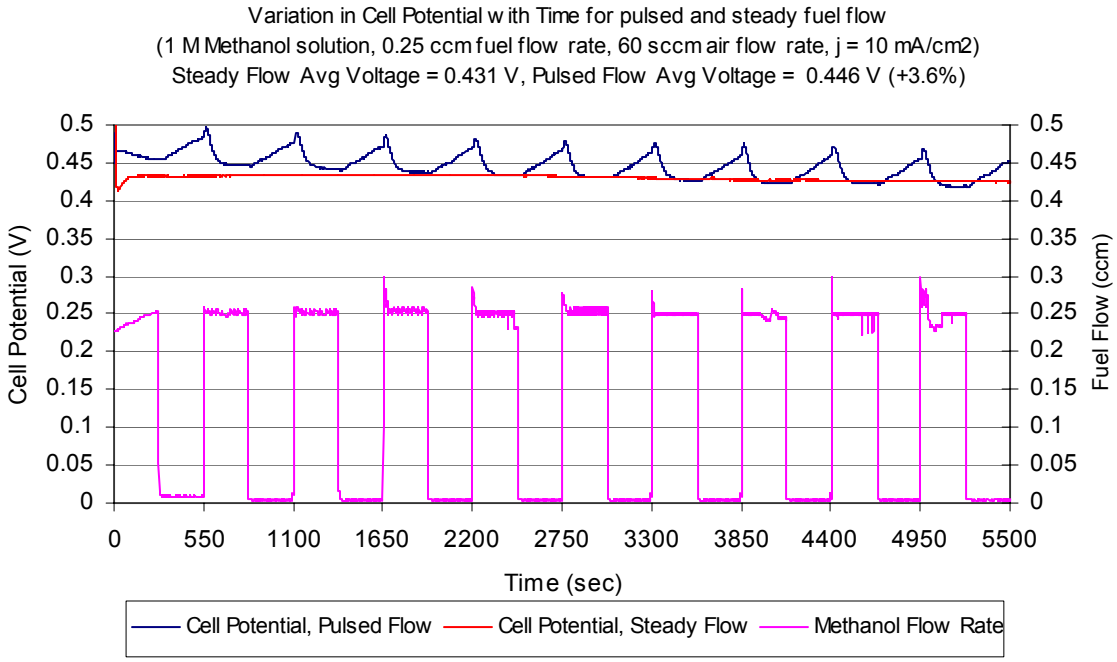

Figure 6.11(a): Oscillation in cell potential with time in response to pulsed fuel flow at 10 mA/cm^2 (NOS_{fuel} = 60.3)

Figure 6.11(b) again shows the effect of pulsed fuel flow on measured cell potential. However, in this case two important parameters are varied from the previous case— the fuel concentration is doubled to a value of 2 M (2 moles of methanol per liter of solution) and catalyst loadings are halved to a level of 2 mg/cm^2 catalyst per electrode. These changes result in greater methanol crossover than the higher loading, lower fuel concentration case considered above. This test was performed as part of a preliminary study to show that pulsed methanol flow is more beneficial with more cost-efficient cells. Reducing catalyst load substantially improves system cost, while increase fuel concentration reduces system volume and pump sizing. Similar to the data shown in Figure 6.11(a), pulsed flow again results in a greater time-averaged cell potential. Furthermore, with the increased fuel concentration and reduced catalyst loading, cell potential decays at a greater rate for both the steady and pulsed flow cases. However,

whereas in Figure 6.11(a) the magnitude of voltage decay with time was slightly greater in the pulsed flow case as compared to the steady flow case, here the magnitude of the change in voltage with time is found to be roughly equal. Thus discontinuation of fuel flow consistently results in a temporary but substantial rise in cell potential over the steady flow case. This rise is greater in magnitude than in the 1 M, 4:4 loading cases presented earlier. As greater methanol crossover is known to occur at higher fuel concentrations and lower catalyst loadings, the fact that a greater rise in cell potential occurs after flow shut-off further supports the conclusion that the effect is realized due to temporarily reduced crossover. Here, an average voltage increase of 8.2% is realized over steady flow conditions.

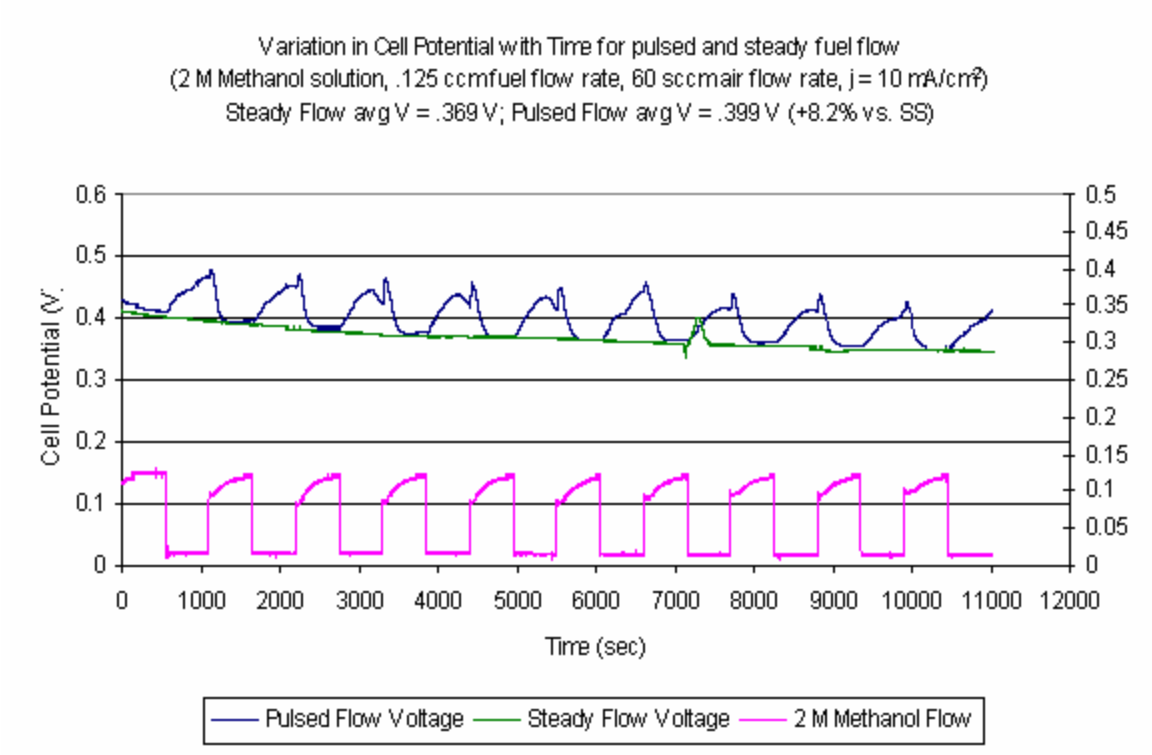

Figure 6.11(b): Oscillation in cell potential with time in response to pulsed fuel flow at 10 mA/cm^2 (NOS_{fuel} = 60.3), 2 M Methanol, 2:2 catalyst loading case

Figure 6.12 makes an illustrative comparison of the effect of using pulsed flow versus the effect of steady flow with the same average fuel flow rates. In Figure 6.12, the average cell potential of pulsed trials at current densities of 10 mA/cm^2, 25 mA/cm^2, and 50 mA/cm^2 are plotted with a VI curve taken with a steady fuel flow rate of 0.125 ccm. During the pulsed trials (such as the example in Figure 6.11), average fuel flow was also 0.125 ccm. Upon initial inspection, it appears that Figure 6.12 indicates that little benefit is realized by pulsing fuel flow. However, the time scales over which the data was collected are quite different. For the steady flow VI curve (red data points), data was acquired for approximately 30 seconds at each current load; however, in each pulsed flow case, at least ten complete fuel flow cycles were caputured and then the average voltage was taken. In contrast to the half-minute duration used for the VI curves, the pulsed flow data was taken over the span of several hours. Therefore, Figure 6.12 actually indicates that pulsing fuel flow helps to maintain the initial "quasi-steady" state voltage measured in the steady flow case.

Also of great importance in the consideration of realizing the benefits of pulsed fuel flow is the dependence of the voltage rise upon the quantity of methanol that has been absorbed by the membrane and also the quantity which has crossed to the cathode. As the sum of methanol which has left the anode varies with operating history, current load on the cell, and time, so too will the benefits of pulsed flow vary. Therefore, the best implementation of pulsed methanol flow may involve any of the following: a cycle which includes only a few on-off oscillations in flow to maximize voltage before resuming steady flow operation; a low duty cycle square wave that allows for periodic reduction in methanol crossover; or a closed loop system that allows for the fuel flow to be controlled by any combination of several parameters, including cell potential, change in potential with time, current load, and carbon (e.g. CO, CO_2) level in the cathode exhaust.

Based upon these observations, it is suggested that pulsed flow be utilized intermittently in order to minimize methanol crossover, thus enhancing performance via mitigation of methanol crossover. As has been stated, the benefit of reduced crossover not only increases power output in the short-term, but it also believed that minimized crossover will have a substantial impact on improved MEA lifetime.

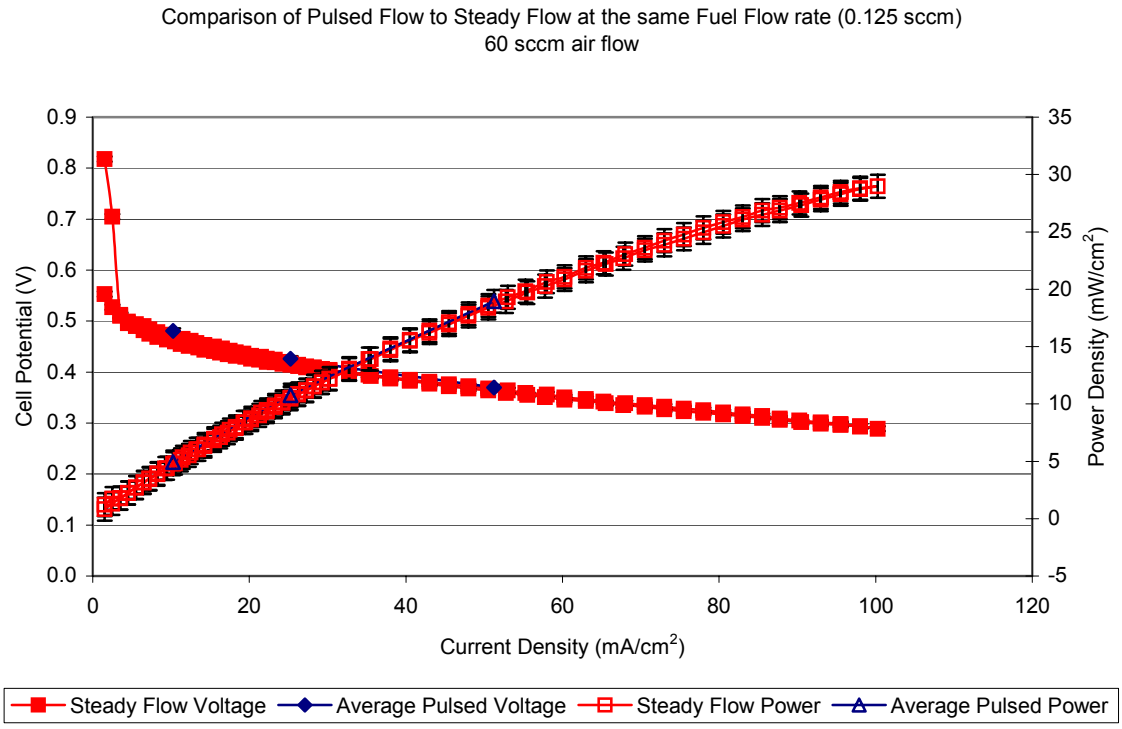

Figure 6.12: Comparison of pulsed fuel flow to steady fuel flow; average fuel flow rate = 0.125 ccm

6.2.3 Comparison to Published Results

Two journal references in particular support the results and theory presented in the previous section. The data presented by Sundmacher, *et al.*, corroborates the

trends presented in the present work, while the work of Scott, *et al*., introduces equations to quantify methanol crossover and ultimately support the theory proposed in the previous section.

As discussed in Chapter 3, Sundmacher, *et al*., reported experimental results showing the effect of pulsed methanol concentration while current load was held constant. This is very similar to the work presented here; however, a distinguishing characteristic of the present work was that the flow rate of the pre-mixed methanol-water solution was varied rather than maintaining a constant water supply rate and varying the concentration of methanol actively mixed into that flow. The control scheme and operating procedures utilized by Sundmacher, *et al.* caused greater methanol crossover during times of steady fuel flow and promoted reduction in methanol crossover during times of zero fuel flow as compared to the flow control scheme presently employed.[6] To briefly restate these potential effects of the control scheme used by Sundmacher, *et al*., recall that the higher concentrations of methanol (such as the 1.5 M concentration used by Sundmacher, *et al*.) at the anode will produce greater crossover. Further recall that maintaining a constant liquid flow rate along the anode of the cell and varying the concentration of methanol in the flow draw latent fuel drawn away from the anode during times when feed-stream methanol concentration is zero. Maintaining a constant liquid flow rate along the anode is believed to accelerate entrance into the "fuel starvation" region described previously. Another distinction between the present work and that of Sundmacher, *et al*., is the catalyst loading on the anode and, to a lesser extent, cathode. The Motorola DMFC used in the present work had catalyst loadings of 4 mg/cm^2 on each electrode as compared to 2 mg/cm^2 per electrode loadings used in the Sundmacher study. With lower catalyst loadings, particularly at the anode, methanol crossover

[6] Refer to Ch. 3 for further comparison of the respective control schemes and operating procedures and for schematic representation of the differences.

increases substantially due to less electrochemical activity. The results of these three important differences are that methanol crossover occurred in larger quantity due to higher concentration (1.5 M vs. 1 M) and lower catalyst loading (2 mg/cm^2 vs. 4 mg/cm^2) and that the reduction in methanol crossover occurs more rapidly and in greater quantity than the method used in the present work. This group reported a 15% improvement by reducing methanol concentration to zero and achieved a 10% improvement in time-averaged power. Though the numerical results reported here differ from the results measured by Sundmacher, *et al*., qualitatively the same trends have been observed; specifically, cell potential increased after fuel flow was reduced and pulsing fuel flow in a periodic manner resulted in an increase in time-averaged voltage.

As discussed in Chapter 3, Scott, *et al*. identified three possible factors that lead to methanol crossover. These factors are included in equation 6.1 below. The first term quantifies methanol crossover due to a concentration gradient (the normal cause of diffusion). The second term is a "leakage rate" brought about by possible pressure differences across the MEA. Finally, the third term captures the methanol crossover associated with electro-osmotic drag. Recall that this is the phenomenon in which methanol molecules are carried across the membrane along with positively charged ions.

$$j = -\frac{D}{t_m}\Delta c - \frac{c_2 K}{t_m}\Delta P + \frac{\lambda}{nF} I \tag{6.1}$$

In this equation, each of the three aforementioned components of methanol crossover is represented. In the first term (concentration gradient) D is the diffusion coefficient of methanol through the MEA, t_m is membrane thickness, and Δc is the methanol concentration difference from anode to cathode. In the second term (the leakage rate

due to pressure), c_2 is the concentration of methanol at the surface of the anode, K is an empirical constant representing the effective hydraulic permeability, and ΔP gives the pressure difference across the MEA. The final term accounts for electro-osmotic drag; the parameter λ gives the moles of methanol that cross through the MEA for every positive ion that permeates the membrane (2.48×10^{-2} $MeOH/H^+$, Scott 1997), n is the number of moles of electrons required to complete the reaction (6 in the case of the oxidation of methanol), F is Faraday's constant (96488 Coulombs/mole electrons), and I is the current density.

In the experimental work presented here, the first and last terms of Equation 6.1 are substantially larger than the second term due to a small differential pressure across the membrane. Pulsing the cell's fuel supply temporarily reduces the concentration difference, thus minimizing the diffusion of methanol through the membrane. Equation 6.1 further indicates that methanol crossover could be mitigated by periodically increasing the current load on the fuel cell such that NOS_{fuel} temporarily is less than unity. This would promote possible reversal of crossover by drawing methanol that had crossed over to the cathode back to the anode where it would be electro-oxidized and thus used to produce useful electrical energy. Recalling that NOS is defined in Chapter 4 as the ratio of the ideal current that can be drawn based on the reactant flow rate to the actual current drawn from the cell, both flow and load pulsing ultimately have the same effect of temporarily reducing NOS_{fuel}, which, in turn, has the effect of minimizing methanol crossover. Table 6.2 gives the first-order relative rates of methanol crossover attributable to diffusion and to electro-osmotic drag. The values for each parameter are either values based on the fuel cell used in this project, such as maximum current load and maximum methanol concentration, or values obtained from Scott, *et al.* These values include the diffusion coefficient, D, and the electro-osmotic drag coefficient, λ.

Both parameters are based on the characteristics of the MEA used. As the materials used by Scott, *et al.* are similar to those used by Motorola to fabricate the MEA used in this work, it is assumed that the coefficients are of sufficient accuracy to estimate these first-order effects upon methanol crossover.

Table 6.2: Relative Effect of Load and Flow Pulsing on Methanol Crossover

Parameter Varied	Maximum Methanol Crossover (mol CH_3OH/s)	Diffusion Equation[7]
Flow	9.7×10^{-8}	$\frac{D}{t_m}\Delta c$
Current Load	1.6×10^{-8}	$\frac{\lambda}{nF} I$

Assuming a maximum concentration gradient equivalent to 1 M methanol solution at the anode and 0 M methanol initially at the cathode and a maximum current load of 100 mA/cm^2 produces the values in Table 6.2. These values suggest that diffusion of methanol through the membrane is primarily due to the concentration gradient across the MEA. At the 0.25 ccm flow rate predominantly used in this study, the total methanol crossover from Table 6.2 of approximately 10^{-7} moles per second is equivalent to several percent (2-3%) of the total methanol flow into the cell.[8] This illustrates the large impact on cell performance of even a seemingly small amount of methanol crossover.

[7] Equations in Table 6.2 are based on Equation 6.1, taken from Scott, *et al*. 1997
[8] A 1 M methanol-water solution flowing at 0.25 sccm is equivalent to (pure) methanol flow of 4.2×10^{-6} mol/s

In addition to temporarily increasing the power produced by the cell, the voltage increase realized through actively varying the fuel flow rate also increases cell efficiency. This effect is twofold: first, simply by increasing cell potential, efficiency is increased; furthermore, by briefly turning off fuel flow, methanol is used more efficiently. As the fuel is supplied in liquid form, when the flow is discontinued, a temporary pool of fuel forms in the flow channels. In order to satisfy the current demand on the cell, methanol from this latent pool is forced to electro-oxidize; a portion of this methanol would normally flow through the cell without reacting. Thus, fuel efficiency is also increased accordingly.

This gain in efficiency from normal, steady flow cell efficiency can be quantified as shown in equation 6.2 below:

$$\Delta\eta_{one-pass} = \frac{i}{HHV_{meth}}\left(\frac{V_{avg,new}}{\dot{n}_{avg.,new}} - \frac{V_{avg,old,ss}}{\dot{n}_{avg.,old,ss}}\right) \tag{6.2}$$

Equation 6.2 indicates that the total increase in cell efficiency as a result of pulsed flow is difference between not only the new voltage and the steady flow voltage, but also the time-averaged flow rates at which these voltages are measured. This quantity (in parentheses) is then multiplied by the current load on the cell to determine the total molar-specific power increase realized before being normalized by the higher heating value of methanol, which is the maximum possible energy that could be obtained by electro-oxidizing methanol.

6.2.4 Consideration of Pulsed Air Flow

Though the air turn-off transient data indicated no performance enhancement as the fuel turn-off data did (refer to Figure 6.2(a)), pulsed air flow was studied to determine the potential for using AFC of oxidant flow as a means of voltage modulation. The

parameters considered for this portion of the study include frequency of oscillation, current load, and amplitude of air flow oscillation.

Figure 6.13 shows the effect of active flow control over a range of current loads and air flow frequencies. The trends revealed in this figure are similar to trends identified in Chapter 5 as part of the study of AFC on the hydrogen fueled PEM cell. The first trend is that as frequency of air flow oscillation increases, the oscillation in cell potential, and thus the amplitude ratio decreases substantially. Secondly, increased current load tends to promote a larger oscillation in cell potential. As stated in the previous chapter, these two trends are observed because increasing the current load upon the cell and reducing the frequency of air flow oscillations causes the cell to exhaust the excess oxidant supply more quickly, thus producing a greater oscillation in cell potential. The data in Figure 6.13 indicate that oscillation in cell potential becomes negligible at or near 1 Hz for even moderately high current densities (i.e. 50 mA/cm^2); at lower current densities, the oscillation in cell potential is only significant at 0.1 Hz. Furthermore, only the highest current density (100 mA/cm^2) produced a substantial oscillation in cell potential up to the assumed frequency limit. This is likely true because of the large amount of excess air that was supplied. Recall that the operating instructions provided by Motorola call for an air flow rate of 60 sccm. All tests were therefore conducted at an average air flow rate of 60 sccm, resulting in a wide range of NOS_{air} values; the NOS_{air} at 10 mA/cm^2 is 10 times larger than the NOS_{air} at 100 mA/cm^2 at a fixed flow rate. The following NOS_{air} values correspond to the respective current densities: $NOS_{air} = 8.6$ for $j = 100$ mA/cm^2; $NOS_{air} = 17.2$ for $j = 50$ mA/cm^2; $NOS_{air} = 34.4$ for $j = 25$ mA/cm^2; and $NOS_{air} = 86$ for $j = 10$ mA/cm^2. This is in contrast to the operation of the PEM cell used, where the level of excess reactant supplied was held constant.

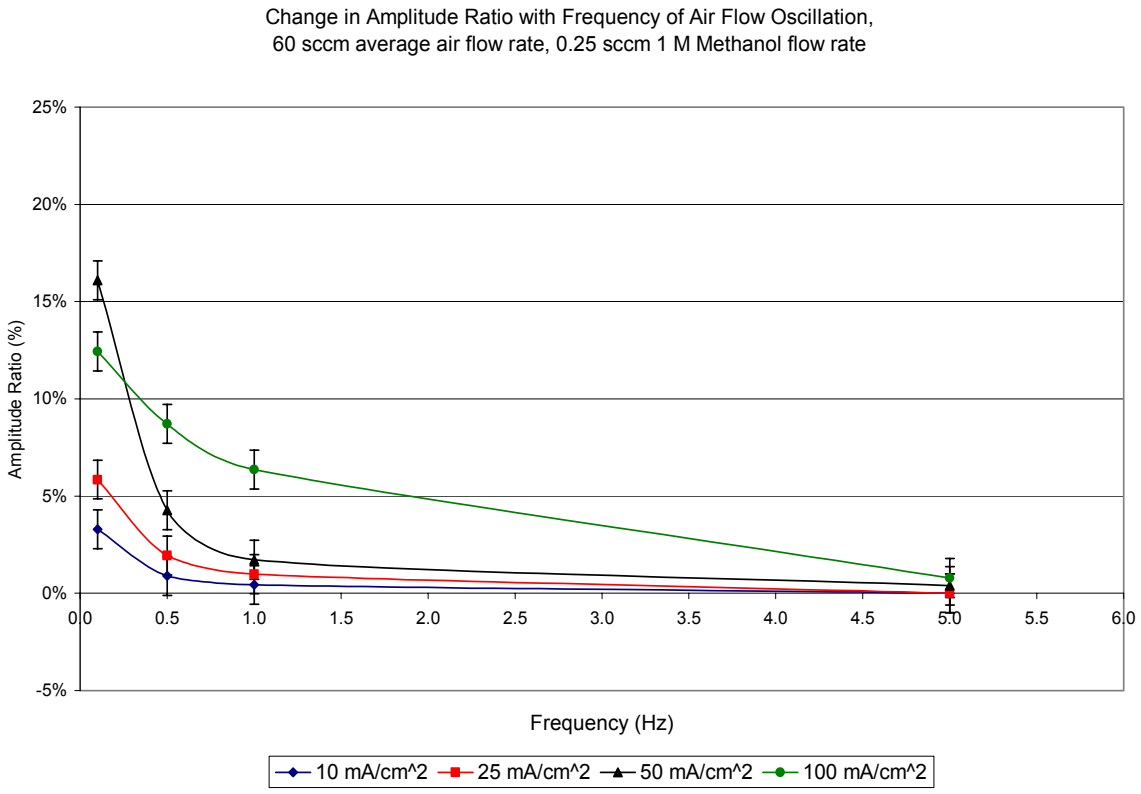

Figure 6.13: Change in voltage oscillation with frequency of air oscillation at 10 mA/cm^2, 25 mA/cm^2, 50 mA/cm^2, and 100 mA/cm^2

As the observed voltage oscillation was small and the frequency limit at moderate current densities is below 1 Hz, this data is most valuable when compared to other results presented here. While the voltage response of a direct hydrogen PEM cell was found to be greater with pulsed air flow than pulsed fuel flow, the effects of pulsed fuel flow on a DMFC were found to be greater than the effects of pulsed air flow. In the PEM case, air flow into the cell has a substantial effect on membrane humidity, which in turn has a substantial effect on cell performance. However, in the DMFC case, the fuel

mixture is in liquid form, primarily composed of water; thus, air flow into a DMFC is thought to have a smaller effect on membrane humidity. Furthermore, the fact that no beneficial effect of pulsing air flow into the DMFC was observed further supports the hypothesis that the improvement realized by pulsing methanol flow is the result of reduced methanol crossover.

7. Conclusions & Recommendations for Future Work

7.1 Conclusions

Numerous trends have been identified in studying the effects of active flow control on solid polymer electrolyte fuel cells. Using direct hydrogen PEM technology, the ability to modulate cell potential via pulsed oxidant flow has been shown. The study of pulsed fuel flow on a DMFC showed potential for increased performance in terms of both cell power output and fuel efficiency. The results of the present work are summarized in Tables 7.1 and 7.2 below.

Table 7.1: Review of trends observed in H_2 PEM study

Parameter Varied	Current Load Increased	Frequency Decreased	NOS Decreased	Flow Amplitude Increased
Effect on Voltage Oscillation	+	+	+	+
Effect on Average Cell Power vs. SS Performance	-	-	-	-

The PEM results presented in this work suggest the possibility that the most relevant parameter in modulating cell potential via active flow control is membrane humidity. By pulsing oxidant flow, the membrane *may* undergo substantial change in humidity level, leading to changes in membrane conductivity that causes the observed oscillation in cell potential. The oscillation in cell potential caused by low-frequency air flow pulses indicates that the ability to modulate cell potential in this way may provide an alternative method to satisfy low-frequency changes in cell load. Responding to sub-Hertz transient load demand using oxidant flow modulation may reduce the cost of

power conditioning equipment currently used in fuel cell systems, potentially resulting in a reduction in total system cost.

Table 7.2: Review of trends observed in DMFC study

NOS_{fuel}	Methanol Crossover	Voltage rise observed?	Sustainable performance enhancement realized?
High (> 60)	High	Yes	Yes
Medium (12 - 24)	Moderate	Yes	Yes
Low (< 6)	Limited	No	No

In the direct methanol portion of the study, pulsed fuel flow was shown to improve cell performance via a reduction in methanol crossover. By periodically turning off methanol flow, an *in situ* latent supply of methanol-water solution, along the anode, is temporarily utilized. As the cell continues to meet the demanded current load, the concentration of methanol in this pool decreases. This pulsing approach has the attendant benefits of reducing methanol crossover and increasing single pass fuel utilization.

There are numerous benefits realized as a product of reduced methanol crossover. Most immediately, the polarization associated with crossover decreases, causing a rise in cell potential, which in turn increases cell power output. Voltage increases of up to 6% over steady flow levels have been observed here. By periodically pulsing flow, a sustainable improvement of up to 5% has been achieved. A longer-term benefit realized due to reduced crossover is increased MEA lifetime. As methanol diffuses to the anode, it bonds irreversibly at the cathode reaction sites, which impedes the reduction of oxygen. Substantial research efforts have focused on developing an

MEA impermeable to methanol. However, these undertakings have shown that the experimental membranes often have lower conductivity due to increased thickness or due to higher internal resistance of the material selected. The lower conductivity of these MEAs results in reduced performance. The hydraulic pulsing work presented here demonstrates that achieving a reduction in methanol crossover is not contingent upon major MEA technology breakthroughs. Furthermore, this work shows that mitigated crossover need not result in reduced cell performance.

The second major benefit shown as the result of hydraulic pulsing is potential for an increase in fuel efficiency. By pulsing the fuel flow in such a manner as to maintain the cell voltage at an acceptable minimum while minimizing fuel flow, fuel efficiency can increase substantially. As fuel efficiency is increased, less fuel storage is required to run the cell for a given time at a given load. This fact is a vital consideration in portable power applications, such as for cell phones, laptops, and possible military applications. Furthermore, if sufficient gains in fuel efficiency are realized, power-consuming recirculating pumps can be eliminated from the fuel cell system, thus reducing parasitic losses and increases total power output from the system.

Finally, the results presented here have shown that cell performance after flow discontinuation is scalable over a wide range of current densities. The energy balance detailed in Appendix A shows that the power consumed after flow discontinuation is approximately constant. This confirms the scalable nature of the variation in cell potential with time after fuel flow discontinuation.

7.2 Recommendations for Future Work

The present PEM work has led to the hypothesis that variation in membrane humidity is the driving factor in producing a time varying voltage signal. Future work should focus on confirming this hypothesis and determining if pulsed reactant flow can assist in maintaining optimal membrane humidity levels. Also, future research efforts should be focused on realizing a net cost savings by reducing the power electronics required to meet slow changes in cell power demand. A first step in such a study should determine if cost savings are feasible when considering the drop in cell power reported here as well as the extra cost associated with the necessary valves and control scheme.

The focus of the DMFC work has been to enhance power output from the fuel cell by modulating current load. However, based on the data presented in Ch. 6, it is also possible to modulate fuel flow so as to maintain a threshold cell potential at a given current load while minimizing the fuel required. Such a scheme could, if properly employed, significantly reduce the need to recirculate methanol flow, thus eliminating parasitic losses associated with extra pumps to reintroduce depleted fuel into the fuel reservoir. Furthermore, design for efficient use of fuel is paramount for a number of the applications for which DMFCs are currently considered to be a viable power source. Such uses include laptop computers, cell phones, and remote sensor applications. In each of these cases, a fixed fuel reservoir would supply the DMFC stack. An important design parameter in cases with a fixed fuel supply will be maximizing the fuel efficiency.

This study of DMFCs has shown potential for benefits in terms of enhanced power output from the cell. The work presented by Argyropoulos, *et al.*, showed that similar improvements in cell power can be realized by pulsing the current load on the cell. Future work should consider the effects of bimodal pulsing, that is, pulsing both fuel

flow and current load on the cell in order to realize optimal levels of performance and fuel efficiency. As has been supported in the present work, the primary mechanism resulting in enhanced performance is understood to be a reduction in methanol crossover. It is suggested that the use of bimodal pulsing could further reduce methanol crossover and thus further improve cell performance.

An additional benefit of the reduction in methanol crossover achieved through bimodal pulsing is to allow for an in increase the concentration of methanol in the fuel solution. Current limitations in membrane technology require that the methanol-water fuel solution must be very dilute. A 1 M methanol-water solution (such as that used for the present work) is only 3-4% methanol by volume; the 1.5 M solution used by Sundmacher, *et al.* was only 6% methanol by volume. Thus, over 90% of the fuel storage tank in a modern DMFC system would be devoted to storing deionized water. To become economical, the energy density of the fuel solution must increase substantially. The present work has shown that methanol crossover can be reduced via modulation of fuel flow in cases using a 1 M methanol solution. The effects of bimodal pulsing will therefore be studies at higher concentrations of methanol.

Other future steps include an accurate quantification of methanol crossover via experimental means and waveform optimization such that cell performance and fuel efficiency are maximized. In this thesis, an approximate value has been calculated for methanol crossover based upon other published data. However, ideally this value would be measured experimentally in real time. Unfortunately, no economical method was found to make the necessary measurements. Also, optimizing the fuel waveform may increase the maximum voltage level attained and also reduce the rate of voltage decline after fuel flow is reintroduced.

Appendix A: Energy Balance Calculations

This appendix contains calculations which compare the total energy contained within the stagnant fuel solution in the anode flow channels of the Motorola DMFC to the work done by the DMFC after flow discontinuation.

The following equations were obtained from 4th degree polynomial curve fits of the data shown in Figure 6.2(b):

Note: The units for each of these equations are Volts; the subscript denotes the NOS(fuel) level.

$t := 0..3000$

$V_{60}(t) := -7\cdot10^{-14}\cdot t^4 + 3\cdot10^{-10}\cdot t^3 - 4\cdot10^{-7}\cdot t^2 + .0002t + .4478$

$V_{24}(t) := -10^{-11}\cdot t^4 + 10^{-8}\cdot t^3 - 4\cdot10^{-6}\cdot t^2 + .0006t + .4022$

$V_{12}(t) := -7\cdot10^{-10}\cdot t^4 + 2\cdot10^{-7}\cdot t^3 - 2\cdot10^{-5}\cdot t^2 + .001t + .3669$

$V_6(t) := -2\cdot10^{-8}\cdot t^4 + 3\cdot10^{-6}\cdot t^3 - .0001\cdot t^2 + .0021\cdot t + .3037$

*Taking the integral of each of these equations and multiplying it by the current load (in Amps) on the cell gives the total work done by the cell after flow discontinuation. The limits of integration are from the time when fuel flow was shut off (t = 0) until the time when voltage was equal to 0 V. (Units are V*s)*

$Vs_{60} := \int_0^{2921} V_{60}(t)\,dt \qquad Vs_{60} = 1.321\times 10^3 \qquad Vs_{24} := \int_0^{670.34} V_{24}(t)\,dt \qquad Vs_{24} = 236.88$

$Vs_{12} := \int_0^{231.258} V_{12}(t)\,dt \qquad Vs_{12} = 79.544 \qquad Vs_6 := \int_0^{124.482} V_6(t)\,dt \qquad Vs_6 = 50.305$

Current load (in Amperes) at each NOS level.

$I_{60} := .04 \qquad I_{24} := .1 \qquad I_{12} := .2 \qquad I_6 := .4$

Energy is the product of current times the integral of Voltage with respect to time: (Units are Joules, 1 J = 1 N-m/s = 1 W-s)

$E_{60} := Vs_{60}\cdot I_{60} \qquad E_{24} := Vs_{24}\cdot I_{24} \qquad E_{12} := Vs_{12}\cdot I_{12} \qquad E_6 := Vs_6\cdot I_6$

$E_{60} =$ ▮ $\qquad E_{24} =$ ▮ $\qquad E_{12} =$ ▮ $\qquad E_6 =$ ▮

These values are the work done after the discontinuation of fuel flow.

The work done by the cell must be less than or equal to the energy available in the anode flow channels (in the form of methanol). The maximum possible energy will now be calculated.

$v := 20$ *Volume per flow channel in mm³*

$n := 18$ *Number of flow channels*

$V := n \cdot v$ $V =$ ∎

Total volume in mL: $V_{tot} := \frac{360}{1000}$ $V_{tot} =$ ∎

Given that the density of methanol is 791 kg/m ³ and the Molar Mass is 32.042 kg/kmol, it can be readily shown that the a 1 M methanol solution contains ***.0247 moles of methanol per mL of solution***

$c := .0247$

$C := V_{tot} \cdot c$ $C =$ ∎ *C is the concentration of methanol in the anode flow channels in moles.*

$HHV := 22700$ $M := 32.042$ $M \cdot HHV =$ ∎

HHV is the higher heating value of methanol in Joules/gram; M is the molar mass in g/mol; the product of the two is energy content of one mole of methanol in Joules/mole methanol. Multiplying the product of these two values by the concentration of methanol in the anode flow channels give the maximum amount of energy (or work) that could be extracted by the fuel cell:

$E_{max} := M \cdot HHV \cdot C$ $E_{max} =$ ∎

Because the work done by the cell after flow discontinuation is less than 1% of the energy contained in the methanol within the anode flow channels, energy has been conserved and the voltage decay data is thus given further credence.

Summary of Calculated Values:

From Decay Data:

$E_{60} = 52.844$
$E_{24} = 23.688$
$E_{12} = 15.909$
$E_{6} = 20.122$

Maximum Possible Energy:

$V_{tot} = .36mL$
$C = 8.892x10^{-3}$
$M \cdot HHV = 7.274x10^{5}$
$E_{max} = 6.468x10^{3}$

REFERENCES

Argyropoulos, P., K. Scott, W. M. Taama, 2000, "Dynamic Response of Direct Methanol Fuel Cell Under Variable Load Conditions", *Journal of Power Sources*, 87, pp. 153 – 61.

Department of Energy, 2002, *Fuel Cell Handbook (Sixth Edition)*, DE-AM26-99-740575, Morgantown, WV, November.

Fisher, Allison, Motorola, May 2003, Dec. 2003, February 2004, correspondence with the author.

Haynes, C. L., G. Gray, D. Parekh, A. Williams, S. Leahy, R. Spadaccini, 2003, "Development of an 'AC' Fuel Cell Stack via Active Flow Control", Georgia Tech Research Institute Year-End IRAD report.

Larminie, J., A. Dicks, 2000, *Fuel Cell Systems Explained*, J. W. Wiley & Sons, New York.

Layton, James, Lynntech Industries, Dec. 2003, Jan. 2004, correspondence with the author.

Nguyen, T. V., and J. S. Yi, 1999, "Multicomponent Transport in Porous Electrodes of Proton Exchange Membrane Fuel Cells Using Interdigitated Gas Distributors, *Journal of the Electrochemical Society*, 146(1), pp. 38-45.

Pukrushpan, J. T., A. Stefanopoulou, H. Peng, 2002, "Modeling and Control for PEM Fuel Cell Stack Systems", Proceedings of the American Control Conference, pp. 3117 – 3122

Rooker, W. E., 2003, *Enhancing the Thermal Design and Optimization of SOFC Technology*, Masters Thesis, Georgia Institute of Technology, Atlanta.

Scott, K. W. Taama, J. Cruickshank, 1997, "Performance and Modeling of a Direct Methanol Solid Polymer Electrolyte Fuel Cell", *Journal of Power Sources*, 65, pp. 159 – 171.

Sundmacher, K., T. Schultz, S. Zhou, K. Scott, M. Ginkel, E. D. Gilles, 2001, "Dynamics of the Direct Methanol Fuel Cell (DMFC): Experiments and Model-Based Analysis", *Chemical Engineering Science*, 56, pp. 333 – 341

Wilkinson, D. P., C. Y. F. Chow, D. E. Allen, E. P. Johannes, J. A. Roberts, J. St-Pierre, C. J. Longley, J. K. K. Chan, 2000, “Method and Apparatus for Operating an Electrochemical Fuel Cell with Periodic Fuel Starvation at the Anode” U. S. Patent 6,096,448.